SYNTHESIS OF CARBON NANOTUBES BY ORIFICE-CHEMICAL VAPOR DEPOSITION REACTOR AND APPLICATIONS IN STYRENE POLYMERIZATION AND NANOCOMPOSITES

BY

Issam Thaher Amr

A Dissertation Presented to the

DEANSHIP OF GRADUATE STUDIES

KING FAHD UNIVERSITY OF PETROLEUM & MINERALS

DHAHRAN, SAUDI ARABIA

In Partial Fulfillment of the
Requirements for the Degree of

DOCTOR OF PHILOSOPHY

In

CHEMICAL ENGINEERING

JANUARY, 2011

KING FAHD UNIVERSITY OF PETROLEUM & MINERALS
DHAHRAN, SAUDI ARABIA

DEANSHIP OF GRADUATE STUDIES

This dissertation, written by **Issam Thaher Amr** under the direction of his dissertation advisor and approved by his dissertation committee, has been presented to and accepted by the Dean of Graduate Studies, in partial fulfillment of the requirements for the degree of **DOCTOR OF PHIOLOSOPHY IN CHEMICAL ENGINEERING.**

Dissertation Committee

A. Al Amer
Prof. Adnan Al-Amer
Thesis Advisor

Dr. Muataz A. Atieh
Co-advisor

U. A. Al-Mubaiyedh
Dr. Usamah Al-Mubaiyedh
Department Chairman

Prof. Naim M. Faqir
Member

Dr. Salam Zummo
Dean of Graduate Studies

عمادة الدراسات العليا
DEANSHIP OF GRADUATE STUDIES

B. A. Sharkh
Prof. Basel F. Abu-Sharkh
Member

12/6/11
Date

Dr. Tahar Laoui
Member

DEDICATED TO

MY LOVING FATHER, MOTHER, WIFE AND DAUGHTERS

ACKNOWLEDGEMENT

All praise and glory be to Allah for his limitless help and guidance. Peace pleasing of Allah be upon his prophet Mohammed.

I would like to express my profound gratitude and appreciation to my advisor Prof. Adnan Al-Amer, and co-advisor Dr. Muataz Atieh for their guidance and patience through this thesis, their continuous support and encouragement can never be forgotten. I'm also grateful to the other members of my thesis committee, Prof. Naim Faqir, Prof. Basel Abu-Sharkh and Dr. Tahar Laoui for their help, suggestions and encouragement.

I wish to express my thanks to all faculty members and staff of Chemical Engineering Department for their support.

My sincere appreciation to all of my friends, not only for the moral support but also for their concern and encouragement in the course of my studies.

My profound gratitude and appreciation to my mother, father, wife, daughters, brothers, sisters, relatives and friends in Jordan for their affection and concern.

Finally, I wish to thank King Fahd University of Petroleum and Minerals for the assistantship and support of this research.

TABLE OF CONTENTS

LIST OF TABLES

LIST OF FIGURES

DISSERTATION ABSTRACT

Name: Issam Thaher Amr

Title: Synthesis of Carbon Nanotubes by Orifice-Chemical Vapor Deposition Reactor and Applications in Styrene Polymerization and Nanocomposites

Major Field: Chemical Engineering

Date of Degree: January 2011

A new generation of catalytic chemical vapor deposition reactor was designed and fabricated locally at the department of chemical engineering, and it is called orifice chemical vapor deposition (O-CVD) reactor, to produce well aligned multiwall carbon nanotube (MWCNT) with high aspect ratio. Reaction parameters such as reaction temperature, reaction time, hydrogen flowrate, hydrocarbon flowrate and orifice diameter were varied in order to study their effect and to find the best parameters for producing MWCNTs with high quality and high aspect ratio. MWCNTs with purity of 97.6% and high aspect ratio (1mm long) were produced at hydrogen flowrate of 240 ml/min, acetylene flowrate of 155 ml/min, orifice diameter of 6 mm, 800^{o}C reaction temperature and 30 minutes reaction time. The production rate was 1.9 gram/hr with total cost of only 6 $US/gram. Scanning electron microscopy (SEM), transmission electron microscopy (TEM) and thermogravimentric analysis (TGA) were used to characterize the produced CNTs.

MWCNT were functionalized by different types of functional groups such as, carboxylic, dodecylamine, phenol and 1-octadecanol functional groups in order to enhance the dispersion of CNTs in styrene monomer solution during polymerization process. The non

functionalized MWCNTs and modified MWCNTs-Amine and MWCNT-COOH showed a clear reduction in the conversion of styrene monomer to polystyrene at high temperature (115 ^{O}C), which indicated that they could be good candidates as polymerization inhibitors by adding them to the styrene monomer solution. MWCNT-Amine was the best in polymerization inhibition.

Polystyrene (PS)/CNT nanocomposites were prepared by thermal bulk polymerization without any initiator at different loadings of CNT. The mechanical, thermal and rheological properties of the nanocomposites were studied. The tensile tests showed that the addition of 5 wt.% of CNT-COOH results in 68% increase in Young's modulus. The DSC measurements showed a decrease in glass transition temperature (T_g) of PS in the composites. The rheological studies at 190^{o}C showed that the addition of untreated CNTs increase the viscoelastic behavior of the PS matrix, while the functionalized CNT act as plasticizer at low loadings. Thermogravimetric analysis indicated that the incorporation of CNT into PS enhanced the thermal properties of the matrix polymer. A comparison between commercial short MWCNTs and long MWCNTs produced by O-CVD was carried out to evaluate the effect of increasing the aspect ratio on the mechanical properties of PS/CNT nanocomposites.

DOCTOR OF PHIOLOSOPHY DEGREE

KING FAHD UNIVERSITY OF PETROLEUM & MINERALS

DHAHRAN, SAUDI ARABIA

ملخص البحث

الإسم: عصام ظاهر عمرو

عنوان الرسالة: تصنيع أنابيب الكربون النانوية بواسطة مفاعل ترسيب البخار الكيميائي ذي الفوهة الضيقة وتطبيقاتها في بلمرة الستيرين و المركبات النانوية

التخصص: الهندسة الكيميائية

تاريخ التخرج: يناير ٢٠١١

تم تصميم وتصنيع جيل جديد من مفاعلات ترسيب البخار الكيميائي المحفزة محليا في قسم الهندسة الكيميائية، وقد اطلق عليه اسم مفاعل ترسيب البخار الكيميائي ذي الفوهة الضيقة، وذلك لانتاج أنابيب كربون نانوية متعددة الطبقات متراصة بشكل جيد وذات نسبة طولية عالية. تم تغيير عوامل التفاعل مثل درجة الحرارة والزمن وتدفق الهيدروجين وتدفق الهيدروكربون وقطر الفوهة وذلك لدراسة تأثيرها ولإيجاد العوامل الأمثل لإنتاج أنابيب الكربون النانوية متعددة الطبقات عالية الجودة وذات نسبة طولية مرتفعة. تم انتاج أنابيب الكربون النانوية متعددة الطبقات ذات نقاوة تصل إلى ٩٧،٦% وذات نسبة طولية مرتفعة (طولها ١ ملم تقريبا) عند تدفق هيدروجين مقداره ٢٤٠ مل/د، تدفق الأستيلين ١٥٥ مل/د، قطر الفوهة ٦ ملم، درجة حرارة التفاعل ٨٠٠ درجة مئوية وزمن التفاعل ٣٠ دقيقة. كان معدل الإنتاج ١،٩ جم/س وبتكلفة مقدارها ٦ دولارات للجرام فقط. تم توصيف أنابيب الكربون النانوية المنتجة باستخدام مجهر المسح الإلكتروني ومجهر النفاذ الإلكتروني والتحليل الحراري الوزني.

تم تعديل أنابيب الكربون النانوية بواسطة مجموعات وظيفية مختلفة مثل مجموعة الكاربوكسيل، ومجموعة الدوديسيل امين، ومجموعة الفينول، ومجموعة الأوكتاديكانول وذلك لتحسين انتشار أنابيب الكربون النانوية في محلول مونمر الستيرين خلال عملية البلمرة. أنابيب الكربون النانوية

الغير معدلة والمعدلة بواسطة مجموعة الأمين ومجموعة الكاربوكسيل أظهرت انخفاضا واضحا في نسبة تحول مونمر الستيرين إلى بوليستيرين على درجة حرارة ١١٥ درجة مئوية، مما يشير إلى أنها مرشحة لتكون مواد جيدة في منع البلمرة من خلال إضافتها إلى محلول مونمر الستيرين. وأفضلها في منع البلمرة كان أنابيب الكربون النانوية مع مجموعة الأمين.

تم تحضير مركبات نانوية من البوليستيرين/أنابيب الكربون النانوية بعملية البلمرة الحرارية الآنية بدون إضافة أي مادة محرضة على البلمرة وبإضافة نسب وزنية مختلفة من انابيب الكربون النانوية. تمت دراسات الخصائص الحرارية والميكانيكة والريولوجية للمركبات النانوية. أظهرت اختبارات الشد أن إضافة ٥% من أنابيب الكربون المعدلة بالكاربوكسيل أدت إلى زيادة في معامل يونغ بنسبة ٦٨%. أظهرت قياسات المسح المسعر التفاضلي إنخفاضا في درجة حرارة الإنتقال الزجاجي. الدراسات الريولوجية التي تمت على درجة حرارة ١٩٠ درجة مئوية أظهرت زيادة في لزوجة البوليستيرين عند إضافة انابيب الكربون الغير معدلة، بينما عملت انابيب الكربون المعدلة كملدنات عند إضافتها بنسب قليلة. التحليل الوزني الحراري أظهر أن إضافة انابيب الكربون النانوية للبوليستيرين حسنت الصفات الحرارية للبوليمر. وأخيرا تم عمل دراسة مقارنة بين أنابيب الكربون القصيرة وتلك الطويلة التي أنتجناها لمعرفة تأثير زيادة النسبة الطولية على الخصائص الميكانيكة لمركبات البوليستيرين النانوية.

درجة الدكتوراة في الفلسفة

جامعة الملك فهد للبترول والمعادن

الظهران ، المملكة العربية السعودية

CHAPTER ONE

INTRODUCTION

1.1 Background

Research on new materials technology is attracting the attention of researchers all over the world. Developments are being made to improve the properties of the materials and to find alternative precursors that can give desirable properties on the materials.

Nanotechnology, which is one of the new technologies, refers to the development of devices, structures, and systems whose size varies from 1 to 100 nanometers (nm). The last decade has seen advancement in every side of nanotechnology such as: nanoparticles and powders; nanolayers and coatings; electrical, optic and mechanical nanodevices; and nanostructured biological materials. Presently, nanotechnology is expected to be influential in the next 10-20 years, in all fields of science and technology.

Great interest has recently been developed in the area of nanostructures carbon materials. Carbon nanotubes have a wide variety of properties and features that are of interest in electronic, mechanical, optical and chemical applications [1,2]. Carbon nanotubes have been formed using an arc discharge method, laser vaporization and through catalytic chemical vapor deposition of hydrocarbons [2,3]. CCVD method has a number of potential advantages over the arc discharge and laser vaporization methods. In particular, CCVD is more amenable to scale-up than arc discharge or laser vaporization, and many successful processes for the large-scale catalytic synthesis of both SWCNTs and MWCNTs have been developed [4]. Catalytic techniques also enable nanotube synthesis to be achieved under relatively mild conditions, giving more control over the growth process. Beside the seeking for large-scale production of CNT, the good quality for the CNT is also needed. Increasing the aspect ratio (length/diameter) of the CNT results in improving the mechanical properties of CNT/Polymer nanocomposites [5,6].

There is an increasing international requirement of polystyrene materials all over the world. As known, polystyrene is glassy elastic material. For this reason, improving on physical and mechanical properties of the PS for many applications are needed.

The present study aims to design new type of CVD for production of high purity and high aspect ratio carbon nanotubes, which can be used in PS nanocomposite application.

1.2 Scope of The Study

Design and fabrication of modified chemical vapor deposition reactor to produce multiwall carbon nanotubes with better properties than those produced by conventional chemical vapor deposition reactors. The modification is to introduce an orifice with different sizes at the beginning of reaction zone. This modification is expected to result in carbon nanotubes with higher aspect ratio and higher purity. The produced CNTs are to be characterized and used in polymerization of styrene to study their effects on the polymerization process and the mechanical properties of polystyrene.

1.3 Objectives

1. To design and fabricate dual furnaces orifice-chemical vapor deposition (O-CVD) reactor to produce multiwall carbon nanotubes (MWCNTs).
2. To control the morphology of carbon nanotubes by optimizing the production condition like reaction temperature, hydrogen and acetylene flow rates, gas residence time, reaction time and diameter of the orifice.
3. To study the effect of CNTs and modified CNTs on the polymerization process of styrene.
4. To study the effect of CNTs and modified CNTs on the mechanical, rheological and thermal properties of polystyrene/CNT nanocompoites.

1.4 Methodology

1.4.1 Production of Carbon Nanotubes

a. Fabrication of Orifice Chemical Vapor Deposition Reactor (O-CVD) which consists of ceramic tube passes two consecutive furnaces. The first one is used to evaporate the ferrocene catalyst, at 120^{o}C, which carried by the inlet gases

into the second furnace. The second furnace is the reaction zone where the carbon nanotubes are formed. We place an orifice at the beginning of the reaction zone to study its effect on the purity, quality, aspect ratio and alignment of CNTs.

b. The reaction parameters will be varied to study their effect and to find the optimum conditions, as follows;
    i. Hydrogen flowrate: (40-540 ml/min)
    ii. Acetelyn flowrate: (15-155 ml/min)
    iii. Reaction temperature: 600, 700, 800, 900 and 1000^{o}C.
    iv. Reaction time: 15, 30, 60 and 120 minutes.
    v. Orifice diameter: 3, 6 and 12 mm.
    vi. Weight and type of catalyst will be fixed for all runs; 100 mg of ferreocene catalyst.
c. The Produced CNTs will be characterized using SEM and TEM.
d. The optimum conditions for producing highest quality and quantity of CNTs will be chosen to produce large amount of CNTs to be used in CNT/PS nanocmposite and styrene polymerization.

1.4.2 Styrene Polymerization

a. Styrene polymerization will carried out in special reactor which is purged with inert gas to remove any oxygen from the reactor. The polymerization process will be carried out under constant temperature and different dosages of normal and modified CNTs as follows:
    i. Temperature: 115^{o}C
    ii. CNTs dosage: 0.1, 0.5 and 1% of weight.
    iii. Modification of CNTs will be done with the following functional groups: COOH, Amine, C18 and Phenol.
b. To study the effect of CNT on the rate of polymerization a sample will be taken at constant time intervals and the monomer conversion will be determined.
c. The mechanical properties of PS/CNT composites will be studied by standard tensile tests, in order to evaluate the effect of the nano additives on the mechanical properties of polystyrene. Also the rheological and thermal properties are studied.

CHAPTER TWO

LITERATURE REVIEW

2.1 History of Carbon Nanotube (CNT)

In 1991, Iijima discovered thin and long carbon straw having the form of nanotubes during the TEM analysis of carbonaceous groups synthesized by an arc discharge method [7]. This carbon nanotube (CNTs) was varied in length from several nanometers to several micrometers, and had an external diameter approximately from 2.5 nm up to 30 nm. In 1992, Ebbesen and Ajayan observed that the increment of pressure in the chambers of an arc exceptionally improved the carbon nanotube yield at the cathode of the graphite [8]. In 1993, Bethune has synthesized carbon nanotubes with diameters about one nm, using methods of arc discharge [9]. In 1996, Smalley and his group [10] reported a method of preparation of the only single walled nanotubes with unusually homogeneous diameters by laser vaporizing of graphite. These tubes had a tendency to form aligned bundles, and they drove Smalley to baptize the bundles ' rope '. Using chemical vapor deposition (CVD) Yacamán et al., (1993) have made large achievement in synthesis and the application

of carbon nanotubes [11]. Since then, the investigations in synthesis and application have been energetically led in the entire world. Figure 2.1 shows the images of the different materials related to carbon.

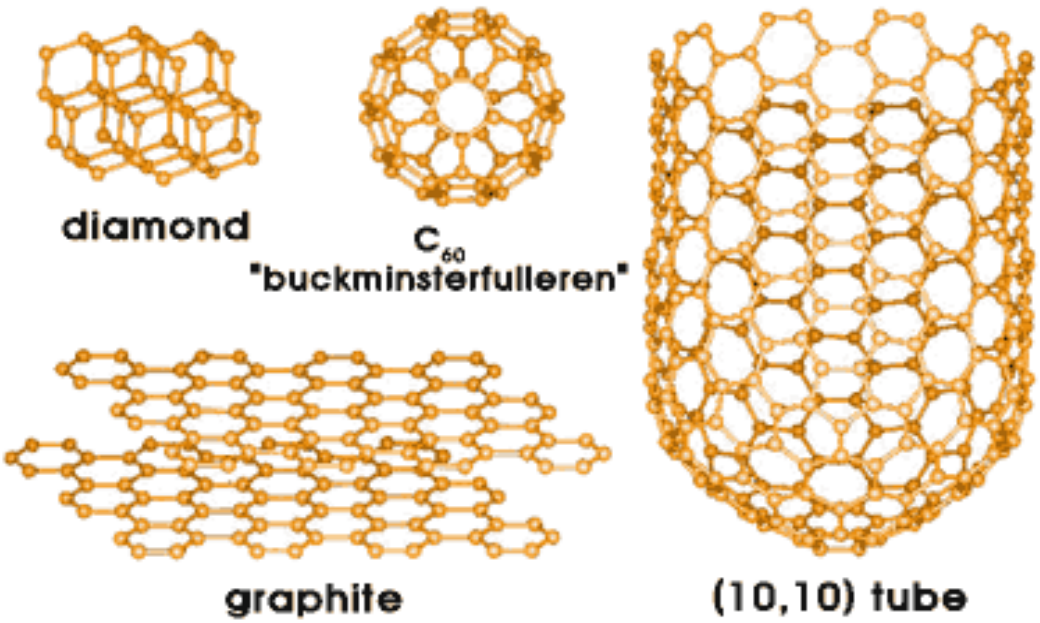

Figure 2.1: Carbon related materials [12].

2.2 Properties of Carbon Nanotubes

A single wall carbon nanotube (SWCNT) has three different structures: chiral; zigzag; and armchair. SWCNT can be either metallic or semiconducting, according to their chirality's vector (n, m), where n and m are two integers. A metallic nanotube is found when the difference n-m is a multiple of three. If the difference is not a multiple of three, a semiconducting nanotube will be formed. Besides, it is also possible to connect nanotubes with different chiralities creating nanotube heterojunctions, which can shape a variety of nanoscale molecular electronic device components [12].

Single and multi-wall nanotubes have very good elasto-mechanical properties. These structural and materials characteristics of nanotubes point towards their possible use in making next generation of extremely lightweight with highly elastic and very strong composite materials.

Nanotubes have high aspect-ratio structures with good electrical and mechanical properties. Consequently, the applications of nanotubes in field-emission displays, and scanning probe microscopic tips for metrology have started to materialize in the commercial sector.

2.2.1 Electronic Properties

Carbon nanotubes have some different electrical properties. One of the important properties of CNT is that it can exhibit the characteristics of a metal or a semiconductor. Depending on their chiral vector, carbon nanotubes with a small diameter are either semi-conducting or metallic. Electronic structure usually characterized using scanning tunneling microscopy [13]. One possible use of the CNTs is as a diode.

One can view carbon nanotubes as giant conjugated molecular wires with a conjugation length corresponding to the whole length of the tube [14, 15]. The differences in conducting properties are caused by the molecular structure that results in a different band structure and thus a different band gap. The differences in conductivity can easily be derived from the graphene sheet properties. It was shown that a (n,m) nanotube is metallic as accounts that: n=m or (n-m) = 3i, where i is an integer and n and m are defining the nanotube. The resistance to conduction is determined by quantum mechanical aspects and was proved independent of the nanotube length [15].

2.2.2 Mechanical Properties

The basal-plane elastic modulus of graphite is one of the largest of any known material. CNTs are the strongest fibers that are currently known. The reason for that, the carbon atoms form a planar honeycomb lattice in which each atom is connected

via a strong chemical bond to three neighbor atoms. Therefore, these compounds are potentially suitable for applications in composite materials that need anisotropic properties. Carbon nanotubes have a very large Young Modulus in their axial direction. The Young Modulus of SWCNT is up to 1TPa, which is 5 times greater than steel (230 GPa) while the density is only 1.3 g/cm^3 [16]. Some of the experimentally estimated that the tensile stress at fracture in the CNT was ~ 55 GPa, based on polymer-NT specimens and if the stress is transferred to the CNTs via the interface shear mechanism [17]. Wagner et al. directly measured the tensile strength of MWCNTs made by CVD by pulling on very long (~2 mm) ropes with a tensile tester [18]. They found the tensile strength of 1.72 ± 0.64 GPa. The tubes had an ID and OD of 12 and 30 nm, respectively, and spacing of about 100 nm between the tubes. To account for this spacing, they use the effective cross sectional area. They treat the CNTs (because isolated) as parallel resistors of conductance 1/R by measuring this value; they estimate the rate at which the tubes break. They measured the tensile strength of the ropes to be an order of magnitude lower than that of graphite whiskers.

Table 2.1 is showing some of the properties of CNTs.

Table 2.1: Typical properties of CNTs [19].

Property	**SWCNT**	**MWCNT**
Tensile strength (GPa)	50–500	10–60
Elastic modulus (TPa)	~1	0.3–1
Density (g/cm3)	1.3–1.5	1.8–2.0
Electrical conductivity (S/m)	$\sim 10^6$	$\sim 10^6$
Thermal stability	>600 ◦C (in air)	>600 ◦C (in air)
Typical diameter	1 nm	~20 nm

2.3 Production Methods of Carbon Nanotubes

Different types of carbon nanotubes, carbon nanofibers, carbon fiber and other types of carbon nanostructure materials can be produced in various ways. In this section, different techniques for nanotube, nanofibers synthesis and their status are briefly described. The most common techniques used nowadays are: arc discharge, laser ablation, and chemical vapour deposition. Economically feasible large-scale production and purification techniques still have to be developed.

2.3.1 Arc Discharge

The carbon arc supplies easy and traditional tools to generate the high temperature necessary for the evaporation of carbon atoms in plasma. Arc-discharge is a method, which was usually used in the synthesis of the carbon nanotubes in the early stage; and it was accidentally discovered by Sumio Iijima (1991). Iijima has observed the structures of the CNTs for the first time during the production of fullerenes using arc-discharge method [7].

To produce nanotubes, this method encloses two carbon electrodes at a distance of 1 mm apart. The electrodes are enclosed in an inert environment using Argon gas, and then DC voltage is applied between the two electrodes [7, 8, 20, 21, 22]. The generated current creates plasma between the two electrodes and vaporizes

carbon. The vaporized carbon from one electrode deposits into pillar-like tubes onto the opposite electrode, hence creating nanotubes.

The electric arc vaporizes a hollow graphite anode packed with a mixture of a transition metal (such as Fe, Co or Ni) and graphite powder. The inert gas flow is maintained at 50-600 Torr. Nominal conditions involve 2000-3000 °C, 100 amps and 20 volts [7, 20]. The gas pressure, flow rate, and metal concentration can be varied to change the yield of nanotubes, but these parameters do not seem to change the diameter distribution.

The Nanotubes created using this method are usually short tubes with diameters ranging from 0.6 to 1.4 nm for single walled and 10 nm diameter multi-walled nanotubes. This method is relatively easy to implement, and will produce yields of 30%. The nanotubes produced contain more impurities compared to other methods, and the consistency of the shape, wall, and lengths of the tubes are somewhat random [12, 21].

Figure 2.2 shows a schematic diagram of arc-discharge apparatus for the synthesis of carbon nanotubes. This apparatus must be connected to a vacuum line with a diffusion pump and a helium supply. The electrodes are two graphite rods, usually of high purity. Typically, the anode is a long rod of 6 mm diameter and the cathode is a 9 mm diameter rod. Efficient cooling of the cathode has been shown to be essential in producing good quality nanotubes [22].

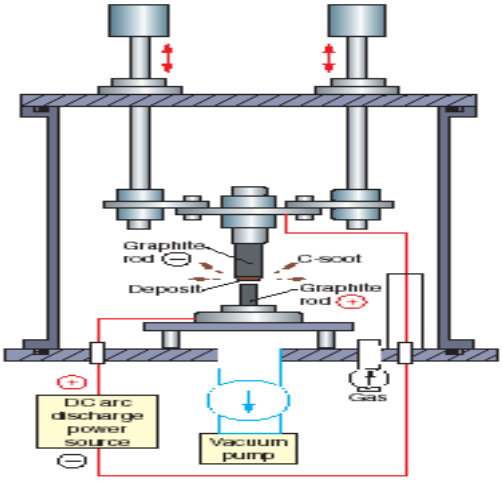

Figure 2.2: Arc-discharge apparatus [12].

2.3.2 Laser Ablation

Pulsed Laser Vaporization, or Laser Ablation, is a newer method currently being developed to create nanotubes. Similar to the carbon Arc-Discharge method, this method vaporizes the carbon and later deposits it onto a substrate. In 1996, Smalley's group [10] at Rice University reported the synthesis of carbon nanotubes by laser vaporization. The laser vaporisation apparatus used by Smalley's group is shown in Figure 2.3. In laser ablation, a target consisting of graphite mixed with a small amount of transition metal particles as catalyst is placed at the end of a quartz

tube enclosed in a furnace. As the vaporised species cool, small carbon molecules and atoms quickly condense to form larger clusters, possibly including fullerenes. The target is exposed to an argon ion laser beam, which vaporizes graphite and nucleates carbon nanotubes in the shockwave just in front of the target. Argon flow through the reactor heated to about 1200 °C by the furnace carries the vapor and nucleated nanotubes, which continue to grow. The nanotubes are deposited on the cooler walls of the quartz tube downstream from the furnace.

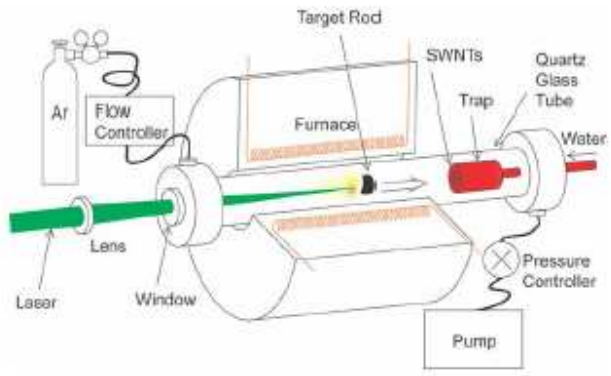

Figure 2.3: Laser ablation apparatus [12].

The condensates obtained by laser ablation are contaminated with carbon nanotubes and carbon nanoparticles. Laser vaporisation results in a higher yield for SWCNT synthesis and the nanotubes have better properties and a narrower size distribution than SWNTs produced by arc-discharge [10].

Nanotubes produced by laser ablation are about 90 % pure, better than those produced using the arc discharge process. The Ni/Y mixture catalyst (Ni/Y is 4.2/1) gave the best yield [23].

2.3.3 Chemical Vapor Deposition (CVD)

Chemical vapor deposition (CVD) is a versatile process suitable for the manufacturing of coatings, powders, fibers, and monolithic components. With CVD, it is possible to produce most metals, many nonmetallic elements such as carbon and silicon as well as a large number of compounds including carbides, nitrides, oxides, intermetallics, and many others. This technology is now an essential factor in the manufacture of semiconductors and other electronic components, in the coating of tools, bearings, and other wear-resistant parts and in many optical, optoelectronic and corrosion applications.

Chemical vapor deposition may be defined as the deposition of a solid on a heated surface from a chemical reaction in the vapor phase. It belongs to the class of vapor-transfer processes, which is atomistic in nature that is the deposition species are

atoms or molecules or a combination of these [24].

In the CVD-method different hydrocarbons such as benzene (C_6H_6), pentane (C_5H_{12}), acetylene (C_2H_2), methane (CH_4) and carbon monoxide is decomposed over different metals (Fe, Co, Ni) at temperatures between 500 and 1200°C. This method was used for a long time for the synthesis of carbon fibers [25] and nanofiber [26, 27], but there were no indications that it could also be used for the synthesis of carbon nanotubes until Yacamán et al. [11] reported this method the first time for the production of nanotubes.

The CVD method deposits hydrocarbon molecules on top of heated catalyst material. Metal catalysts dissociate the hydrocarbon molecules. Figure 2.4 shows the apparatus of the CVD process. The CVD method produces both single-wall and multi-wall nanotubes. The CVD process uses hydrocarbons as the carbon source. Hydrocarbons flow through the quartz tube where it is heated at a high temperature [28]. The energy source is used to “crack” the molecule into reactive atomic carbon. Then, the carbon diffuses towards the substrate, which is heated and coated with a catalyst (usually a first row transition metal such as Ni, Fe or Co) where it will bind. Carbon nanotubes will be formed if the proper parameters are maintained. Excellent alignment, as well as positional control on nanometer scale, can be achieved by using CVD. Control over the diameter, as well as the growth rate of the nanotubes can also be maintained [29, 30]. The appropriate metal catalyst can preferentially grow single rather than multi-walled nanotubes.

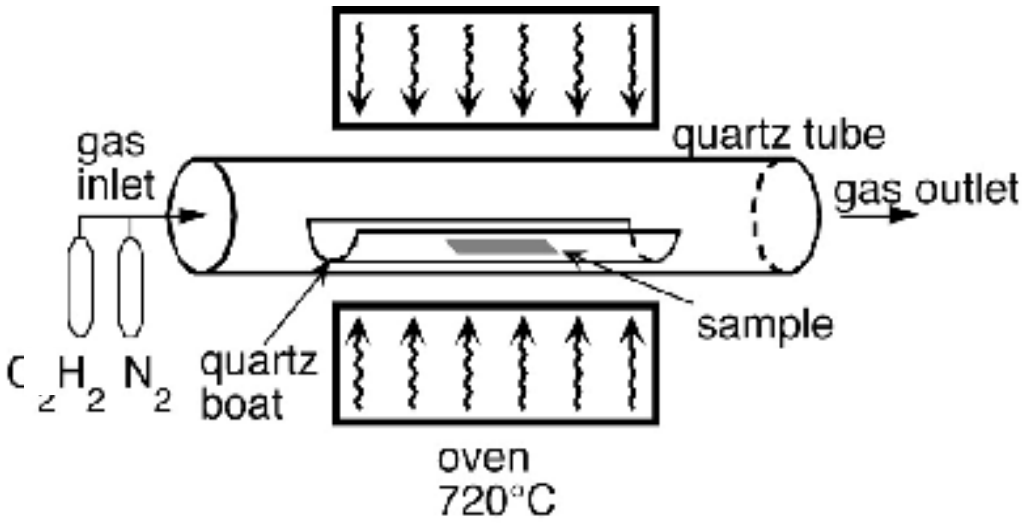

Figure 2.4: CVD deposition oven [12].

2.3.3.1 Different CVD Techniques:

Different techniques for the carbon nanotubes synthesis with CVD have been developed, such as: i) vapor phase growth CVD; ii) substrate catalyst CVD; iii) plasma enhanced CVD; iii) fluidized-bed CVD. These different techniques are explained in more detail as follows [12]:

i) Vapour Phase Growth

Vapour phase growth is one of the synthesis methods which have been used to produce carbon nanotubes [11, 31, 32, 33], carbon nanofiber [27] and vapor grown carbon fiber [25, 34] directly by supplying reaction gas and catalytic metal in the chamber without a substrate, this method also called floating catalyst chemical vapor deposition . The catalyst is introduced in the flowing gas stream e.g. in form of volatile organometallic molecules like ferrocene and nickelocene. This method has been suggested as a good method for mass production of carbon nanostructure materials and fiber.

Figure 2.5 shows a schematic diagram of a vapour phase growth apparatus. The flow controller for the gas flow rate is placed in one corner and a ceramic boat for catalytic metal powder in the chamber. Two furnaces are placed in the reaction chamber. In the first furnace, vaporization of catalytic carbon is maintained at a relatively low temperature while higher temperature is maintained in the second furnace where the synthesis occurs. The hydrocarbon gas in the first furnace will not decomposed, while the low temperature at this furnace will be supplied to vaporize the catalysis. During the vaporization of the catalyst fine catalytic particles will form. When this particle reaches the second furnace, the decomposed carbons are absorbed and diffused on the surface of the catalytic metal particles [35, 36].

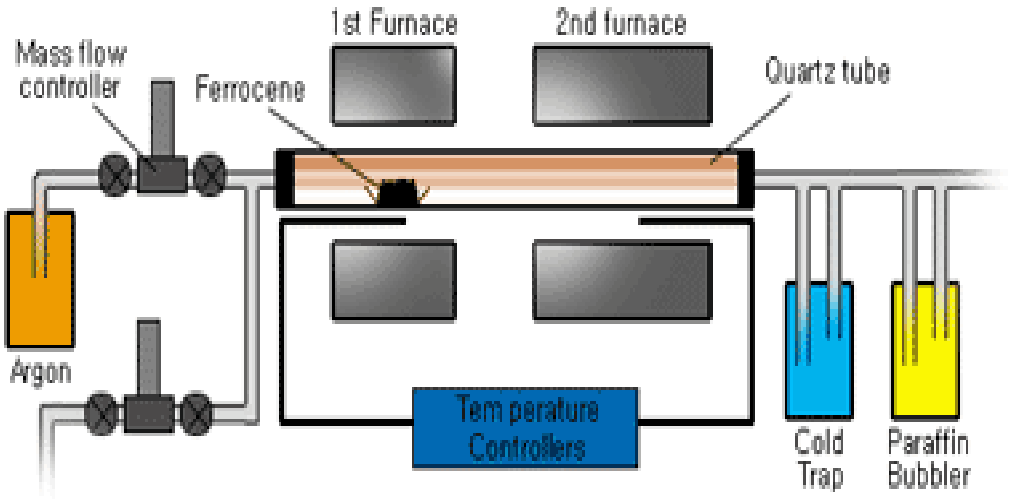

Figure 2.5: Vapor phase growth apparatus [12].

Liu et al. [37] simultaneously synthesized single-walled carbon nanotubes (SWNTs) and double-walled carbon nanotubes (DWNTs) by catalytic decomposition of CH_4 over Fe–Mo/Al_2O_3 catalyst. High-resolution transmission electron microscopy observation shows that produced carbon materials consist of about 70% SWNTs and about 30% DWNTs. The diameters of SWNTs are in the range of 0.8–1.5 nm while the outer and inner diameters of DWNTs are in the range of 1.75–3.1 and 0.95–2.3 nm, respectively. Raman analysis indicates that the synthesized SWNTs and DWNTs have high-quality graphite structure.

Tatsuki et al. [38] have synthesized double-wall carbon nanotubes (DWNTs) in high-yield (>80%) by catalytic chemical vapor deposition (CCVD) of acetylene over well dispersed metal particles (typically Co/Fe binary system) embedded in heat resistant zeolites at temperatures above 900 °C. The synthetic yield of DWNTs has been sensitively affected by reaction conditions of the CCVD such as zeolite support materials, the sintering of the metal particles, hydrocarbon sources and reaction temperatures. High-resolution transmission electron microscopy together with Raman spectroscopy shows that the outer tube diameter varies from 3 to 6 nm with inner–outer tube separations of 0.36–0.37 nm, which is much larger than the interlayer distance of graphite (0.335 nm).

Jieshan et al. [39] were successfully synthesized SWNTs from coal gas with ferrocene as catalyst by catalytic chemical vapor deposition. The results lead one to believe that coal gas is an ideal carbon-containing precursor for preparing SWCNTs. This new approach to SWCNTs should be of potential in the production of carbon nanotubes in large scale. More work is needed to further establish the influence of process parameters on the formation, yield and quality of the SWCNTs, and to clarify the possible synergic effects of gaseous species in the coal gas.

Yoichi et al. [40] were synthesized high purity single-walled carbon nanotubes (SWCNTs) from ethanol by catalytic CVD method. The yield of SWCNTs was determined based on TGA complemented by Raman and TEM analyses. The

effects of CVD reaction time and pre-reduction of catalytic metal on the yield and quality of synthesized SWNTs were investigated. The SWCNT yield of more than 40% was achieved over the weight of zeolite support powder with Fe/Co catalyst, which corresponded to more than 800% yield over the weight of the catalytic metal, within the CVD reaction time of 120 min assuring as-grown high quality.

Kobayashi et al. [41] investigated single-walled carbon nanotube (SWCNT) growth using a novel Fe_3O_4 nanoparticle catalyst synthesized with a simple organic chemistry process. They characterized the structure of the grown SWNTs through scanning electron microscopy (SEM), atomic force microscopy (AFM) and microscopic Raman spectroscopy. Discrete nanoparticles with a uniform diameter of ~4 nm could be deposited on Si substrates with a thermal oxide layer by spin coating with a nanoparticle solution. Nanoparticles prepared under optimum conditions remained discrete and uniform without aggregation even after chemical vapor deposition (CVD) process and their diameters were reduced to ~1.7 nm due to decomposition reactions during CVD. These nanoparticles were found to have remarkable catalytic activity in the CVD growth of the SWCNTs. SWCNTs with diameters of around 1 nm were produced from the reduced nanoparticle catalyst. The diameters of the grown SWCNTs were closely correlated with those of the catalytic nanoparticles and tended to be slightly smaller than the particle size.

Flahaut et al. [42] have reported the influence of catalyst preparation conditions for the synthesis of carbon nanotubes (CNTs) by catalytic chemical vapor deposition (CCVD). Catalysts were prepared by the combustion route using either urea or citric acid as the fuel. They found that the milder combustion conditions obtained in the case of citric acid can either limit the formation of carbon nanofibers (defined as carbon structures not composed of perfectly co-axial walls or only partially tubular) or increase the selectivity of the CCVD synthesis towards CNTs with fewer walls, depending on the catalyst composition. It is thus for example possible in the same CCVD conditions to prepare (with a catalyst of identical chemical composition) either a sample containing more than 90% double- and triple-walled CNTs, or a sample containing almost 80% double-walled CNTs.

Kim et al. [43] described synthesis of very unusual multi-walled carbon nanotubes through a catalytic chemical vapor deposition method using a floating reactant method and subsequent thermal treatment up to 2600 °C in a large quantity. Main characteristics of these nanotubes are (1) relatively wide distribution of diameters ranging from 20 to 70 nm and linear, long macro-morphology (aspect ratio >100), (2) highly straight and crystalline layers, (3) high purity through removal of metallic impurity, (4) very low interlayer spacing (0.3385 nm) and low R value (I_D/I_G = 0.0717), (5) high G' intensity over intensity of G band (G'/G = 0.85) and strongly negative magnetoresistance value of -1.08% at 77 K and 1 T. The unusual microstructure of thin multi-walled carbon nanotubes with a partially facetted cross-

sectional shape caused by thermal treatment is mainly ascribed to abrupt density changes (from 1.89 to 2.1 g/cm^3) within a confined nanosized space, accompanying with the phase separation.

Pinault et al. [44] have reported a study of the initial stages of growth of aligned multiwalled carbon nanotubes (MWCNT) synthesised by catalytic chemical vapour deposition (CCVD) of liquid aerosol obtained from toluene/ferrocene solution. A special experimental procedure has been developed to stop the process after short durations (30 s to 2 min). Two different pyrolysis temperatures are considered: 800 and 850 ºC. Both scanning and transmission electron microscopy (SEM, TEM) coupled to energy-dispersive X-ray (EDX) analyses are used in order to determine the location of catalyst particles and to examine their chemical nature, morphology and size distribution when nanotubes start to grow. During the early stages (30s), they observe the formation of a layer of catalyst particles on silicon substrates before the growth of nanotubes. X-ray diffraction (XRD) and X-ray photoelectron spectroscopy (XPS) measurements indicate the occurrence of iron oxide (C-Fe_2O_3 or Fe_3O_4). In addition, XPS analysis reveals the formation of graphite-like carbon, demonstrating that iron oxide particles catalyst the decomposition of toluene vapour. SEM and TEM observations show that these particles are most often located at the nanotube root, suggesting a base growth mechanism responsible for the formation of aligned nanotube when prolonging growth time (2 min).

ii) CVD Method using Substrate Catalyst

In this method substrate like silicon (Si), Silicon dioxide (SiO_2), and aluminum were used to deposit different types of catalysts such as Fe, Ni, Co on the substrate. After the substrate was washed with distilled water and diluted HF solution, the substrate was placed in a ceramic boat. The ceramic boat was positioned in the center of the CVD furnace (as shown in Figure 2.6). Very thin film of catalyst was deposited over the substrate catalyst when the catalyst was injected with hydrocarbon source into the chamber of the furnace tube. During the injection of the hydrocarbon with catalyst precursor, the organic catalyst was decompose into fine cluster catalyst and deposited over the substrate. Another method to deposit the catalyst was using sputtering machine in which the catalyst was prepared by sputtering a transition metal onto a substrate and then using either a chemical etching or thermal annealing to induce catalyst particle nucleation. The thickness of the transition metal layer before the annealing step ranges from 1-200 nanometers. The diameter range of the carbon nanotubes depends on the thickness of the catalytic film [45, 46].

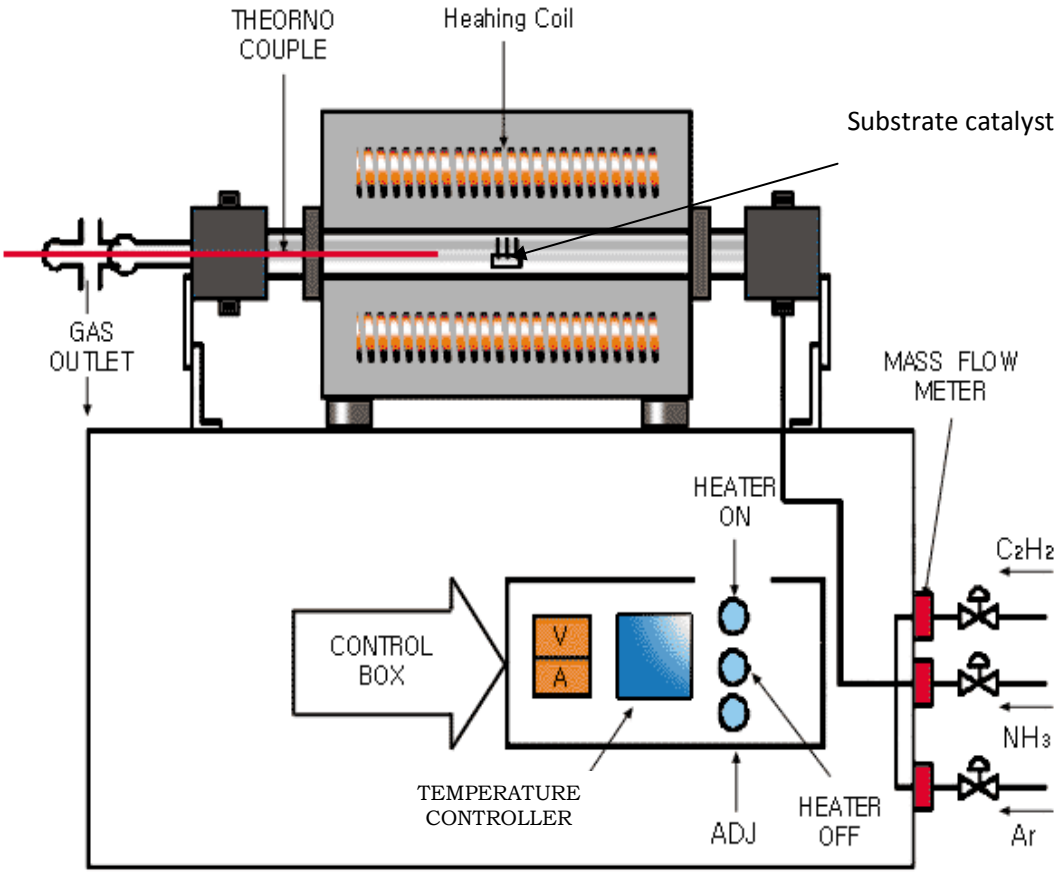

Figure 2.6: Thermal CVD apparatus [12].

.

Bei and Ping [47] have studied the effect of thickness ratio of Ni:Cr on the density and alignment of CNTs synthesized by CVD. Changing the layer thickness ratio of Ni:Cr can change the density and alignment of CNTs dramatically. It is found the density and alignment can be controlled by adjusting the thickness ratio of Ni:Cr. Meanwhile, the catalyst encapsulated in the CNT was confirmed to be Ni by EDX and HRTEM measurement. They have concluded that only Ni has catalysis and Cr acts as dispersant in these experiments. Thus, their investigations are significant in providing a better understanding of the acting of catalyst and the controlling of the desirable density and alignment of CNTs for various applications.

iii) Plasma Enhanced Chemical Vapour Deposition (PE-CVD)

In PE-CVD method, carbon nanotube grows over the substrate catalyst, which is coated with catalyst, located inside plasma. In this method, usually the source of the plasma is RF- (radio frequency), MW- (microwave) or a DC-plasma (direct current). The plasma enhanced CVD method generates a glow discharge in a chamber or a reaction furnace by a high frequency voltage applied to both electrodes. Figure 2.7 shows a schematic diagram of typical plasma CVD apparatus with a parallel plate electrode structure [12].

.

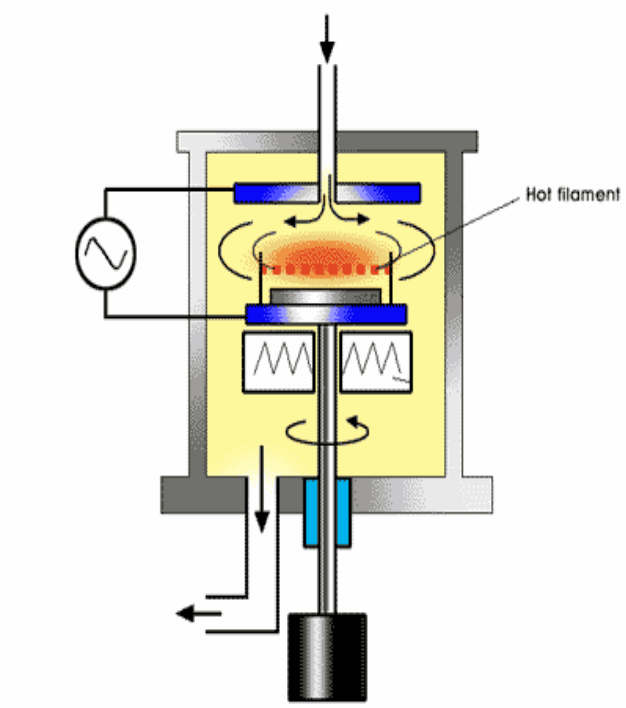

Figure 2.7: Plasma Enhanced CVD apparatus [12].

Often a methane (CH_4) and hydrogen (H_2) gas mixture with a ratio of 1% CH_4 to 99% H_2 is used at a total pressure between 1 to 40 mbar and a temperature of 900 °C.

iv) Fluidized-Bed CVD Method [3]

In the FBCVD process, the CVD reaction occurs within a fluidized bed of catalyst particles. Freestanding CNTs required in applications such as composite materials and energy-storage devices can be produced cost effectively with this technique; and clearly, cost is a key factor that underpins successful large scale processes. An illustration of a typical fluidized-bed system is given in Figure 2.8. The setup consists of a cylindrical reactor affixed within a high-temperature furnace, with a control and data-logging system. Environmental impact mitigation systems, e.g., off-gas scrubbers and cyclones, are also employed.

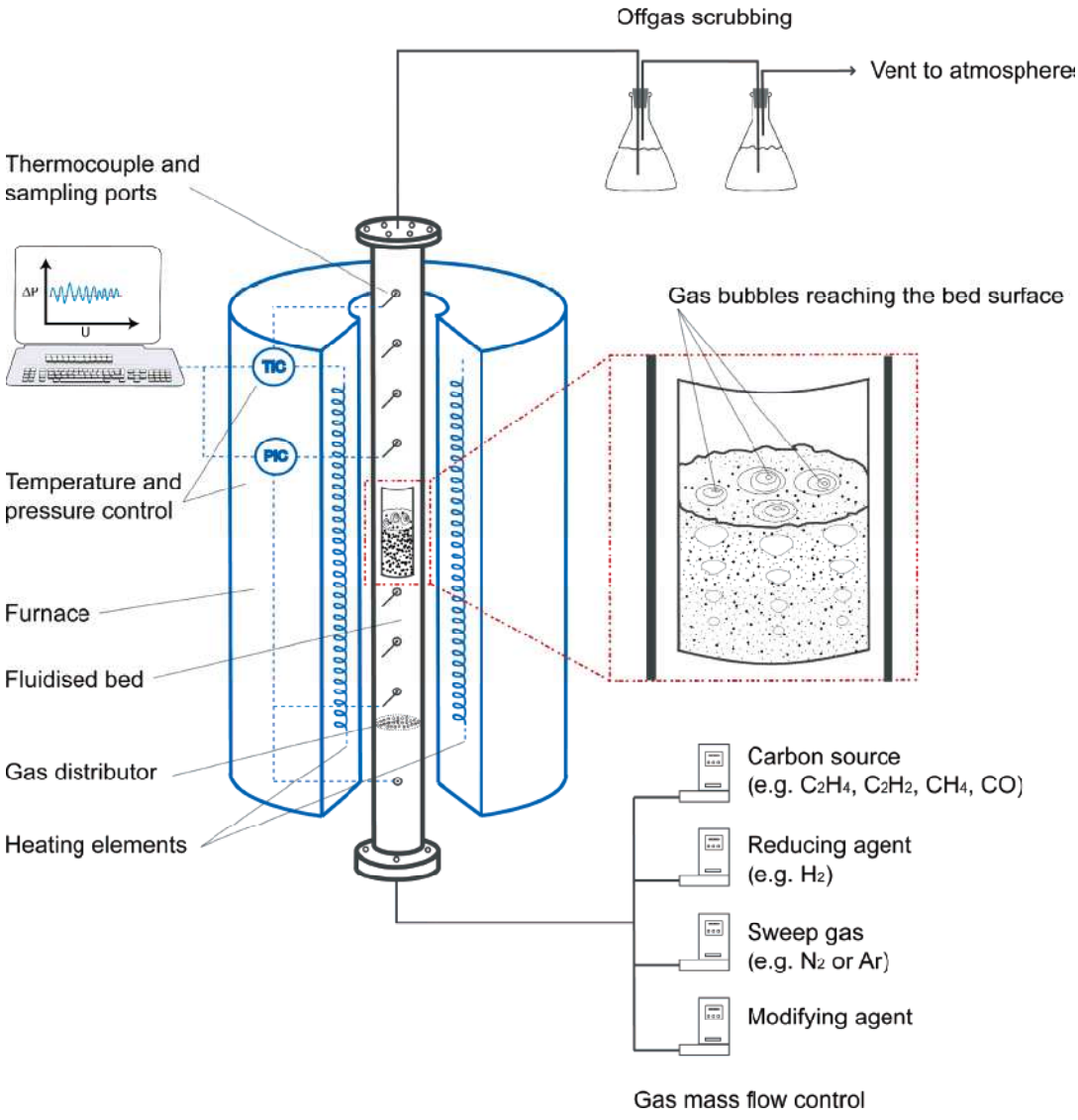

Figure 2.8: Sketch of a typical fluidized-bed reactor setup [3].

2.3.3.2 CVD Parameters:

Produced CNTs features, including dimensions, wall number, chirality and graphitization are determined by the growth mechanism and process conditions. Therefore, parametric factors which affect the CCVD should be well considered in order to synthesize the desired clean CNTs. According to the literatures, the key parameters which are discussed in following sections include temperature, catalyst, carbon feedstock and other parameters [48].

i) Temperature: [48]

CNTs morphology dependence on the temperature is one of the most popular topics under investigation [48]. Muataz et al. [49] studied the role of reaction temperature in CNTs synthesis by floating catalyst method, in which benzene and ferrocene were utilized as carbon precursor and catalyst, respectively. They pointed out that MWCNTs synthesis occurs at temperatures greater than 500 ◦C and maximum wall numbers with less impurity is obtained at 850 ◦C. The higher the reaction temperature the more pronounced is the formation of non-tubular carbon like nanofibers. They also revealed that there is a positive correlation between the average diameter and the length of CNTs and temperature. As a result, they proposed that temperature is a dominating factor for CNT diameter control. The main effects of increasing the reaction temperature are to increase the metal particle size during the CVD growth of CNTs, and consequently the nanotube diameter. However there are

some inconsistencies about the exact effect of the temperature on CNTs growth mechanism. Kim et al. [50] failed to observe any significant effects of temperature on average diameter of MWCNTs but observed that elevating the temperature had increased the length aswell as the crystallinity of the nanotubes. Son et al. [51] concluded that the CNT diameters synthesized from methane in fluidized bed decreases as the reaction temperature increases. Nevertheless, the effect of temperature was evident on the growth rate, purity and the crystallinity of CNTs in all mentioned studies [48].

There is a great paradox of CNTs synthesis where even though the higher growth temperature is favored for less defective, wellcrystallized nanotube, including such parameters of interest such as yield and purity, but a too high temperature is not suitable due to some disadvantages like deformation of catalyst, sintering of the supported catalysts, formation of alloy in bimetallic catalyst and the formation of pyrolytic amorphous carbon [48]. Although in a few rare cases, CNTs were produced at temperatures higher than 1000 ◦C, but most reported that the CVD products are in non-tubular form of carbon at these temperatures [48]. It can be attributed to the fact that not only pyrolysis of carbon sources is generally promoted around 1000 ◦C, but also pyrolysis of the CNTs will begin. Other effects of the reaction temperature are related to the diameter distribution and chirality issue especially in SWCNTs synthesis [48].

ii) Catalyst: [48]

Catalysts play a crucial role in the CCVD synthesis of CNTs and therefore improving the desired characteristics of catalyst will enhance the obtained CNTs quality as well as the process yield. Materials with capability of decomposing hydrocarbon and CNTs formation are employed as catalyst in CCVD processes. However, it has been found that only the hydrocarbon molecules' decomposing ability of catalyst could not be accounted for CNT formation [48]. These results emphasize that careful selection of the catalyst is a dominating factor in CCVD synthesis of CNTs. Transition metals in the form of nanoparticles are considered as the most effective catalysts. The peculiar ability of transition metals to promote CNT growth is strongly related to these factors: (a) catalytic activity for decomposition of volatile carbon compounds, (b) ability of metastable carbides formation, and (c) diffusion of carbon through and over the metallic particles [48]. The CCVD process for CNTs growth utilizes heterogeneous catalysts, which are the catalytically active metal particles, typically with diameter of 1–10 nm, anchored on a high surface inert area [48].

Iron (Fe), cobalt (Co), and nickel (Ni) have been enumerated as the most effective catalysts for CNTs growth. However, the challenge is that which metal is more active and provide better quality CNTs. An alloy of two transition metals with each other or with other non-transition metals can dramatically improves the catalyst performance in terms of CNT quality and lowering the reaction temperature [48].

Although catalyst selection and preparation is the most significant factor in CNTs synthesis, there are a number of mechanisms that can lead to catalyst deactivation, and hence loss of reactor performance. These mechanisms are poisoning, fouling and sintering of the catalyst due to elevated temperature or long reaction time. Phase change in catalyst support also sometimes occurs due to the high temperature and this can lead to a surface area reduction, and therefore reducing the reaction rate on account of impact on the access to active sites. Consequently other process parameters effects on CNTs synthesis should be taken into account.

iii) Carbon Feedstock:

Numerous carbon sources have been used for CNT synthesis, including carbon black [52], and fullerenes [53], used in arc-discharge and laser-ablation techniques; and carbon monoxide [54], methane [55], ethylene [56], acetylene [57], benzene [58], camphor [59], methanol [60], and ethanol [61], used in CVD processes. Mixtures of carbon sources have also been used to increase the yield of CNTs. In the HiPCO process, it was observed that the yield of CNTs increased by 25% with the addition of a small percentage (0.7%) of methane to carbon monoxide because of the increase in carbon availability. However, the “optimum” yield and type of CNTs produced for each carbon source is highly dependent upon the associated temperature, pressure, co- reactant species, and choice of catalyst metal [62]. The exact relationship between these variables remains unclear.

Li et al. [63] found that the chemical structure of hydrocarbons, i.e., straight-chained, ring, or benzene-like structures, was significantly more influential than the thermodynamic properties (e.g., enthalpy) of the carbon source on the type of CNTs formed. Li and co-workers observed that methane and aromatic molecules favor the formation of SWNTs. In a similar study, Hernadi et al. [64] suggested that C_6 units could not incorporate directly into the CNT structure, leading to lower carbon deposit yields. They also observed that CNT morphology was independent of the carbon feedstock when the same catalyst was used, a result supported by Qian et al. [65] The decomposition temperature of each feedstock places an additional constraint on the range of possible operating temperatures, e.g., methane is relatively more stable than acetylene at 900 °C. Nonetheless, acetylene has been used in experiments above 900 °C to produce CNTs with little amorphous carbon formation [66, 67]. Once again, the exact relationship between these variables is unclear, suggesting that further research is necessary.

A summary of the three well established techniques for producing CNTs is given in table 2.2.

Table 2.2: Comparison between arc discharge, laser ablation and CVD techniques used for producing CNTs [3, 4].

Method	Arc Discharge	Laser Ablation	CVD
Description	Arc evaporation of graphite in the presence of inert gas; CNT formed on electrodes during quenching	Vaporization of graphite target by laser; CNT formed on receiver during quenching	Decomposition of hydrocarbons over transition metal catalyst to form CNT
Operating Temperature	>3000 °C	>3000 °C	500-1200 °C
CNT length (µm)	~1	~1	$0.1 - 10^5$
Yield	low	low	high
Quality	low	high	medium to high
Purity	low	medium to high	medium to high
Scale up	difficult	difficult	easy

2.4 Applications of CNT in Polymer Nanocomposites

Carbon nanotubes have a reported Young's modulus and tensile strength of up to 1 TPa [68] and 60 GPa [69] respectively, while their densities can be as low as ~1.3 g cm^{-3} [70]. These values make nanotubes of much interest in polymer reinforcement [71]. The high aspect ratio of CNT allows enhancement in polymer properties even at lower concentrations as compared to conventional fillers such as carbon black or nanoclays [72]. Several studies have shown that the addition of small amounts of CNT can considerably improve the mechanical properties and thermal stability of polymer nanocomposite [6, 73, 74, 75]. However, it has been well known that as-produced CNTs are very difficult to be dispersed in polymer matrices as CNTs have large aspect ratio and surface area and possess large van der Waals forces between themselves, which can lead to the formation of aggregates or bundles that are tightly bound. Therefore, the dispersion of CNTs and incorporation of CNT individuals into polymer matrices is one of the most important tasks to optimize the effective utilization of polymer/CNT composites. Lately, the CNTs have been functionalized by various agents in order to get good dispersion in polymers so that the properties will be enhanced. A large number of simple and complex molecules are being used to functionalize CNTs [19, 76]. The incorporation of CNTs into polymer matrices has frequently been achieved by solution mixing [77], in situ polymerization [78] and melt blending [79].

2.4.1 Preparation Methods of Polymer/CNT Nanocomposites [76]

2.4.1.1 Solution Mixing:

Solution mixing is the most common method for the fabrication of CNT/polymer nanocomposites because it is amenable to small sample sizes. Typically, solution blending involves three major steps: dispersion of CNTs in a suitable solvent by mechanical mixing, magnetic agitation or sonication. The solvent can also dissolve polymer resins. Subsequently, the dispersed CNTs are mixed with polymer matrix at room or elevated temperatures. The nanocomposite is finally obtained by precipitating or casting the mixture. This method is often used to prepare composite films.

2.4.1.2 Melt Blending:

Melt blending is another commonly used method to fabricate CNT/polymer nanocomposites. Thermoplastic polymers, such as polypropylene, polystyrene, poly(ethylene 2,6-naphthalate), can be processed as matrix materials in this method. The major advantage of this method is that no solvent is employed to disperse CNTs. Melt blending uses a high temperature and a high shear force to disperse CNTs in a polymer matrix, and is most compatible with current industrial practices. Special equipments, such as extruder, injection machine, which are capable of being operated at an elevated temperature and generating high shear forces, are employed to disperse

CNTs. Melt blending or variants of this technique are frequently used to produce CNT/polymer composite fibers. Compared with the solution mixing methods, this technique is generally considered less effective to disperse CNTs in polymers than that of solution mixing, and its application is also limited to low filler concentrations in thermoplastic matrices.

2.4.1.2 *In-situ* Polymerization:

In situ polymerization is an efficient method to realize uniform dispersion of CNTs in a thermosetting polymer. In this method, CNTs are mixed with monomers, either in the presence or absence of a solvent, and then these monomers are polymerized via addition or condensation reactions with a hardener or curing agents at an elevated temperature. One of the major advantages of this method is that covalent bonding can be formed between the functionalized CNTs and polymer matrix, resulting in much improved mechanical properties of composites through strong interfacial bonds.

The following table (2.3) summarize and compare the three methods for preparing polymer/CNT nanocomposites.

Table 2.3: Polymer/CNT nanocomposites preparation techniques.

Method	**Solution Mixing**	**Melt Blending**	**In-situ Polymerization**
Description	Dispersion of CNTs in a suitable solvent and polymers are mixed in solution. The CNT/polymer composite is formed by precipitation or by evaporation of the solvent	CNTs are mechanically dispersed into a polymer matrix using a high temperature and high shear force mixer or compounder	CNTs are dispersed in monomer followed by polymerization
Solvent	Must	No	Can be used
Special equipment	No	Yes	No
Dispersion of CNT	Medium	Low	High

2.4.2 Properties of Polymer/CNT Nanocomposites

The carbon nanotubes-polymer composites were initially reported in 1994 by Ajayan et al. [80]. They just mechanically mixed the purified MWNTs with epoxy resin. Since then, attention has been paid to composite materials with uniform and high nanotubes loading. Carbon nanotube epoxy composites are most widely studied as nonconjugated polymer-based composites.

There are certain advantages that have been realized in using carbon nanotubes for structural polymer (e.g., epoxy) composites. Nanotube reinforcements will increase the toughness of the composites by absorbing energy during their highly flexible elastic behavior. This will be especially important for nanotube-based ceramic matrix composites. An increase in fracture toughness on the order of 25% has been seen in nano-crystalline alumina nanotube (5% weight fraction) composites, without compromising on hardness [81]. Other interesting applications of nanotube-filled polymer films will be in adhesives where a decoration of nanotubes on the surface of the polymer films could alter the characteristics of the polymer chains due to interactions between the nanotubes and the polymer chains; the high surface area of the nanotube structures and their dimensions being nearly that of the linear dimensions of the polymer chains could give such nanocomposites new surface properties.

Other than for structural composite applications, some of the unique properties of carbon nanotubes are being pursued by filling photoactive polymers with nanotubes. Recently, such a scheme has been demonstrated in a conjugated luminescent polymer, poly (m-phenylenevinylene-co-2, 5-dioctoxy-p-phenylenevinylene) (PPV), filled with MWCNTs and SWCNTs [82]. Nanotube/PPV composites have shown large increases in electrical conductivity (by nearly eight orders of magnitude) compared to the pristine polymer, with little loss in photoluminescence/electro-luminescence yield. In addition, the composite is far more robust than the pure polymer regarding mechanical strength and photo-bleaching properties (breakdown of the polymer structure due to thermal effects). Preliminary studies indicate that the host polymer interacts weakly with the embedded nanotubes, but that the nanotubes act as nanometric heat sinks, which prevent the build up of large local heating effects within the polymer matrix. While experimenting with the composites of conjugated polymers, such as PPV and nanotubes, a very interesting phenomenon has been recently observed [82]; it seems that the coiled morphology of the polymer chains helps to wrap around nanotubes suspended in dilute solutions of the polymer.

Multi-walled carbon nanotube/epoxy resin composites have been fabricated [83]. By choosing an over-aged hardener, relatively soft and ductile matrix, a rubbery epoxy resin, has been obtained. This made possible to evaluate the effect of nanotube addition on the whole stress-strain curve up to high strain level. Sandler et al. [84]

reported that untreated carbon nanotubes were dispersed in an epoxy matrix. The use of carbon nanotubes not only reduces the percolation threshold to below 0.04 wt%, but also increases the overall conductivity. While using ethanol in ultrasound with intense stirring process improves the dispersion of the nanotubes, and it is not impossible to break up all the entanglements of the carbon nanotubes. Even on the millimeter scale, the distribution of nanotubes is not uniform. Gong et al. [85] reported that using surfactants as wetting agents might improve dispersion and thermomechanical properties of carbon nanotube/polymer (epoxy) composites, but even with the addition of the surfactant, complete homogeneous dispersion of the nanotubes was not obtained. Better surfactants and different concentration of polymer were not investigated in this case.

Composite films of poly (vinyl alcohol) and nanotubes were prepared. Followed by casting to make films, chemically treated nanotubes were carefully mixed with aqueous poly (vinyl alcohol) solution in order to prevent reaggregation. Each nanotube must be covered with a layer of polymer to form a stable mixture before it is able to interact with a number of other nanotubes. It was believed that “in colloidal terms”, the absorbed polymer sterically stabilizes the nanotube dispersion and protects it against bridging flocculation and depletion aggregation. The electrical conductivities of composites shows a typical percolation behavior and the presence of the nanotubes stiffen the material, particularly at high temperature [86]. However, the plausible mechanism seems too simple and was not confirmed directly.

Poly (methly methacrylate) (PMMA)/nanotubes composites were fabricated by in situ process. In the process treated nanotubes can be initiated by AIBN and open their π-bonds. With the opened π-bonds nanotubes can link with the PMMA, thus obstruct the growth of PMMA and produce a C-C bond between the nanotubes and the PMMA. The dispersion ration of nanotubes in the PMMA matrix is improved and the properties of the composites rise due to high interfacial strength [87].

Thin film of PMMA/SWCNT composite was also fabricated by spin coating. It was found that the polymers intercalated between nanotubes into bundles. At low nanotubes concentration, amorphous carbon was dispersed well, thus more uniform films were prepared. A combination of solvent casting and melt mixing was used to fabricate SWCNT/PMMA composites. Melt mixing produced compositionally uniform films on the micrometer scale, while the films prepared by solvent casting were heterogeneous. Mechanical properties and electrical conductivity of the aligned nanocomposite fibers were improved by melt spinning [88]. Jia et al. [89] reported on PMMA/carbon nanotube composites. This paper shows that processing of the polymer can improve CNT/polymer composite behavior. CNTs participate in PMMA polymerization; effective properties decrease for greater than 7 wt% CNTs due to residual stresses in the matrix. Carole et al. [90] reported composites consisting of different quantities of carbon nanotubes and nanofibrils in a poly (methyl methacrylate) (PMMA) matrix have been prepared using a polymer extrusion technique. The nanotubes or nanofibrils were first dispersed over the polymer matrix

particles using a dry powder mixing method. The final composite specimens contained well-dispersed and aligned nanofibrils and nanotubes. The orientation distribution of carbon fibrils and nanotubes in the composite was determined by image analysis and found to be maximized in the extrusion flow direction.

The issue of nanotube dispersion is critical to efficient reinforcement. Schadler et al. [17] discussed slipping of nanotubes when they are assembled in ropes. The result shows that there is a significantly affects on the elastic properties. In addition to slipping of tubes that are not bonded to the matrix in a composite, the aggregate of nanotube ropes effectively reduce the aspect ratio (length/diameter) of the reinforcement. Shaffer and Windle [91] were able to process carbon nanotube/polyvinyl-alcohol composite films for mechanical characterization. The tensile elastic modulus and damping properties of the composite films were assessed in a dynamic mechanical thermal analyzer (DMTA) as a function of nanotube loading and temperature. From the theory developed for short-fiber composites, a nanotube elastic modulus of 150 MPa was obtained from the experimental data. This value in a microscopic composite is well below the values reported for isolated nanotubes. It is not clear whether this result is a consequence of imperfections in the graphite layers of catalytically grown nanotubes used for the investigation or whether it relates to a fundamental difficulty in stress transfer.

Even with improved dispersion and adhesion, micro-mechanical characterization of these composites is difficult because the distribution of the nanotubes is random. Thus, attempts have been made to align nanotubes in order to elucidate the reinforcement mechanisms. Jin et al. [91] showed that aligned nanotube composites could be obtained by mechanical stretching of the composite. X-ray diffraction was used to determine the orientation and degree of alignment. Haggenmueller et al. [93] showed that melt spinning of single wall nanotubes in fiber form can also be used to create a well-aligned nanotube composite. In addition to alignment of the carbon nanotubes, researchers have attempted to spin carbon fibers from carbon nanotubes.

Hsu-Chiang et al. [94] have successfully prepared a novel nanocomposite consists of multiwall carbon nanotube (CNT)/waterborne polyurethane (WPU) nanocomposite. Carbon nanotube was modified to be compatible with waterborne polyurethane via covalent bonding or ionic bonding. Thermal properties show that adding carbon nanotube enhanced the thermal stability by 26 °C (from 315 to 341 °C) when carbon nanotube content was 2.5 phr (part per hundred parts of resin). After the surface modification, carbon nanotube can be dispersed effectively, and improve the interfacial strength between it and waterborne polyurethane matrix. Consequently, the physical properties of nanocomposite are enhanced, especially in the covalent bonding system. Mechanical property tests show that adding multiwall carbon nanotubes improve the tensile properties very significantly (370% in tensile strength).

SEM and TEM microphotographs prove that carbon nanotube can be effectively dispersed in waterborne polyurethane matrix. Rheological tests show that carbon nanotube can increase the melt viscosity and reduce the variation of processing viscosity.

Tony et al. [95] have prepared polyethylene (PE) and multiwalled carbon nanotubes (MWCNTs) with weight fractions ranging from 0.1 to 10 wt% by melt blending using a mini-twin screw extruder. The morphology and degree of dispersion of the MWCNTs in the PE matrix at different length scales was investigated using scanning electron microscopy (SEM), transmission electron microscopy (TEM), atomic force microscopy (AFM) and wide-angle X-ray diffraction (WAXD). A percolation threshold of about 7.5 wt% was obtained and the electrical conductivity of PE was increased significantly, by 16 orders of magnitude, from 10^{-20} to 10^{-4} S/cm. The storage modulus (G') versus frequency curves approached a plateau above the percolation threshold with the formation of an interconnected nanotube structure, indicative of 'pseudo-solid-like' behaviour. The ultimate tensile strength and elongation at break of the nanocomposites decreased with addition of MWCNTs. The diminution of mechanical properties of the nanocomposites, though concomitant with a significant increase in electrical conductivity, implies the mechanism for mechanical reinforcement for PE/MWCNT composites is filler-matrix interfacial interactions and not filler percolation. The temperature of crystallisation (T_c) and fraction of PE that was crystalline (F_c) were modified by incorporating MWCNTs.

The thermal decomposition temperature of PE was enhanced by 20 K on addition of 10 wt% MWCNT.

2.4.3 Polystyrene/CNT Nanocomposites

Polystyrene (PS) is a versatile polymer with the features of low price, good optical transparency, excellent electric insulation and mechanical properties. The dispersion of carbon nanotubes into PS matrix for the fabrication of PS/CNT composite has naturally stimulated significant interest among researchers [75].

Qian et al. [6] fabricated PS/MWCNT films by solvent evaporation. With only the addition of 1% by weight they achieved between 36–42% increase in the elastic stiffness and a 25% increase in the tensile strength. Figure 2.9 is a TEM micrograph of their nanotube film showing the mechanisms of fracture.

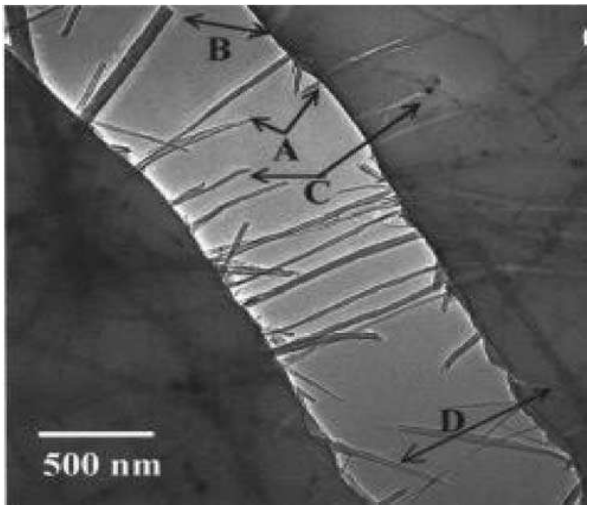

Figure 2.9: TEM image shows significant pullout of the nanotubes from the PS matrix [6].

Thostenson et al. [96] also utilized solvent evaporation followed by microscale twin screw extrusion to obtain highly aligned PS/MWCNT films that exhibited a 49% increase in elastic modulus.

Andrews et al. [97] prepared PS/MWCNT nanocomposites via melt mixing and reported a good dispersion with an electrical percolation at 0.25 vol %.

Safadi et al. [77] prepared PS/MWCNT films via spin-casting and reported the transformation from insulating to conducting behavior and a 100% increase in the tensile modulus at 5 wt %.

Mitchell et al. [98] added functionalized single-wall carbon nanotubes (SWCNTs) to PS and studied the melt rheology of the nanocomposites, and

demonstrated the presence of a percolated network of SWCNTs at concentration exceeding 1.5 wt %.

Choi et al. [99] synthesized PS/MWCNT nanocomposites via an in-situ bulk sonochemical polymerization and studied their morphology, thermal and rheological properties. Meanwhile, Kim and co-workers [78] applied the same method and observed that MWCNT played an important role as initiator consumer during the polymerization reaction.

Kota et al. [100], prepared PS/MWCNT nanocomposites by solvent evaporation method using two different solvents; Dimethyl formamide, (DMF), and Tetrahydrofuran**,** (THF), to study the correlation between electrical and rheological properties at the onset of percolation.

CHAPTER THREE

EXPERIMENTAL SECTION

3.1 Production of Carbon Nanotubes

The orifice-chemical vapor deposition (O-CVD) reactor consists of one ceramic tube passes and two consecutive furnaces. The first one is used to evaporate the ferrocene catalyst, at 120^{o}C, which is carried by the inlet gases into the second furnace. The second furnace is the reaction zone where the carbon nanotubes are formed. Stainless steel orifice was placed at the beginning of the reaction zone to study its effect on the purity, quality, aspect ratio and alignment of CNTs.

O-CVD reactor is a ceramic tubular reactor with diameter of 50 mm and length of 180 cm passing through two consecutive furnaces, see figures 3.1 and 3.2. A catalyst boat containing 100 mg of ferrocene ($FeC_{10}H_{10}$ 98 % purity) catalyst is placed within the first reaction chamber. The ferrocene evaporated at 120^{o}C and carried by the inlet gases into the second furnace which is the reaction zone where the carbon nanotubes were formed. Stainless steel orifice was placed at the beginning of

the reaction zone to study its effect on the purity, quality, aspect ratio and alignment of CNTs. It is followed by a ceramic boat for collecting the produced CNT.

Argon gas is introduced into the reactor for flushing and removing air while the second reaction chamber is being heated for 1 hour at the required reaction temperature. After switching off the argon gas, the furnace of the first chamber is switched on and the temperature is set at 120 ^{o}C. The hydrogen gas (purity 99%) is introduced as carrying gas and reducing agent, while acetylene (purity 99%) is introduced as a carbon source. The reaction time is set to the required value, after which the process is stopped and the product is collected.

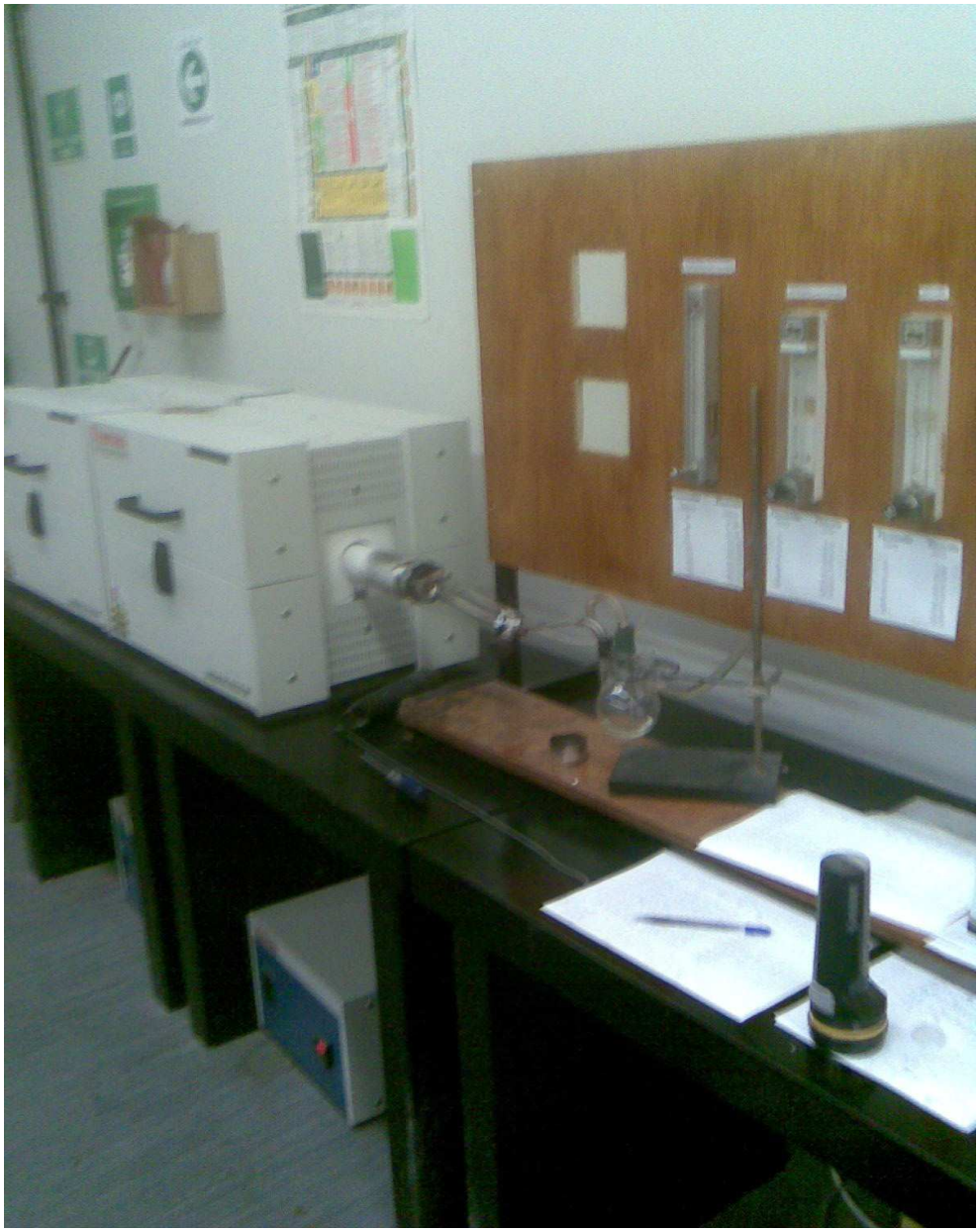

Figure 3.1: Photo for the O- CVD Reactor.

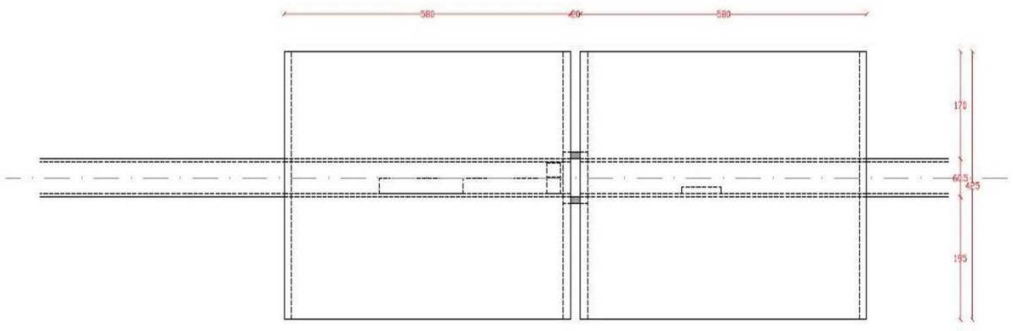

Figure 3.2: Engineering drawing for O-CVD reactor

3.2 Characterization of Produced Carbon Nanotubes

The scanning electron microscopy (SEM), model (JEOL JSM 6460LV), was used to characterize the morphology (diameter and the length) of the deposited material, while the structure was characterized using the transmission electron microscopy (TEM), model (FEI Tecnai G^2), for the selected sample. The SEM gives good results in characterizing the length and the diameter of the CNT because it is used to scan only the surface of the sample, while the TEM is the best way to study the internal structure of the product. The purity of the samples was measured by thermal gravimetric analysis (TGA), while the amount of deposited material was calculated from the weight difference of the collection boat before and after the reaction.

3.3 Functionalization of Carbon Nanotubes

In order to enhance the dispersion of CNTs in Polystyrene nanocomposites, commercially available pristine MWCNTs (produced by Nanostructured and Amorphous Materials Inc., USA, 8 -15nm diameter, 10-50μm length, 95% 230 m^2/g) was functionalized with COOH followed by modification with different surfactants as explained below. The Procedure given by Abuilaiwi et al. [101] was used to functionalize CNTs with different functional groups.

3.3.1 Acid Modification of MWCNT

The CNTs were mixed with concentrated nitric acid at a weight ratio of 1:10 (CNT:acid) in a round bottom flask and refluxed for 48 hours at 130 °C under continuous stirring to obtain CNT-COOH modified MWCNTs [102]. Upon cooling, the mixture was thoroughly filtered, washed continuously with deionized water to remove the last traces of unreacted acid until the pH value was 7 which signifies zero acidity. The acid modified multiwall carbon nanotubes, henceforth MWCNT-COOH was finally filtered and dried at 60 °C [102].

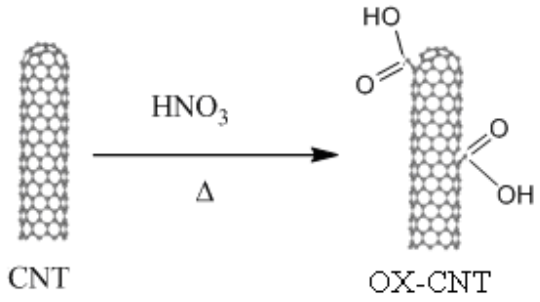

Figure 3.3: Mechanism of acid modification of carbon nanotubes (MWCNT) via thermal oxidation

3.3.2 Substitution of Carboxyllic (–OOH) Group with Different Surfactants

Surface functionalization of CNTs with different types of surfactants was achieved by substitution of the MWCNT-COOH with appropriate surfactant such as 1-Octadecanol (C18), Phenol and Dodecyamine (Amine) at the surfactant melting temperature [103]. The first functionalization carried out was the substitution carboxylic group in MWCNT-COOH with 1-Octadecanol ($C_{18}H_{38}O$). For this purpose, 5g of MWCNT–COOH nanotubes was collected from the bulk samples of the acid modified CNTs and reacted with C18 in a few drops of sulfuric acid at a MWCNT-COOH to C18 ratio of ratio 1:10 and a temperature of 59.8°C for six (6) hrs under continuous stirring. The reaction takes place as shown in the scheme below

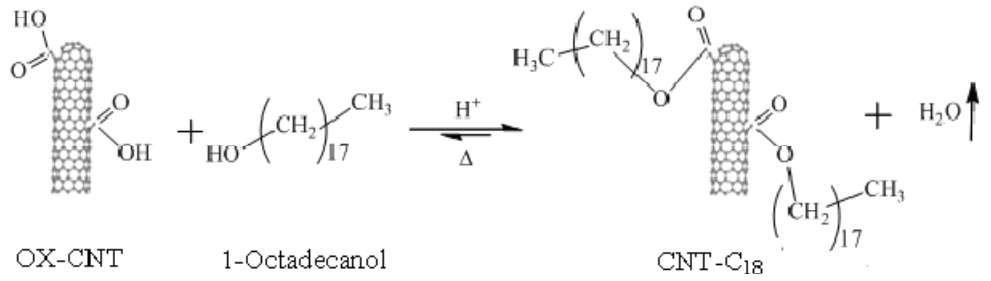

Figure 3.4: Mechanism of C18 modification of MWCNT (MWCNT-C18)

The resulting mixture was allowed to cool down, then washed and filtered in excess toluene solution and deionized water to remove traces of unreacted 1-Octadecanol and sulfuric acid respectively.

For functionalization with Amine group, Dodecylamine was used as a surfactant. In this case, 5g of MWCNT-COOH was added into a round bottom flask containing few drops of sulfuric acid. 50g of Dodecylamine was added and the mixture was heated with continues stirring at 30 °C for six (6) hrs. The content was allowed to cold, washed with Toluene and excess deionized water. The scheme was shown in figure 3.5.

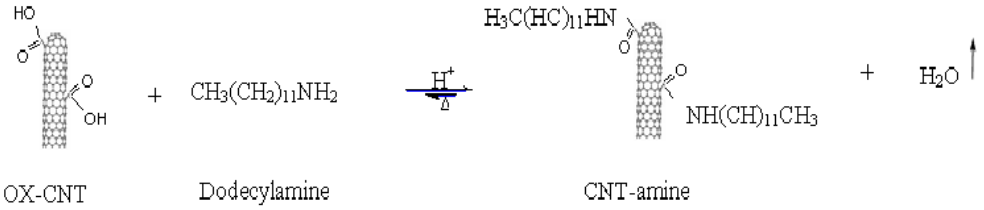

Figure 3.5: Mechanism of Amine modification of MWCNT (MWCNT-amine)

The last substitution of MWCNT-COOH with surfactants was for the phenol group. Here, phenol was mixed with MWCNT-COOH in a few drops of sulfuric acid at a ratio 10:1. The mixed was then heated at 42 °C with continuous stirring for about six (6) hrs to obtained phenol modified CNTs. The content was allows to cool as with the previous substitution processes, then washed with Toluene and excess deionized water to removed any unreacted phenol and sulfuric acid.

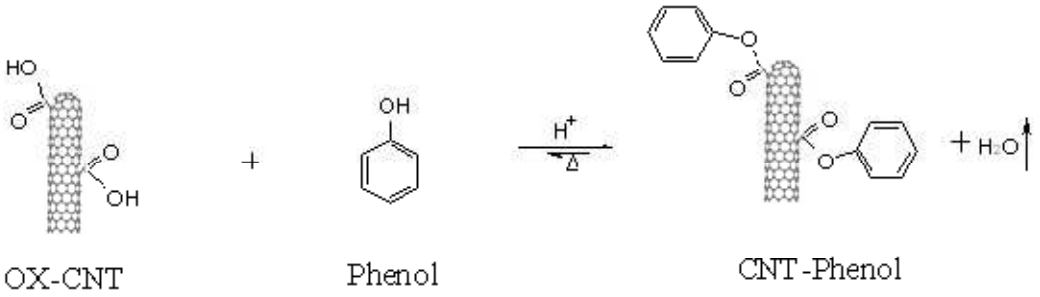

Figure 3.6: Mechanism of phenol modification of MWCNT (MWCNT-phenol)

3.3.3 Characterization of Functionalized Carbon Nanotubes

Fourier transform infrared spectroscopy (FTIR) was used for the study of the surface chemistry of both the pure and modified carbon nanotubes. The spectra emitted by each surfactants i.e. -COOH, -C18, -amine and -phenol was determine qualitatively within a range of 400 and 4000 cm-1 by using Nicolet 6700 FITR spectrometer from the Nicolet Instrument Corporation USA.

3.4 Preparation of Polystyrene/CNT Nanocomposites

Styrene monomer purchased from Sigma-Aldrich was washed and distilled to remove the inhibitor before using it. The required wt% of CNT, CNT-COOH, CNT-C18, CNT-Phenol or CNT-amine and a magnetic stirrer was placed in a round-bottom flask that was sealed with a rubber septum and purged with nitrogen through repeated vacuum/nitrogen cycles. Then, 20 g of the monomer (styrene) was injected using a syringe and a transfer needle. The flask was placed in a sonicator bath (Branson 1510) for 30 min to reduce the agglomeration of carbon nanotubes. Then, the flask was immersed in an oil bath that kept the reaction temperature at 115^{o}C to enhance autocatalytic polymerization since there is no initiator is used. After 12 hours, the flask was removed from the oil bath and the product mixture was dissolved in toluene. Then the mixture was poured into a clean aluminum plate and kept under fume hood until it is dried and the nanocomposites were collected.

In case of studying the conversion of styrene monomer to polystyrene, the reaction time was fixed at 6 hours and the product mixture was diluted with Tetrahydrofuran THF. Then methanol was added to precipitate the formed polymer, which was recovered by filtration followed by drying at 70^{o}C.

3.5 Studying the Properties of Polystyrene/CNT Nanocomposites

To investigate the effect of different CNT loadings and different modifications the mechanical, rheological and thermal properties of PS/CNT nanocomposites were studied according to the following methods.

3.5.1 Transmission Electron Microscopy (TEM)

100 to 120 nm thick section of the nanocomposite sample were prepared using an ultramicrotome (Leica) at room temperature. Sections were put on an uncoated copper EM grid or pre-coated with a holey carbon film (Quantifoil). The examination was done using a Titan cryo twin equipped with a field emission gun (FEI Company) operating at 300kV, equipped with a 4k x 4k CCD camera (Gatan, Inc.).

3.5.2 Tensile Testing

The tensile testing was conducted according to ASTM-D3638 using Instron Machine (Model 5567) at room temperature with a speed of 1 mm/min. The test specimen (dog bone shape) dimensions were 13 mm x 3.2 mm x 2 mm. A minimum of five samples for each composition were tested.

3.5.3 Differential Scanning Calorimetry (DSC)

Non-isothermal DSC analysis was performed using TA Q1000 instrument equipped with liquid nitrogen cooling system and auto sampler. The standard procedure performed in non isothermal scans was the following: samples of about 5-10 mg were heated in hermetic aluminum pans from 25 to 280°C at a scan rate of 10°C/min and held for 5 minutes to erase any thermal history. The samples were then non-isothermally crystallized from 280°C to 25°C at a cooling rate of 5°C/min. Subsequently, the glass transition temperature was measured by raising the temperature to 280°C at a similar heating rate of 10°C/min.

3.5.4 Rheological characterization

Oscillatory rheological properties of the samples were determined using an ARES-rheometer (Rheometrics Scientific). The measurements were performed in dynamic mode under liquid nitrogen atmosphere using 25 mm parallel plate geometry and a constant gap width of approximately 1.5 mm. Compression moulded polymer discs of diameter 25 mm were used and the tests performed at 190^{o}C. Rheological properties were measured as a function of angular frequency which was varied from 0.1 to 100 rad/s and the strain amplitude was chosen to be within the viscoelastic range of the composites.

3.5.5 Thermogravimetric Analysis

Thermogravimteric analysis of the composites was done in nitrogen atmosphere using SDT Q600 instrument from TA instruments. The temperature range was from 25-1000^{0}C and the heating rate was 10^{0}C/min.

CHAPTER FOUR

RESULTS AND DISSCUSION

4.1 Production of Carbon Nanotubes Using Orifice Chemical Vapor Depostition (O-CVD) Reactor

In order to improve the quality and purity of CNTs, we developed new generation of CCVD reactors called orifice-chemical vapor deposition (O-CVD) reactor. The orifice chemical vapor deposition reactor (O-CVD) consists of ceramic tube passes two consecutive furnaces. The first one is used to evaporate the ferrocene catalyst, at 120^{o}C, which carried by the inlet gases into the second furnace. The second furnace is the reaction zone where the carbon nanotubes are formed. We place an orifice at the beginning of the reaction zone to study its effect on the purity, quality, aspect ratio and alignment of CNTs. The reaction parameters will be varied to study their effect and to find the optimum conditions. These parameters are; reaction temperature (600-1000^{o}C), hydrogen flowrate (40-540 ml/min), acetylene flowrate

(15-155 ml/min), and orifice diameter (3, 6, 12 mm). We started with varying the hydrogen and acetylene flowrates and the orifice diameter at constant temperature (800 ^{o}C) and constant time (30 min). Then, at the best conditions, the effect of reaction temperature was studied.

4.1.1 Effect of Hydrogen and Acetylene Flowrates

4.1.1.1 Effect of Hydrogen and Acetylene Flowrates on the Amount of Deposited Carbon Nanomaterials

Table 4.1 shows the results of the amount of deposited carbon for different combination of hydrogen and acetylene flow rates. These experiments were conducted without orifice at the beginning of reaction zone. The reaction temperature and reaction time were fixed at 800^{o}C and 30 min respectively.

Table 4.1: The weight of deposited carbon produced by O-CVD at different acetylene and hydrogen flowrates without orifice at reaction temperature and reaction time of 800^{o}C and 30 min respectively.

Orifice Diameter (mm)	Acetylene Flowrate (ml/min)	Hydrogen Flowrate (ml/min)	Weight of Deposited Carbon (g)
None	15	40	0.112
None	15	100	0.166
None	15	240	0.166
None	15	320	0.140
None	15	540	0.165
None	70	40	0.318
None	70	240	0.362
None	70	320	0.591
None	70	540	0.484
None	155	40	0.412
None	155	100	0.545
None	155	240	0.502
None	155	320	0.705
None	155	540	0.635

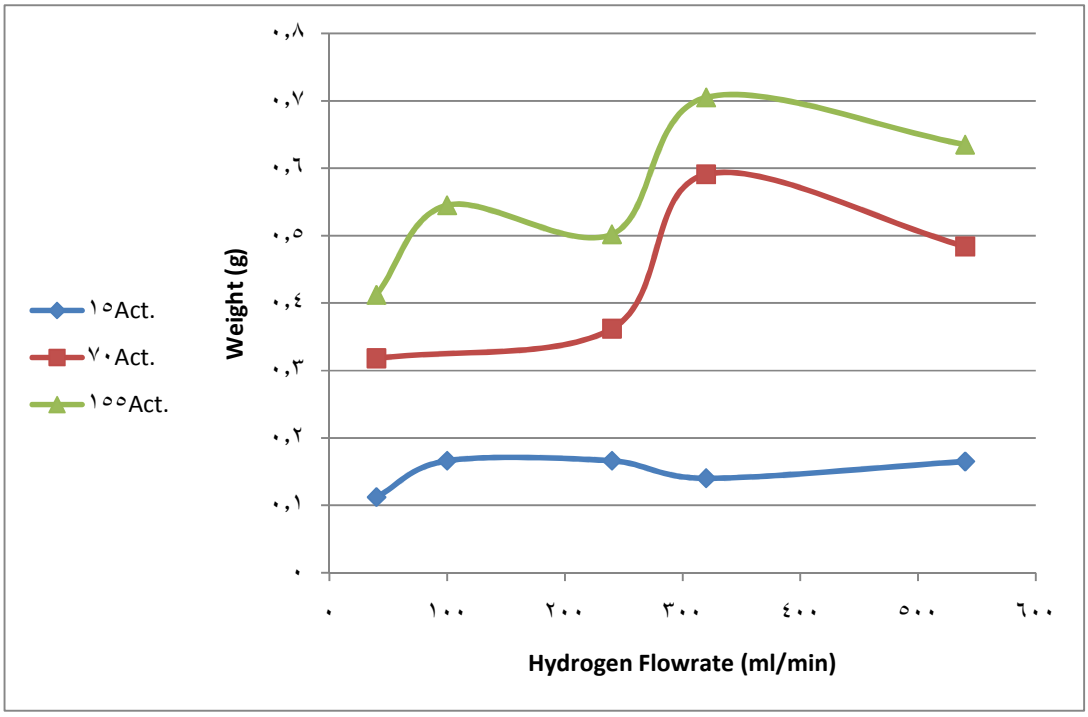

Figure 4.1: Weight of deposited carbon produced by O-CVD without orifice versus hydrogen flowrate at different acetylene flowrates (15, 70 and 155 ml/min).

It is clear from Figure 4.1 that increasing the acetylene flowrate increases the amount of deposited carbon. However, the effect of hydrogen flowrate is not the same for the whole range. Hydrogen flow rate plays a significant role in the formation of carbon nanotubes, as being the carrier and reactant gas in the floating catalyst

method. During the process of synthesis of CNTs, hydrogen gas carried into the reaction chamber. The ferrocene vaporized at 120 °C and reduced to Fe ions in the presence of hydrogen. The Fe particles aggregate into nanoscaled catalyst for the growth of the CNTs. The effect of hydrogen can be both acceleration and suppression. The effect of hydrogen acceleration on carbon formation may be interpreted in two ways. The first interpretation suggested that, hydrogen decompose inactive metal carbides to form catalytically active metal. The other interpretation pertains to the removal, by hydrogen, of the surface carbon and precursors of carbon, which block the active site. The suppressing effect has also been reported to be due to the surface hydrogenation reactions to form methane. For the acetylene flowrates of 70 and 155 ml/min, increasing the hydrogen flowrate causes an increase in the amount of deposited carbon until the value of 320 ml/min of hydrogen, after which the weight starts to decrease. This suggests that below 320 ml/min the hydrogen accelerates the reaction by reducing more catalyst. Increasing the hydrogen flowrate more than this value results in surplus amount which leads to surface hydrogenation and suppressing the formation of CNT. For low flowrate of acetylene (15 ml/min) the amount of deposited carbon is very low and there is no significant effect of hydrogen.

4.1.1.2 Effect of Hydrogen and Acetylene Flowrates on the Purity

The purity of the sample means the amount percentage of CNT with respect to other carboneous species like carbon ash and carbon fibers. The purity was determined by thermo gravimetric analysis and inspected by SEM images. In order to study the effect of both hydrogen and acetylene flowrates we varied them with different combinations to reflect different hydrogen to acetylene ratio. Table 4.2 and figure 4.2 shows the results of the purity for different combination of hydrogen and acetylene flow rates.

Table 4.2: The purity of CNTs produced by O-CVD at different acetylene and hydrogen flowrates without orifice at reaction temperature and reaction time of 800^{o}C and 30 min respectively.

Orifice Diameter (mm)	Acetylene Flowrate (ml/min)	Hydrogen Flowrate (ml/min)	Purity %
None	15	40	19.17
None	15	100	21.99
None	15	240	24.73
None	15	320	33.09
None	15	540	55.04
None	70	40	1.29
None	70	100	10.35
None	70	240	35.09
None	70	320	40.23
None	70	540	39.37
None	155	40	9.35
None	155	100	25.02
None	155	240	39.15
None	155	320	26.34
None	155	540	16.95

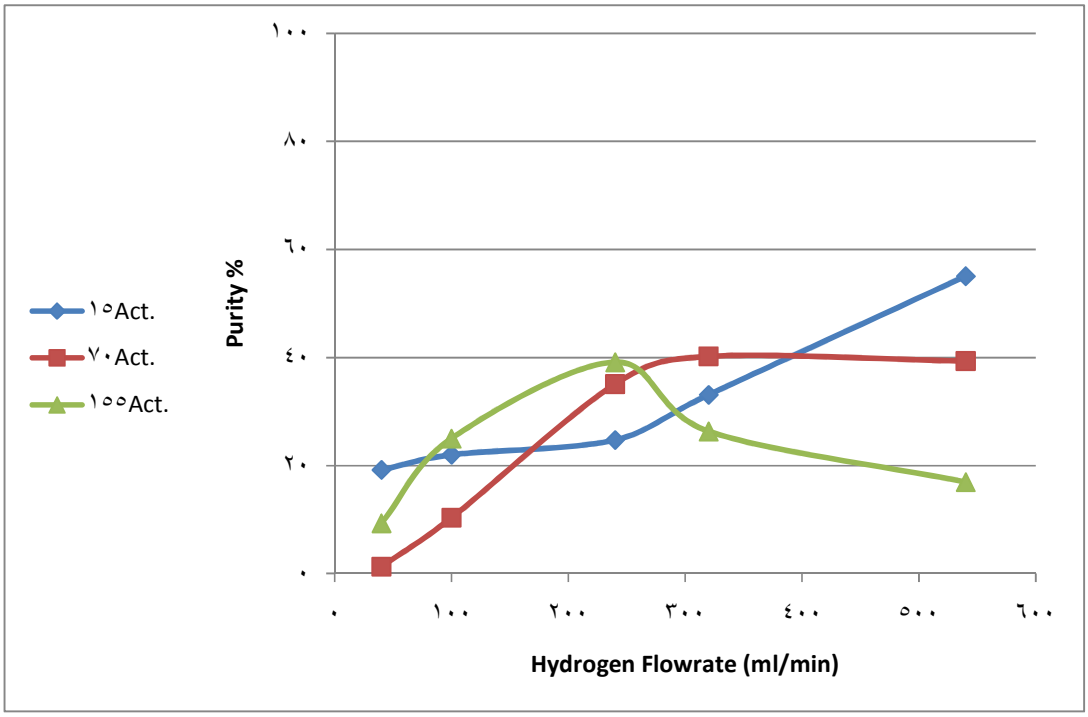

Figure 4.2: Purity of CNT produced by O-CVD without orifice versus hydrogen flowrate at different acetylene flowrates (15, 70 and 155 ml/min).

It is shown in figure 4.2 that increasing the hydrogen flowrate keeps increasing the purity in case of low acetylene flowrate (15 ml/min) because the hydrogen flowrate is always higher than that of acetylene and the hydrogen activates the surface of the catalyst [104] and this activation affects significantly the purity of the CNTs by increasing the chance of their formation. The SEM images for acetylene flowrate of 15 ml/min are given in figure 4.3 (a-c)

For higher acetylene flowrate (70 ml/min) the purity at hydrogen flowrate of 40 ml/min was very low (less than 10%), where another carbon materials else than CNT were formed as shown in the SEM images (figure 4.3 (d, g). The reason for this is that increasing the acetylene flowrate will increase the concentration of the carbon atom in the reaction chamber which will cause an increase in the impure carbon materials. Also, the high amount of carbon atoms will cover the active sites of the catalyst, beside that the low hydrogen flowrate with respect to the acetylene flowrate will result in less amount of activated catalyst which is necessary for the growth of CNTs. However, further increase in the hydrogen flowrate increases the purity because more catalyst is activated and increase the dissociation of acetylene to produce carbon atoms that will deposite in the catalyst and grow as carbon nanotubes. For acetylene flowrate of 155 ml/min, increasing the hydrogen flowrate beyond 240 ml/min, a decrease in purity is noticed. This is because increasing the flowrate will decrease the residence time which means the atoms will not have more time to grow as carbon nanotubes.

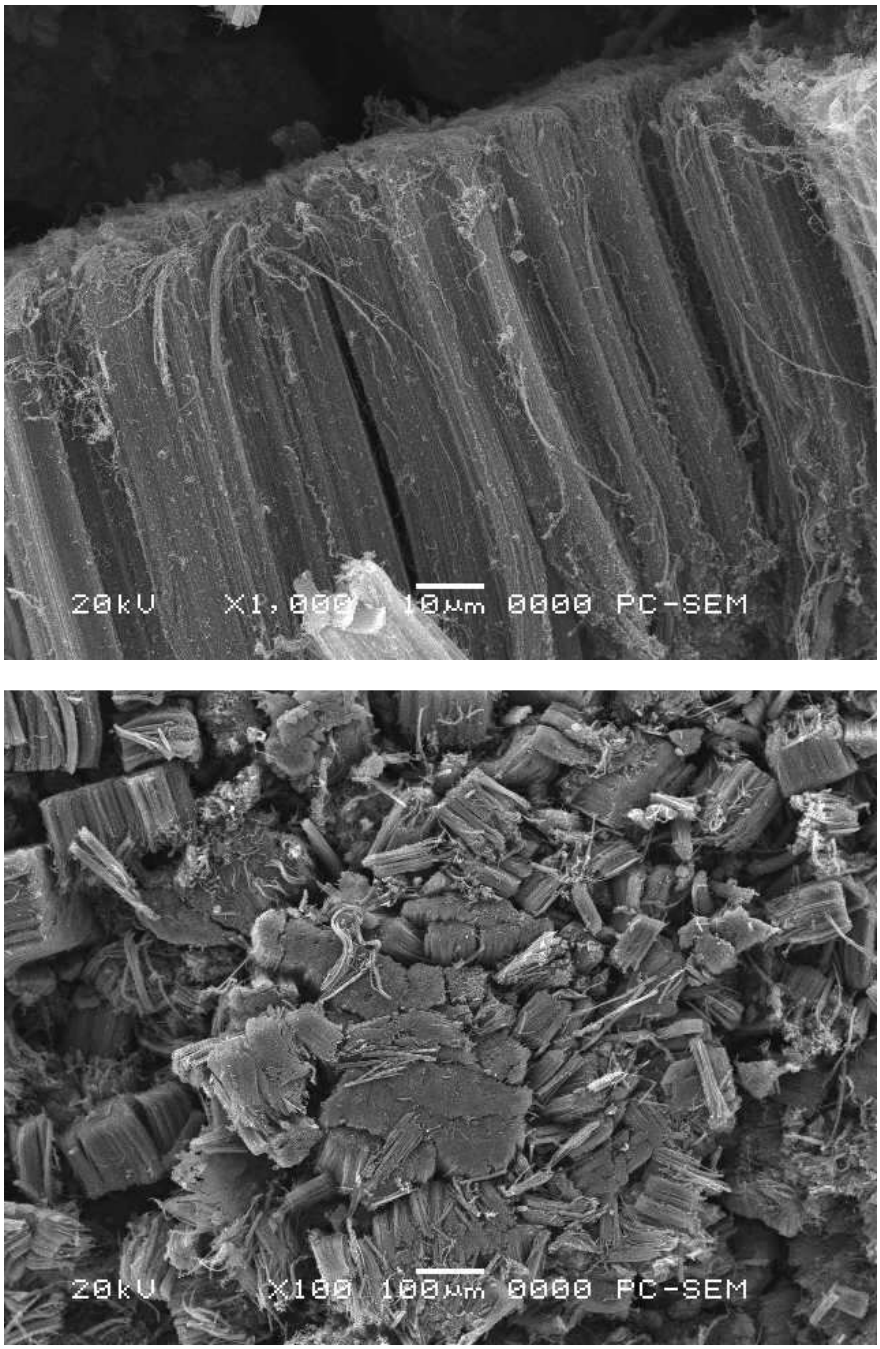

(a) A15 - H40

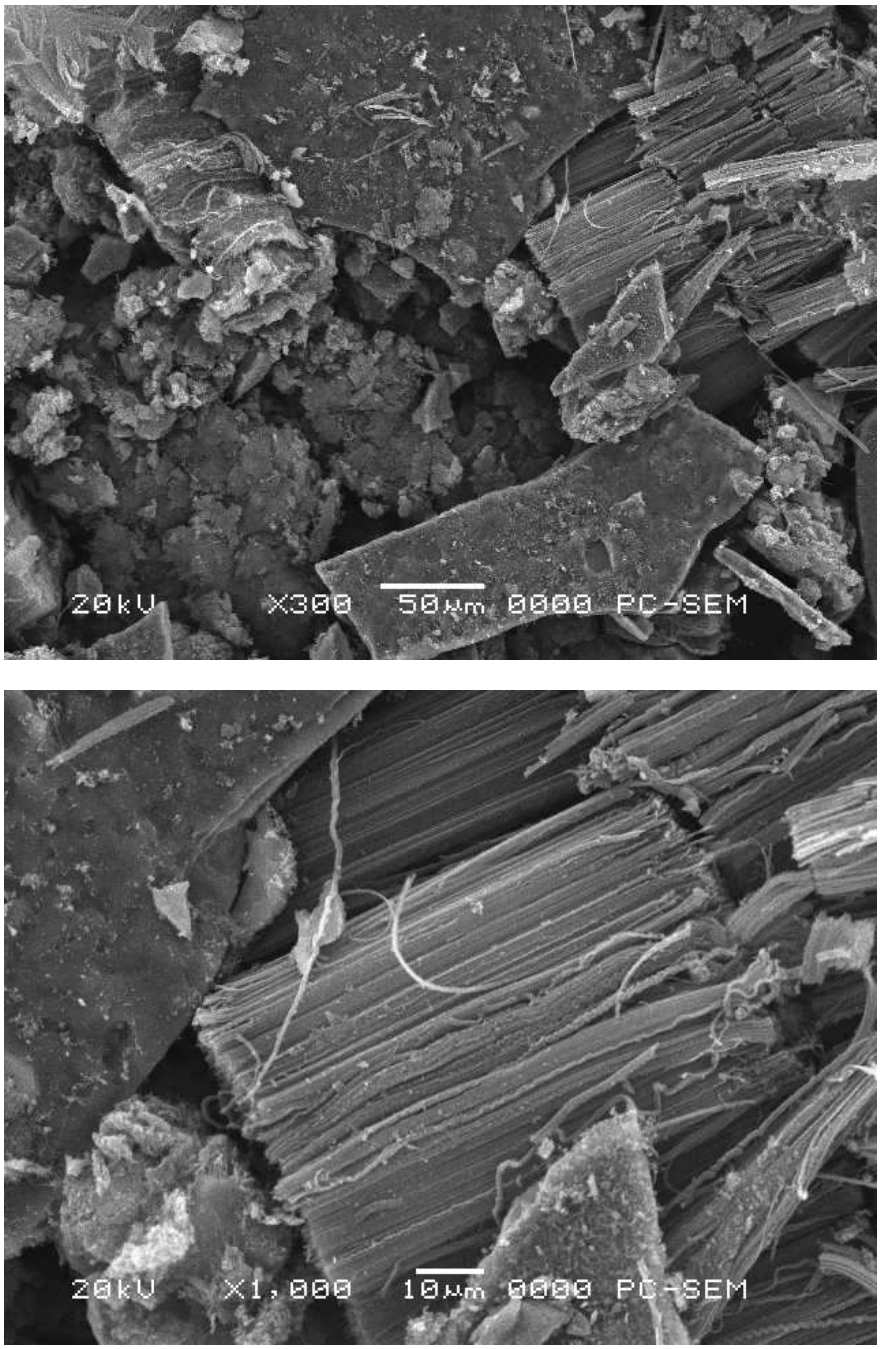

(b) A15 – H240

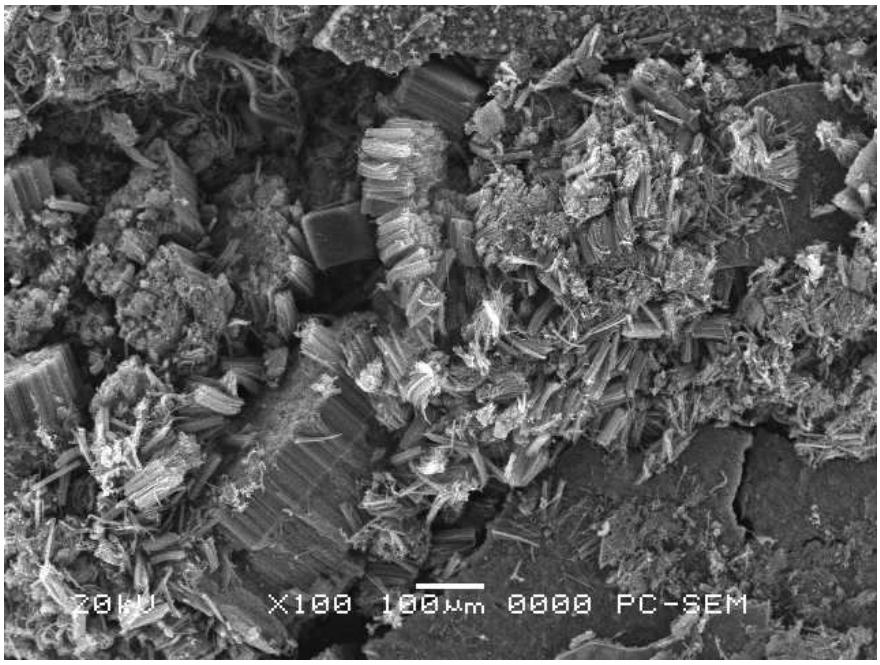

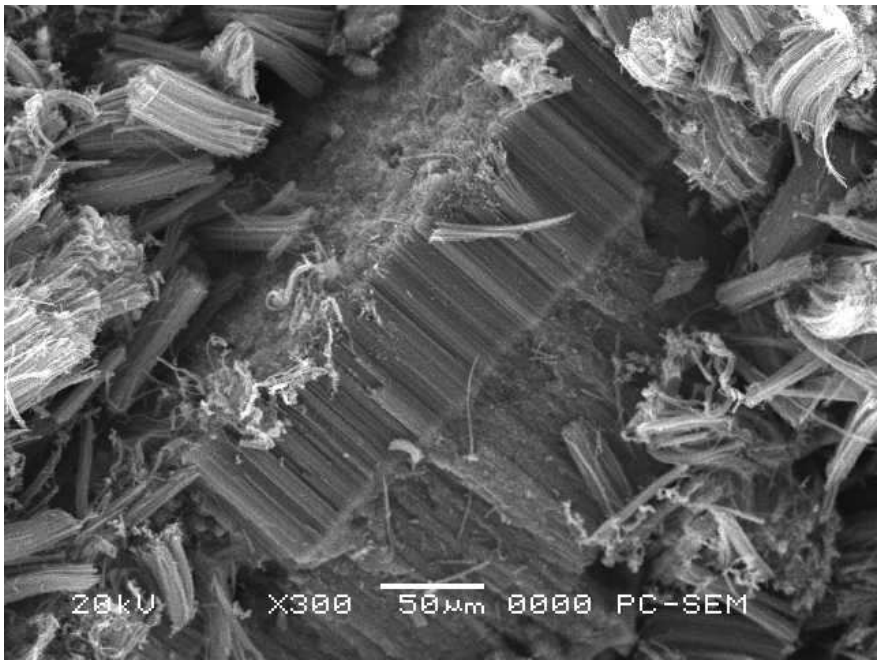

(c) A15 – H540

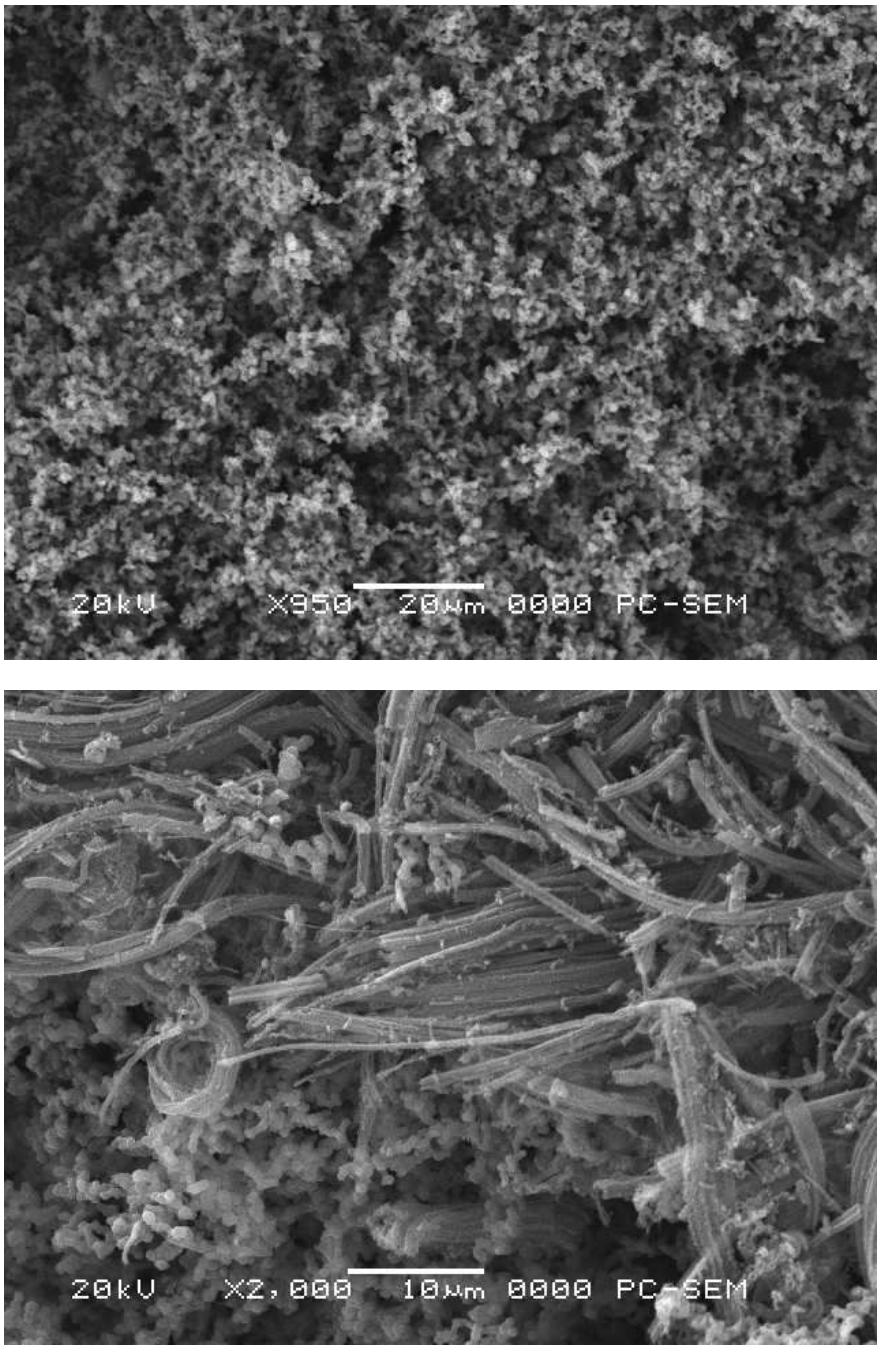

(d) A70 – H40

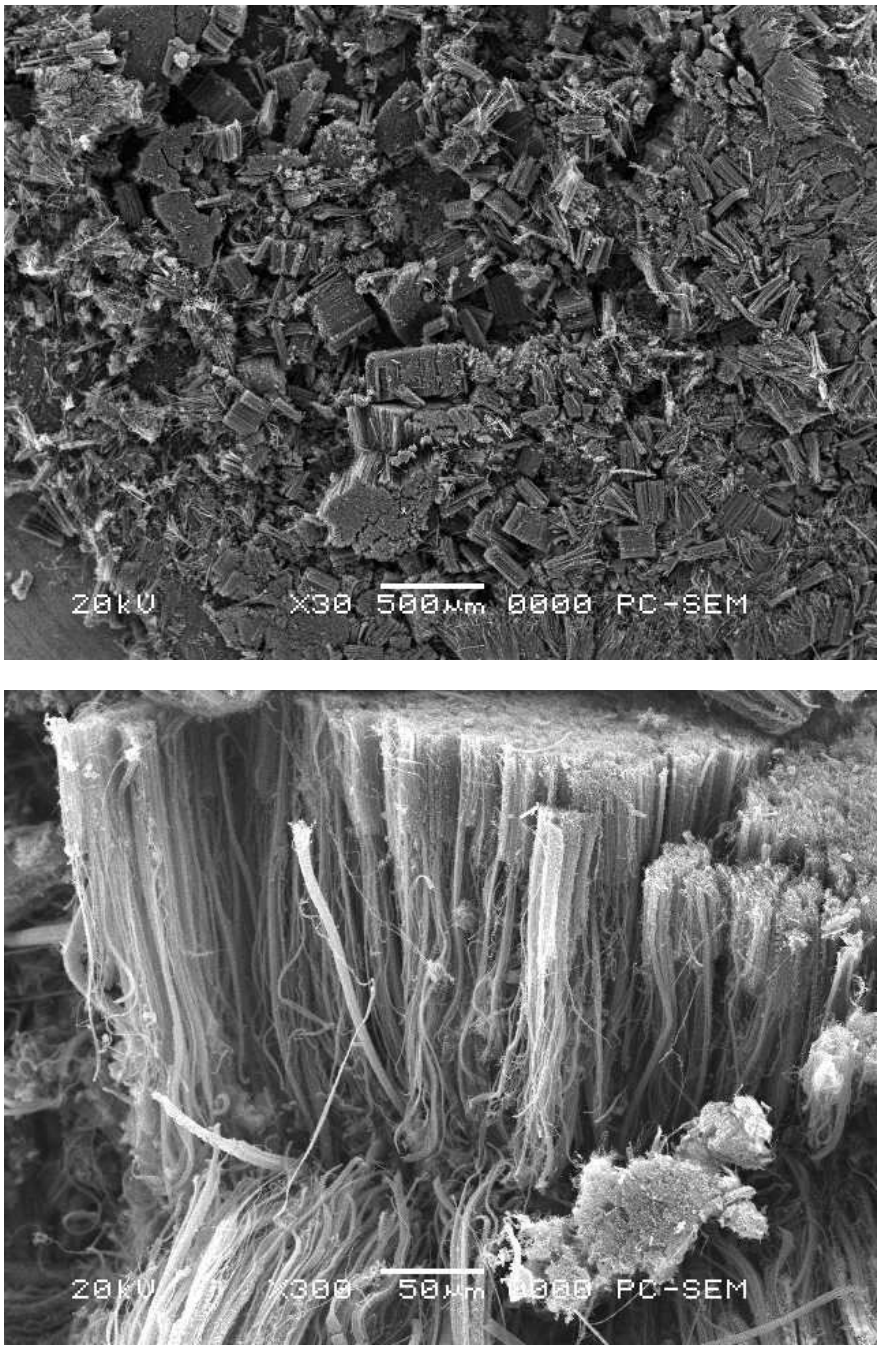

(e) A70 – H240

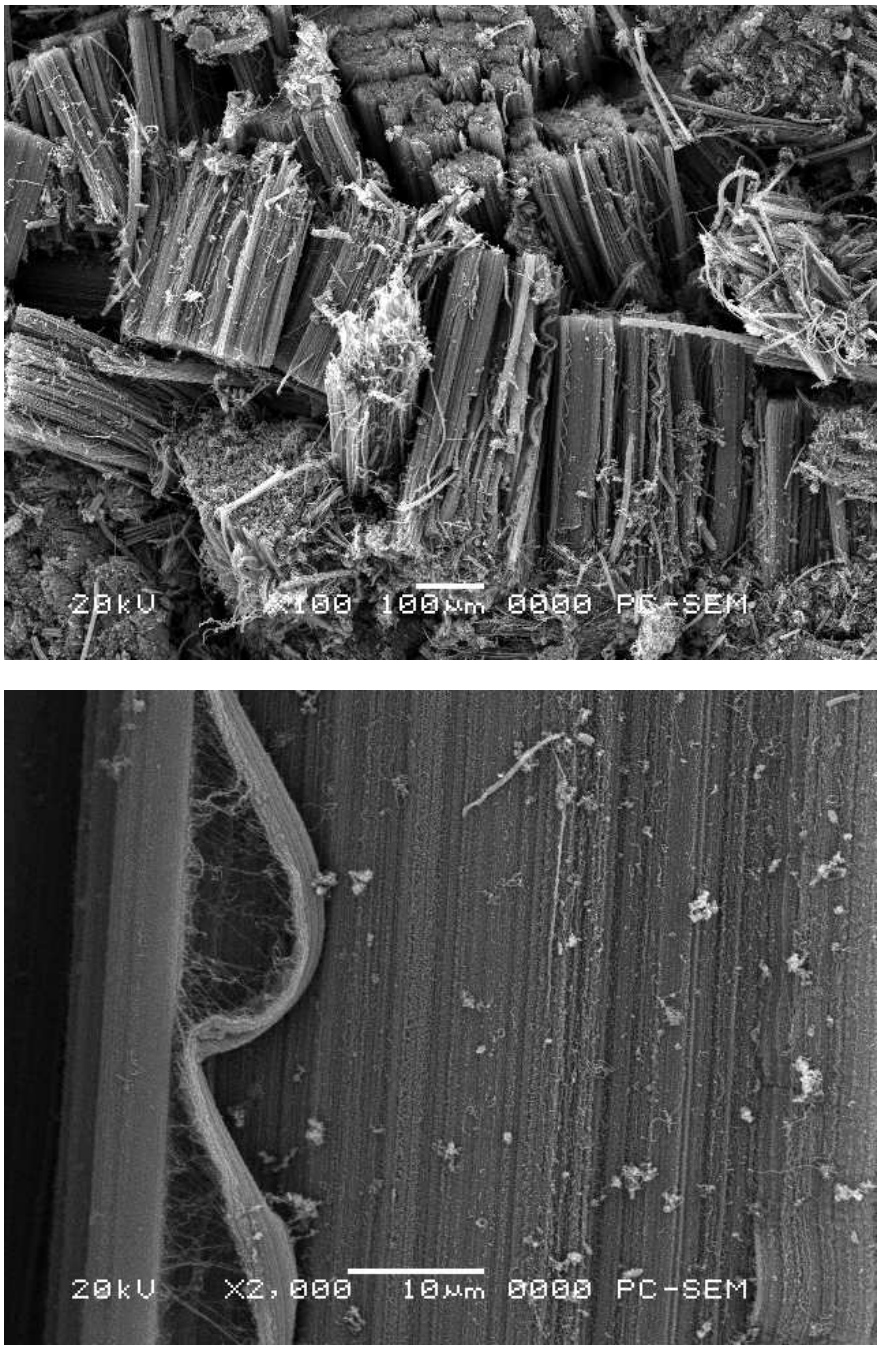

(f) A70 – H540

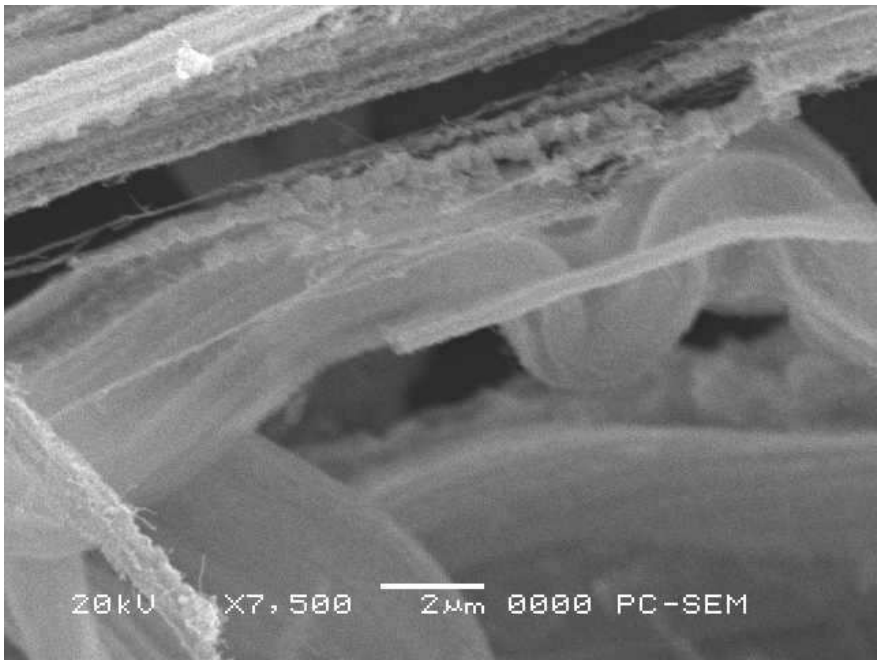

(g) A155 – H40

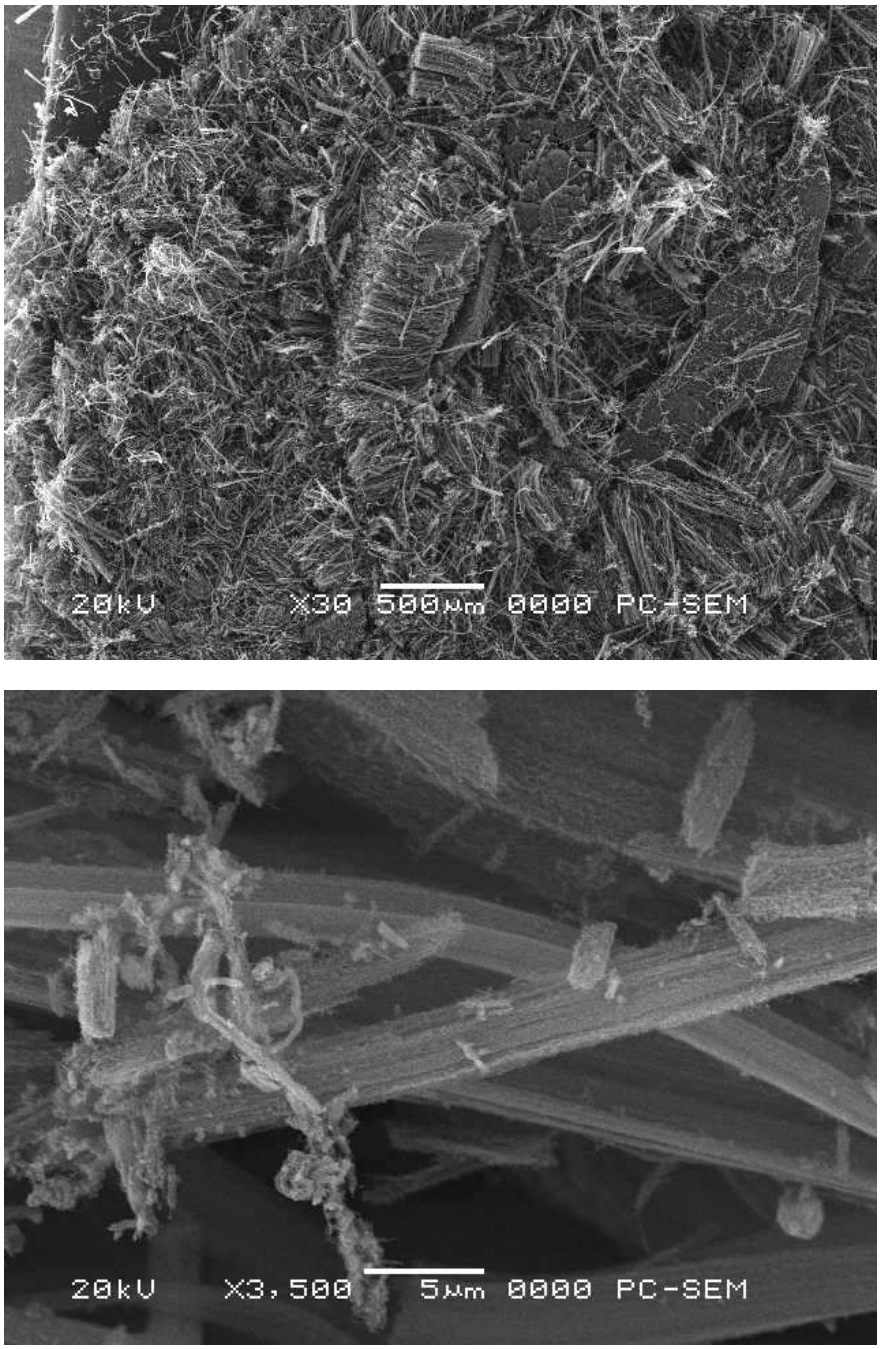

(h) A155 – H240

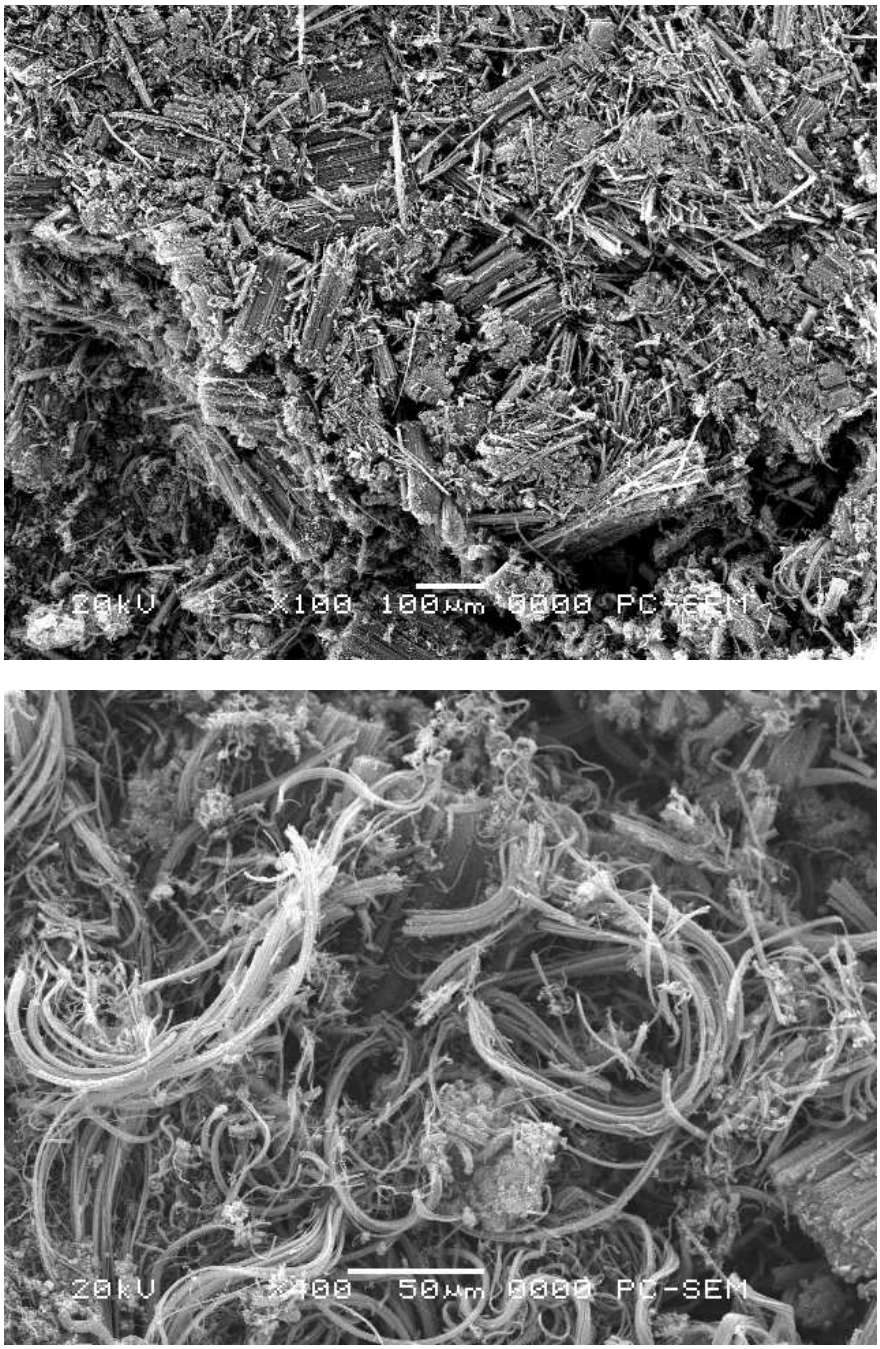

(i) A155 – H540

Figure 4.3: SEM images for CNTs produced by O-CVD without orifice at different acetylene and hydrogen flowrates.

3.1.1.3 Effect of Hydrogen and Acetylene Flowrates on the Length of Aligned CNTs

It is known that increasing length of carbon nanotubes increases the aspect ratio (length/diameter) which means improvement of the mechanical properties. The results of the length of aligned CNTs for different combination of hydrogen and acetylene flow rates are given in Table 4.3 and Figure 4.4.

Table 4.3: The length of CNTs produced by O-CVD at different acetylene and hydrogen flowrates without orifice at reaction temperature and reaction time of 800^{o}C and 30 min respectively.

Orifice Diameter (mm)	Acetylene Flowrate (ml/min)	Hydrogen Flowrate (ml/min)	Length of CNTs (μm)
None	15	40	0
None	15	100	90.6
None	15	240	87.5
None	15	320	54.2
None	15	540	28.7
None	70	40	332.7
None	70	240	305.6
None	70	320	310.4
None	70	540	202.4
None	155	40	394.4
None	155	100	416.7
None	155	240	425.7
None	155	320	503.2
None	155	540	583.3

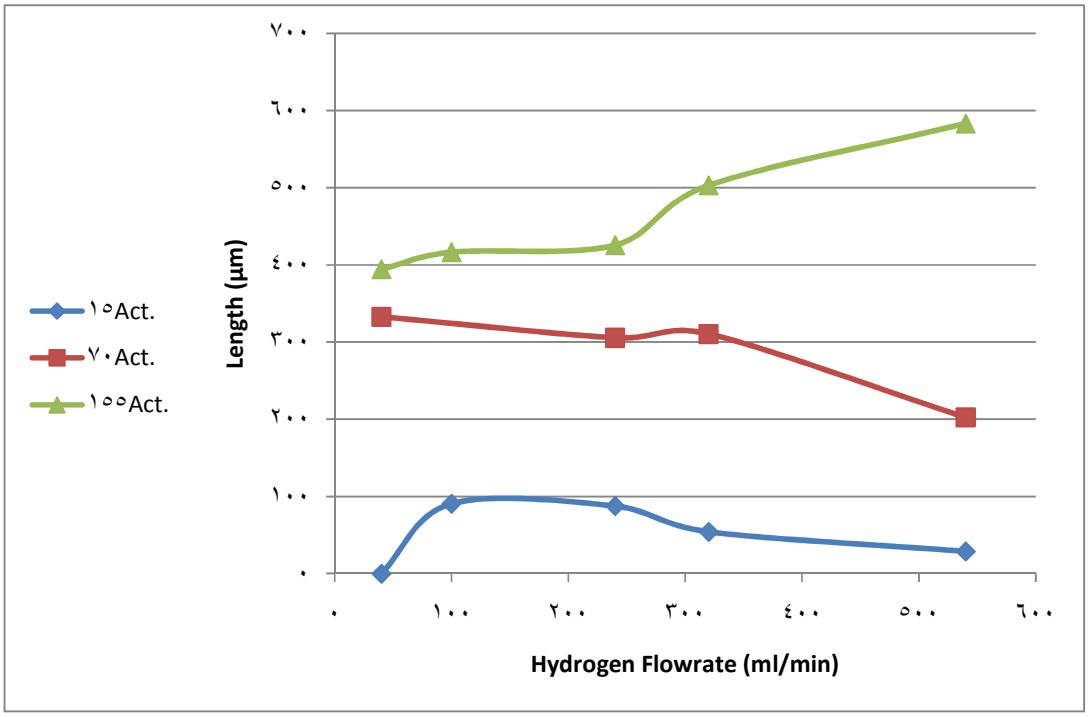

Figure 4.4: Length of CNTs produced by O-CVD without orifice versus hydrogen flowrate at different acetylene flowrates (15, 70 and 155 ml/min).

It is clear from the figure that increasing the acetylene flowrate results in increasing the length of the CNT. This is due to the increment in the number of carbon atoms which participate in building the nanotube. As the hydrogen flowrate increases a slight decrease in the length is noticed, this might be due to the increment in the number of active catalyst particles over which a carbon nanotube is grown. So,

increasing the number of catalyst particles will increase the number of carbon nanotubes for the same number of carbon atoms which results in shorter CNTs. However, this is not the case for acetylene flowrate of 155 ml/min because the amount of carbon atoms is in surplus and long CNTs can still be formed.

4.1.2 Effect of Orifice on the Production of CNTs

In order to improve the quality and quantity of the produced CNT we introduced a stainless steel orifice with small diameter, compared to the diameter of the reaction tube, at the beginning of the reaction zone. To study the effect of the orifice we repeated the same experiment while an orifice with diameter of 6 mm was inserted. The effect of this orifice on the amount, purity and length of CNTs is studied by comparison with the pervious experiments which were conducted without orifice. The result for another two orifices with diameter of 3 and 12 mm are given in appendix A since orifice 6mm gave the best conditions.

4.1.2.1 Effect of Orifice on the Amount of Deposited Carbon Nanomaterials

Table 4.4 shows the results of the amount of deposited carbon for different combination of hydrogen and acetylene flow rates while an orifice with 6 mm diameter was inserted at the entrance of reaction zone.

Table 4.4: The weight of deposited carbon produced by O-CVD at different acetylene and hydrogen flowrates with 6mm orifice at reaction temperature and reaction time of 800^{o}C and 30 min respectively.

Orifice Diameter (mm)	Acetylene Flowrate (ml/min)	Hydrogen Flowrate (ml/min)	weight of Deposited Carbon (g)
6	15	40	0.122
6	15	100	0.133
6	15	240	0.184
6	15	320	0.187
6	15	540	0.206
6	70	40	0.303
6	70	100	0.530
6	70	240	0.404
6	70	320	0.621
6	70	540	0.423
6	155	40	0.393
6	155	100	1.010
6	155	240	0.951
6	155	320	1.341
6	155	540	0.662

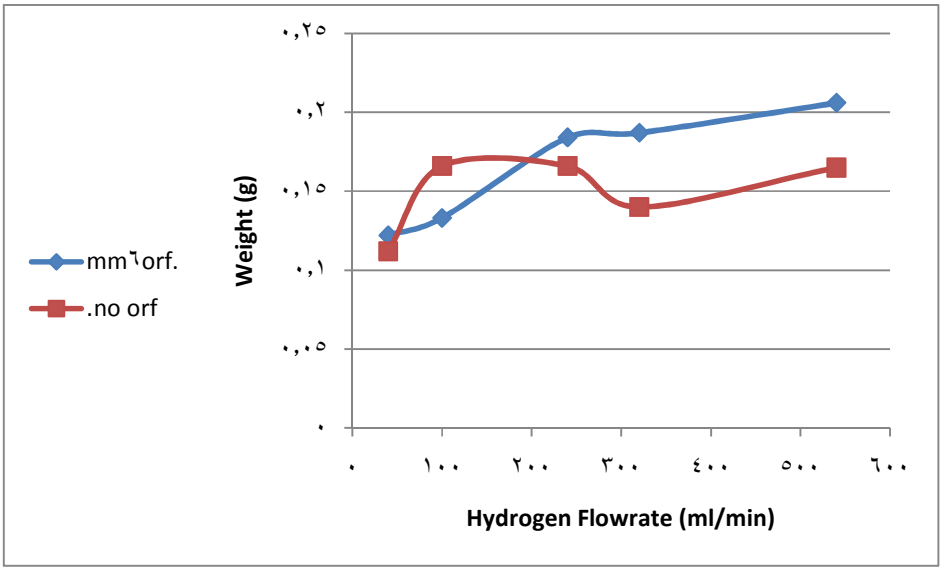
٠,٢٥
٠,٢
٠,١٥
٠,١
٠,٠٥
٠
Weight (g)
mm٦orf.
.no orf
٠
١٠٠
٢٠٠
٣٠٠
٤٠٠
٥٠٠
٦٠٠
Hydrogen Flowrate (ml/min)

(a)

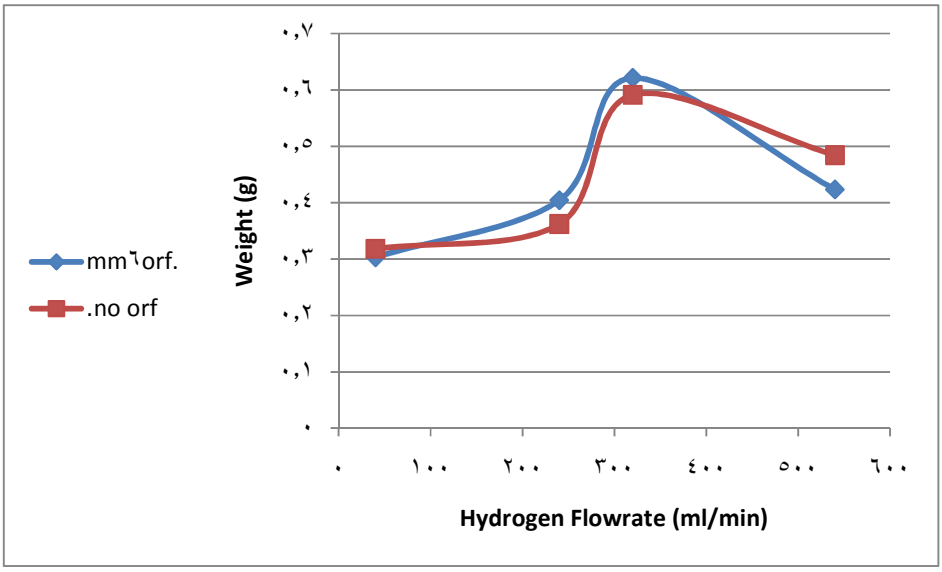
٠,٧
٠,٦
٠,٥
٠,٤
٠,٣
٠,٢
٠,١
٠
Weight (g)
mm٦orf.
.no orf
٠
١٠٠
٢٠٠
٣٠٠
٤٠٠
٥٠٠
٦٠٠
Hydrogen Flowrate (ml/min)

(b)

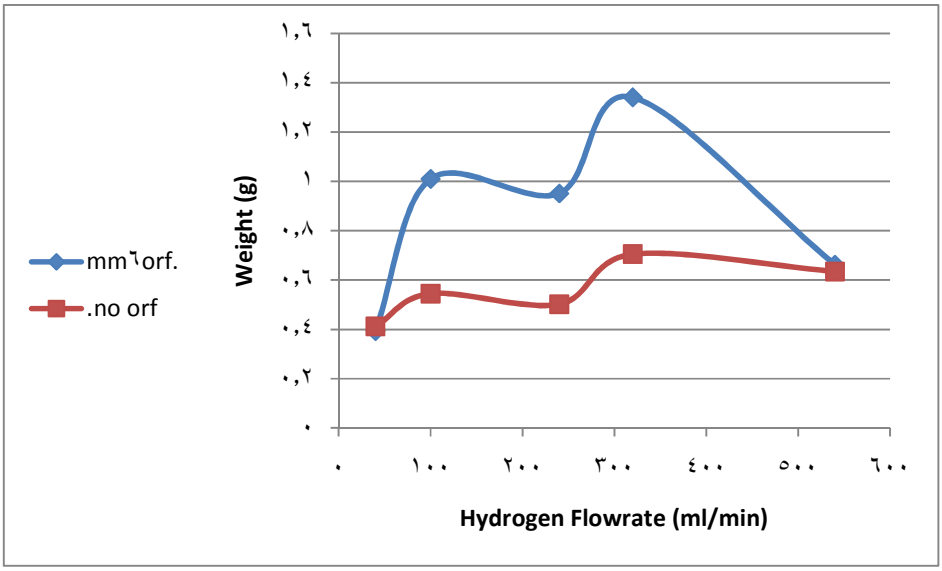

(c)

Figure 4.5: Weight of deposited carbon produced by O-CVD without orifice and with 6 mm orifice versus hydrogen flowrate at acetylene flowrate of (a) 15 ml/min, (b) 70 ml/min and (c) 155 ml/min

.

It is clear from Figure 4.5 that introducing the orifice has increased the weight of deposited carbon. This increment was significant with high acetylene flowrate (155 ml/min) and reach about 91% higher than it without orifice. The orifice was made of stainless steel which consists of iron, chromium and nickel. The suggested reason for the yield increase is that the orifice enhances the dissociation of acetylene into carbon atoms because of its composition and its hot surface.

4.1.2.2 Effect of Orifice on the Purity

Table 4.5 and figure 4.6 show the results of the purity for different combination of hydrogen and acetylene flow rates while an orifice with 6 mm diameter was inserted at the entrance of reaction zone.

Table 4.5: Results of purity of CNT produced by O-CVD at different acetylene and hydrogen flowrates with 6mm orifice at reaction temperature and reaction time of 800^{o}C and 30 min respectively.

Orifice Diameter (mm)	Acetylene Flowrate (ml/min)	Hydrogen Flowrate (ml/min)	Purity %
6	15	40	25.06
6	15	100	29.95
6	15	240	17.61
6	15	320	23.21
6	15	540	35.56
6	70	40	80.62
6	70	100	95.04
6	70	240	95.82
6	70	320	96.48
6	70	540	96.63
6	155	40	39.56
6	155	100	54.84
6	155	240	96.34
6	155	320	98.27
6	155	540	97.23

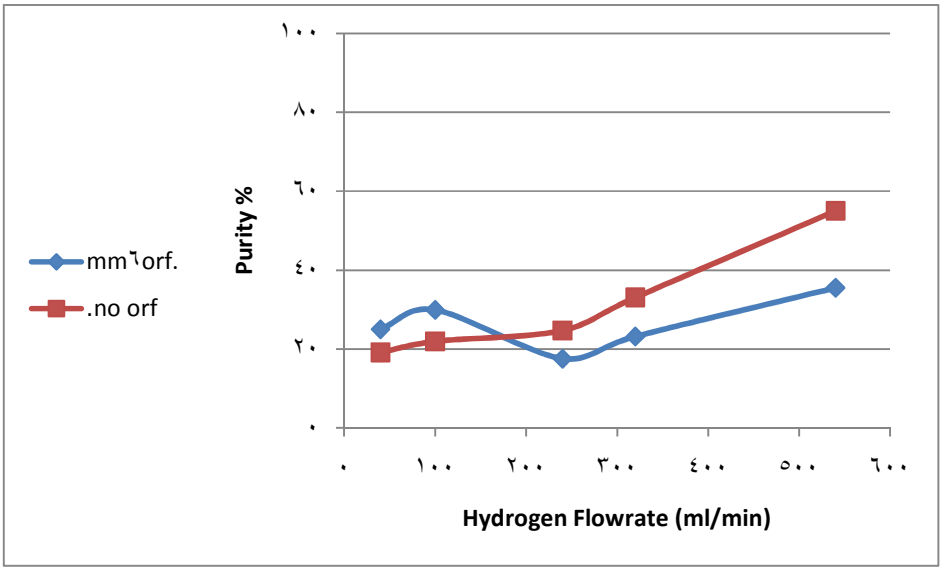
١٠٠
٨٠
٦٠
٤٠
٢٠
٠
Purity %
mm٦orf.
.no orf
٠
١٠٠
٢٠٠
٣٠٠
٤٠٠
٥٠٠
٦٠٠
Hydrogen Flowrate (ml/min)

(a)

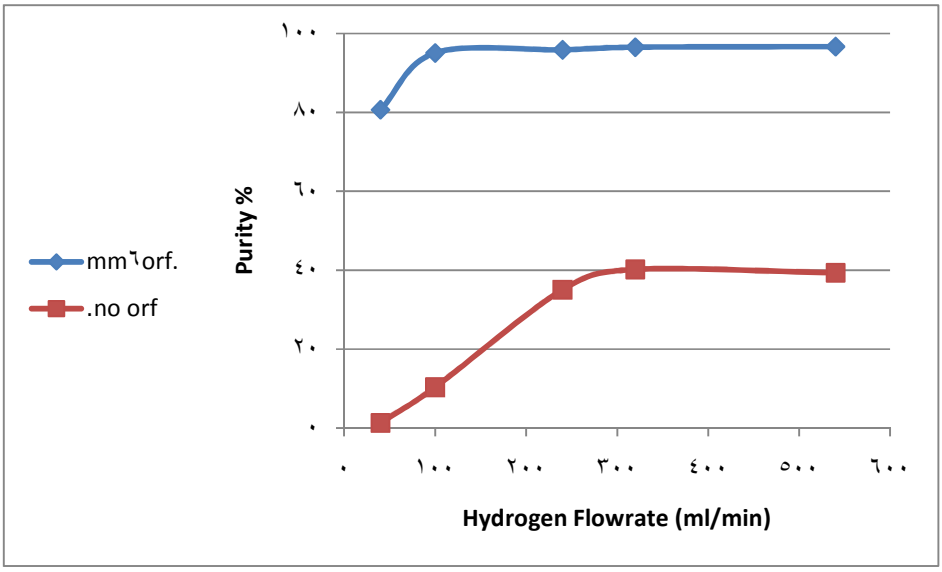
١٠٠
٨٠
٦٠
٤٠
٢٠
٠
Purity %
mm٦orf.
.no orf
٠
١٠٠
٢٠٠
٣٠٠
٤٠٠
٥٠٠
٦٠٠
Hydrogen Flowrate (ml/min)

(b)

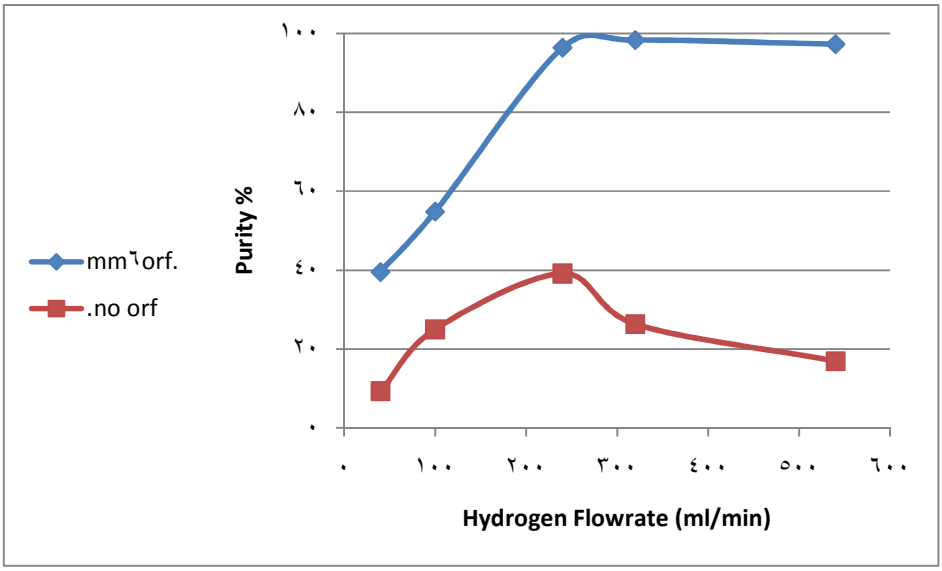

(c)

Figure 4.6: Purity of CNTs produced by O-CVD without orifice and with 6 mm orifice versus hydrogen flowrate at acetylene flowrate of (a) 15 ml/min, (b) 70 ml/min and (c) 155 ml/min.

Figure 4.6(a) shows that for low acetylene flowrate of 15 ml/min, introducing the orifice has no significant effect on the purity of CNTs, except a little decrease in its value for higher hydrogen flowrates in comparison with the case without orifice. However, when acetylene with 70 ml/min and 155ml/min flowrates was used, figure 4.6(b and c) is showing that the purity after introducing the orifice is much higher and reaches around 97% in the case of acetylene flowrate of 155ml/min and hydrogen

flowrate of 240 ml/min. The suggested reason for this is that the orifice surface act as a catalyst that increase the dissociation of acetylene to produce carbon atoms that will deposit in the catalyst and grow as carbon nanotubes. Also, introducing the orifice enhanced the mixing between hydrogen and catalyst vapor which results in increasing the reduced or activated catalyst particles on which CNT will be formed. It is also noticed from figure 4.6(b and c) the purity increased with increasing the hydrogen flowrate until certain value after which the purity be almost constant. This means that the amount of ferrocene catalyst which has been used was activated and was enough to enable most of the carbon atoms to deposit and grow as CNTs.

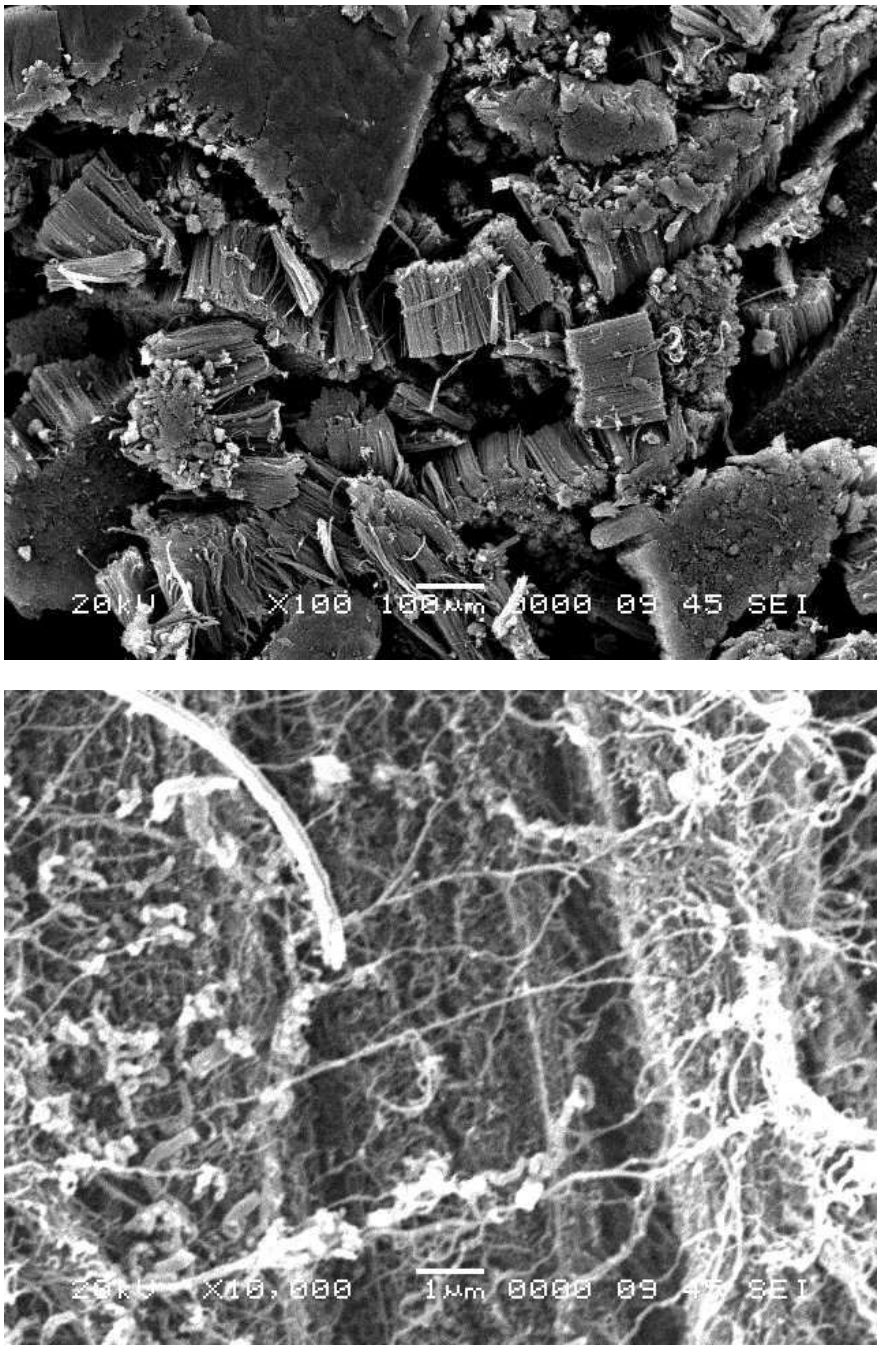

(a) A15 - H40

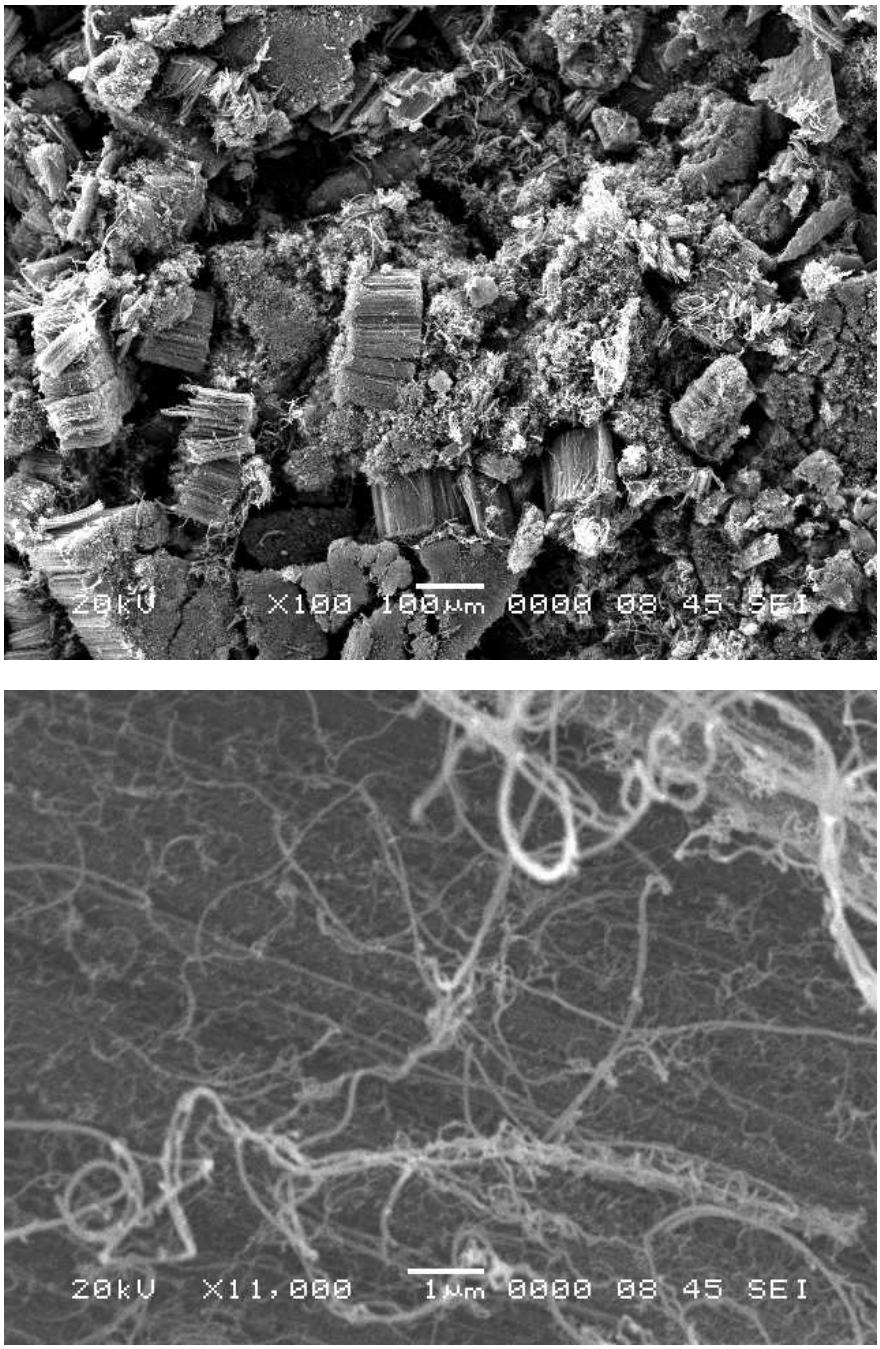

(b) A15 – H240

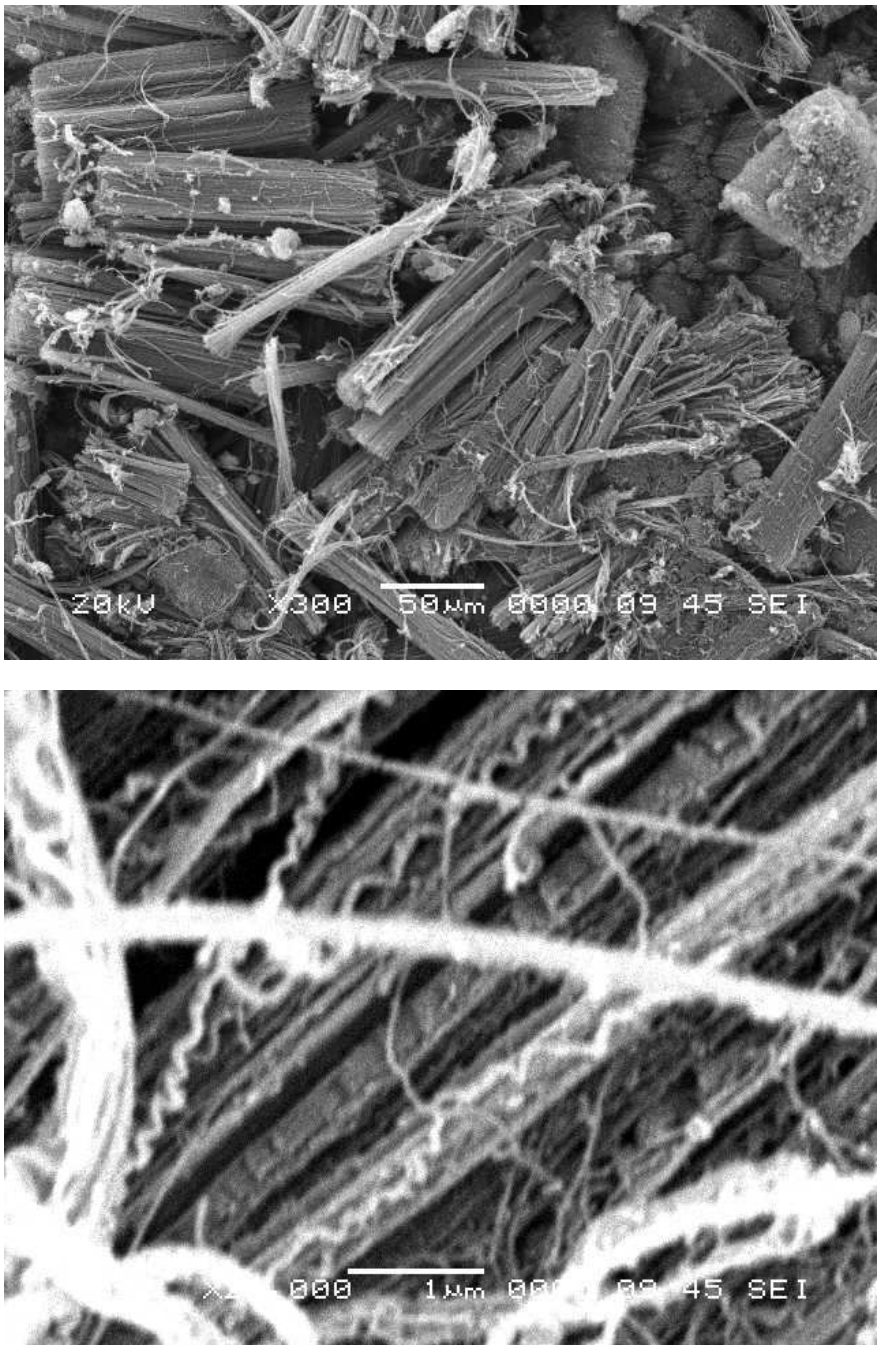

(c) A15 – H540

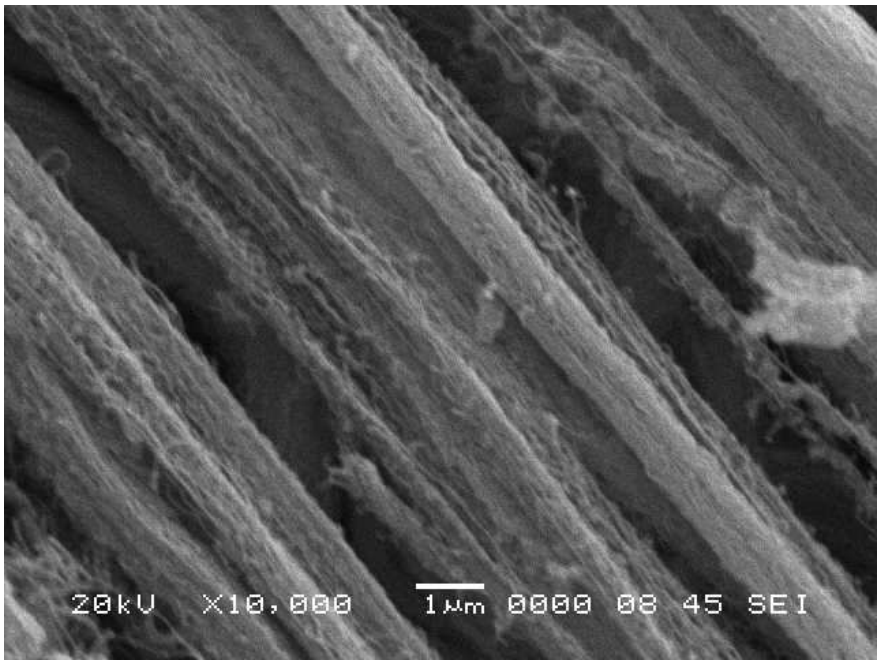

(d) A70 – H40

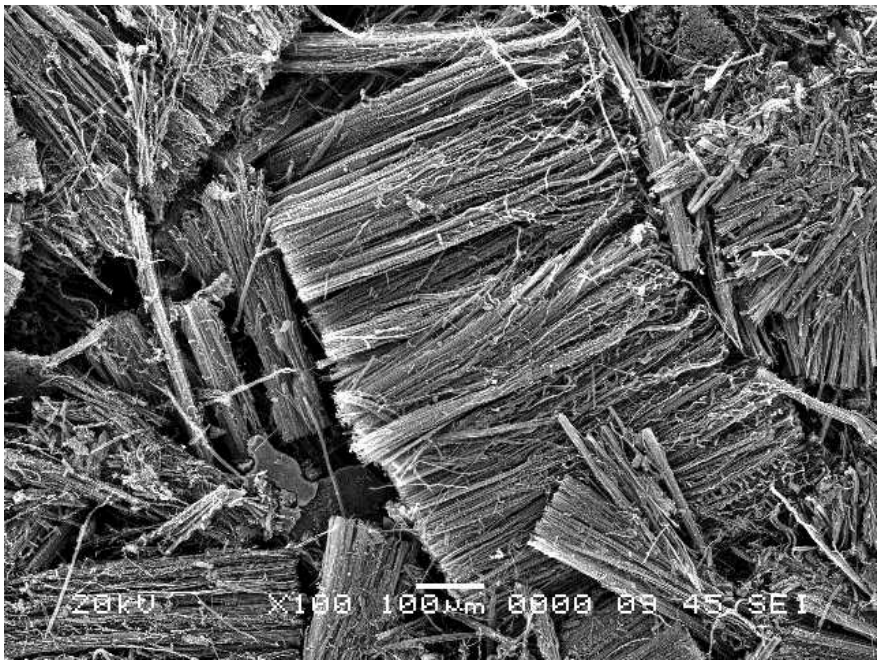

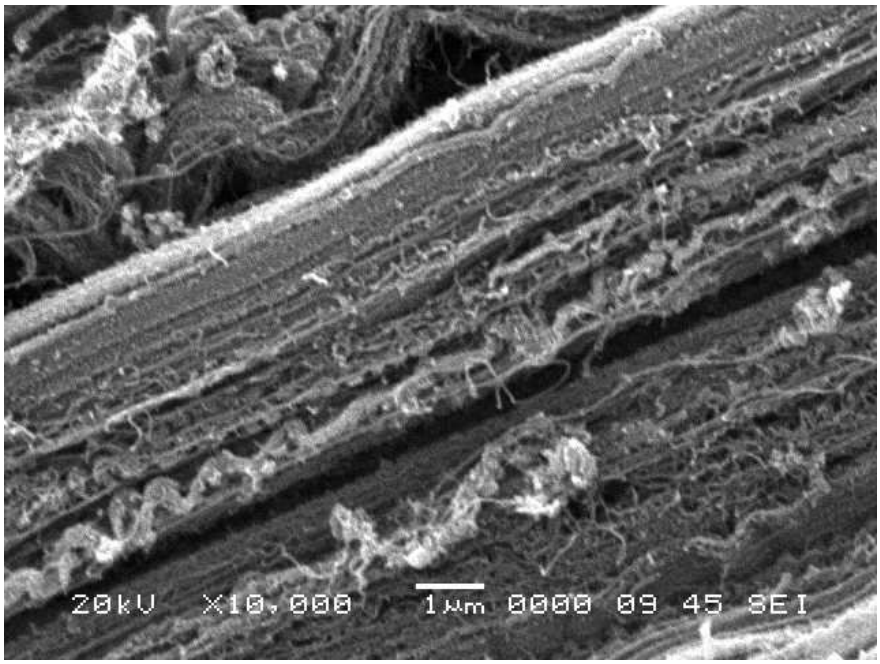

(e) A70 – H240

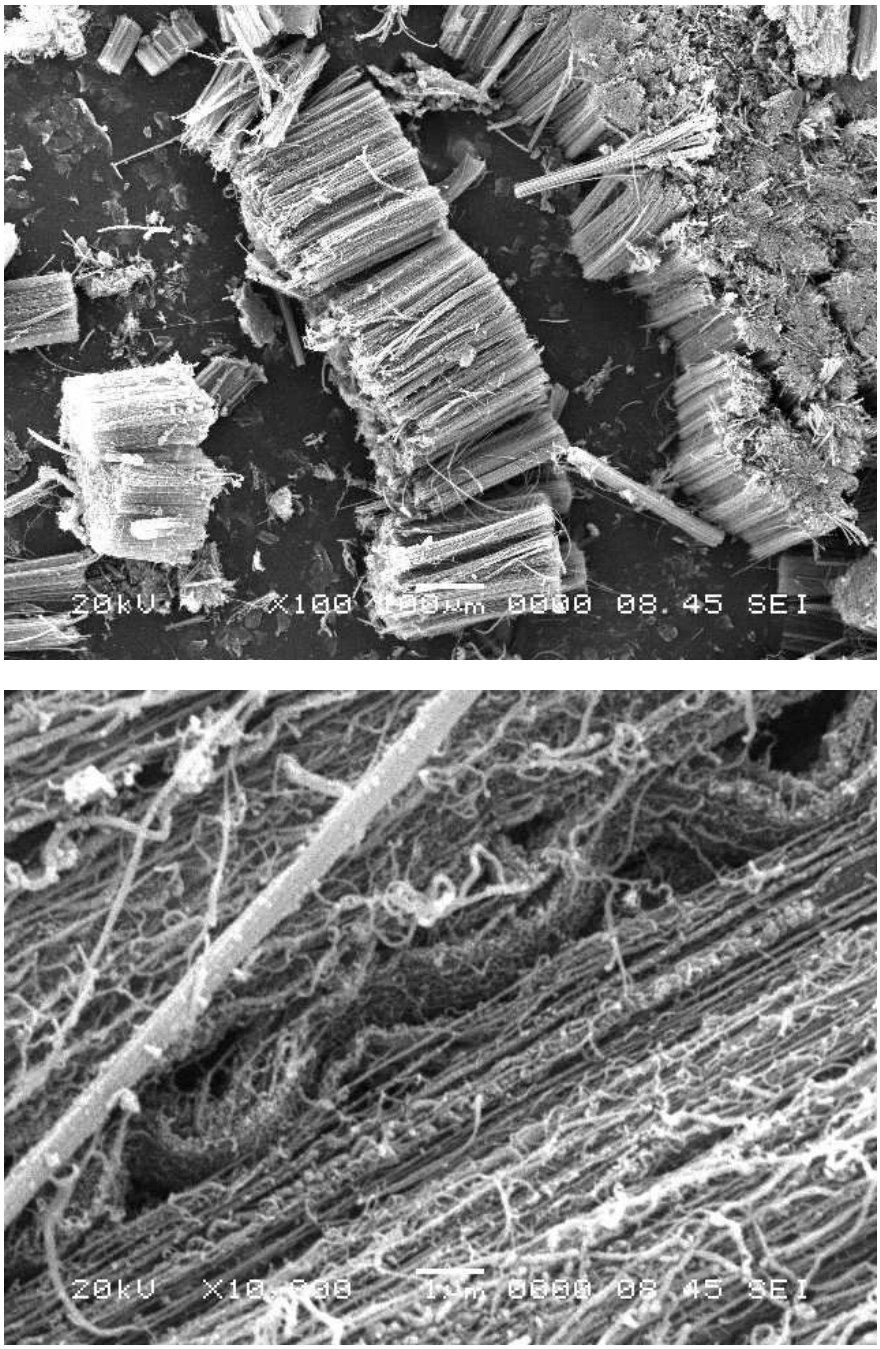

(f) A70 – H540

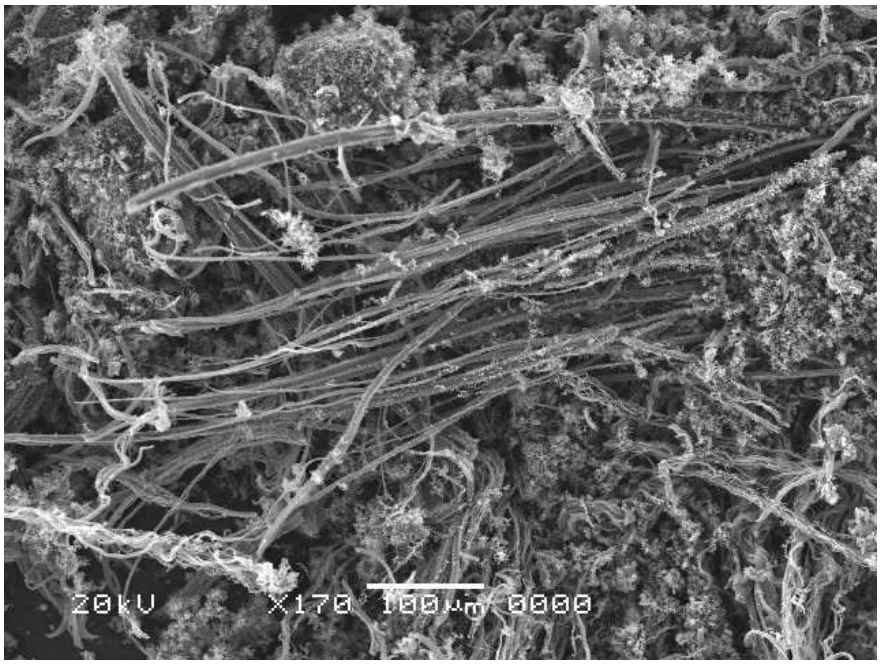

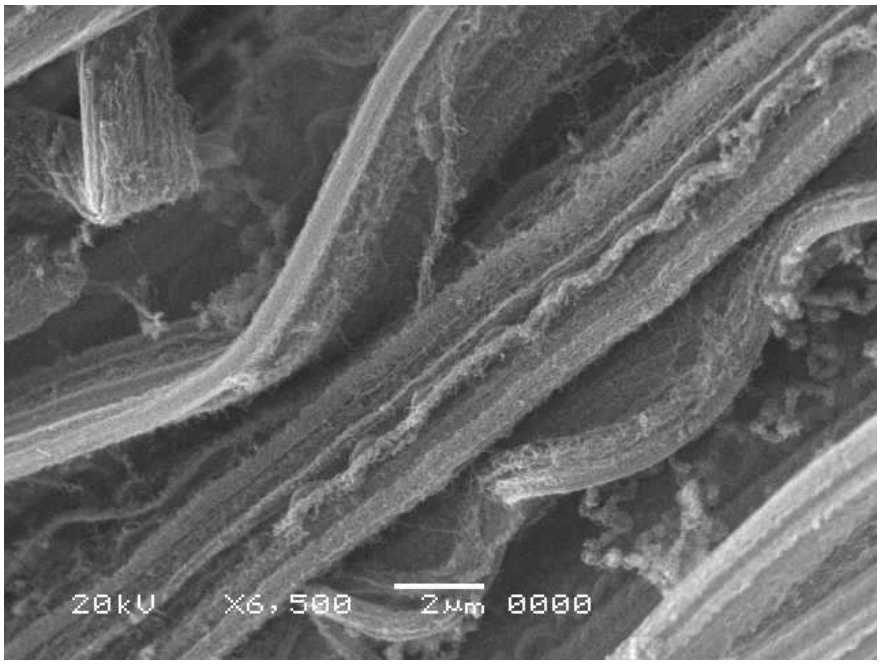

(g) A155 – H40

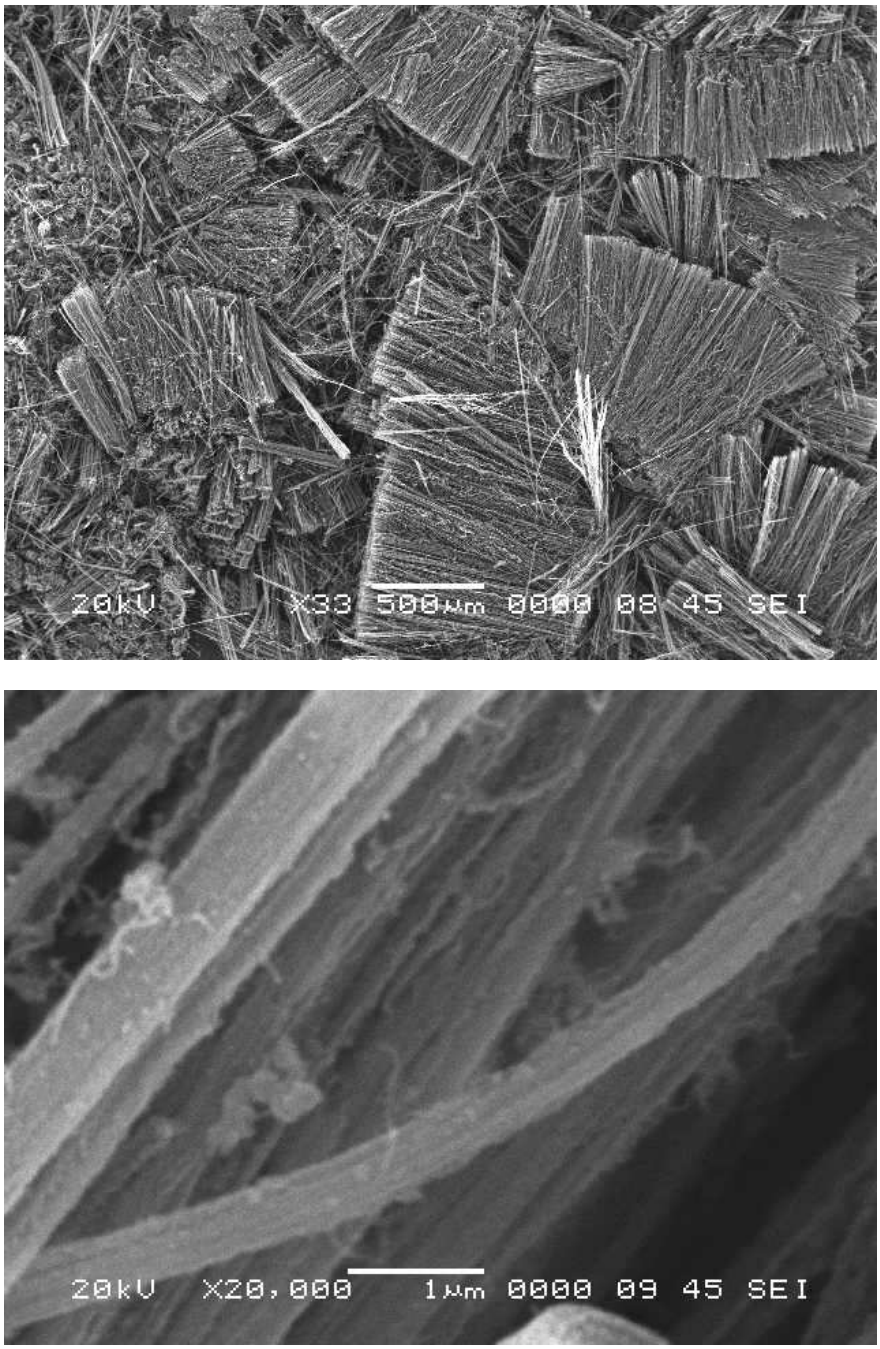

(h) A155 – H240

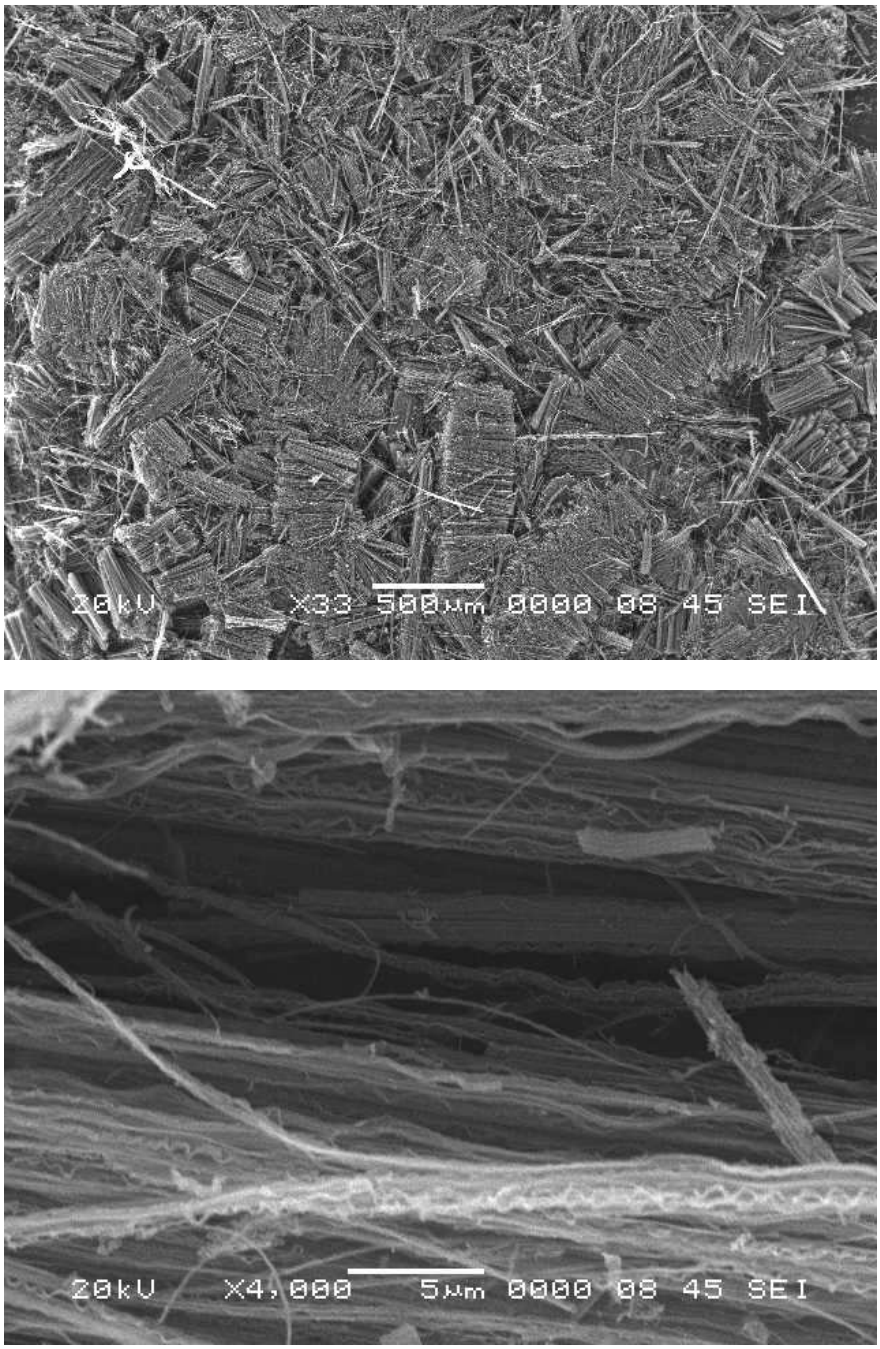

(i) A155 – H540

Figure 4.7: SEM images for CNTs produced by O-CVD with 6mm orifice at different acetylene and hydrogen flowrates.

4.1.2.3 Effect of Orifice on the Length of Aligned CNTs

Table 4.6 and figure 4.8 show the results of the length of aligned CNTs for different combination of hydrogen and acetylene flow rates while an orifice with 6 mm diameter was inserted at the entrance of reaction zone.

Table 4.6: The length of aligned CNT produced by O-CVD at different acetylene and hydrogen flowrates with 6mm orifice at reaction temperature and reaction time of 800^{o}C and 30 min respectively.

Orifice Diameter (mm)	Acetylene Flowrate (ml/min)	Hydrogen Flowrate (ml/min)	Length of CNTs (µm)
6	15	40	121.9
6	15	240	133.3
6	15	320	130.8
6	15	540	109.6
6	70	40	717.3
6	70	100	504.3
6	70	240	523.8
6	70	320	519.7
6	70	540	250.4
6	155	40	515.4
6	155	100	850.1
6	155	240	970.1
6	155	320	770.4
6	155	540	552.8

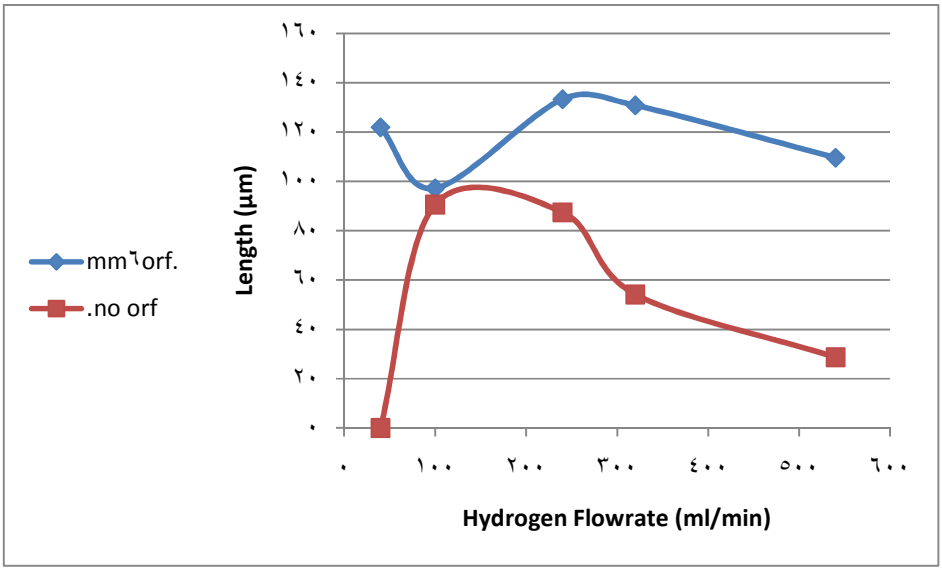
mm٦orf.
.no orf
Length (µm)
١٦٠
١٤٠
١٢٠
١٠٠
٨٠
٦٠
٤٠
٢٠
٠
٠
١٠٠
٢٠٠
٣٠٠
٤٠٠
٥٠٠
٦٠٠
Hydrogen Flowrate (ml/min)

(a)

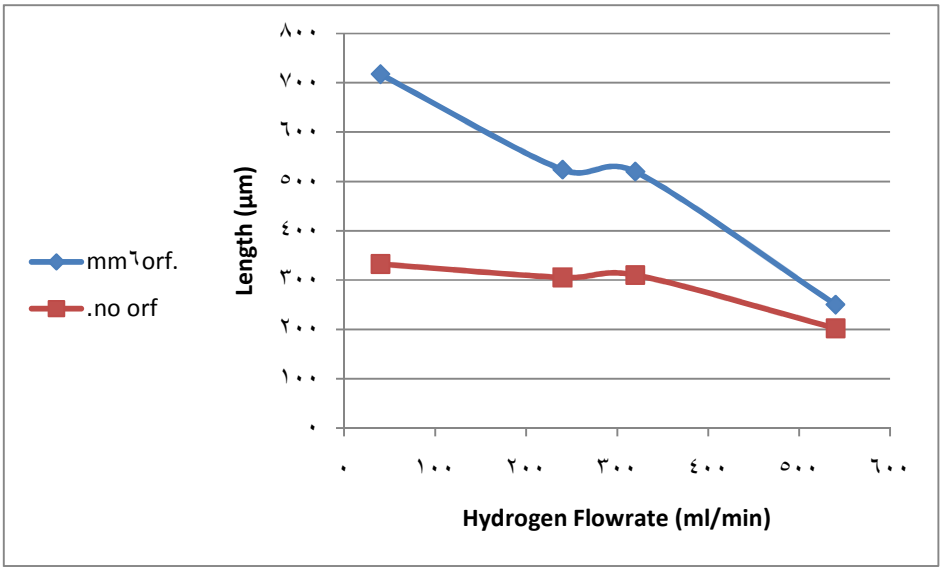
mm٦orf.
.no orf
Length (µm)
٨٠٠
٧٠٠
٦٠٠
٥٠٠
٤٠٠
٣٠٠
٢٠٠
١٠٠
٠
٠
١٠٠
٢٠٠
٣٠٠
٤٠٠
٥٠٠
٦٠٠
Hydrogen Flowrate (ml/min)

(b)

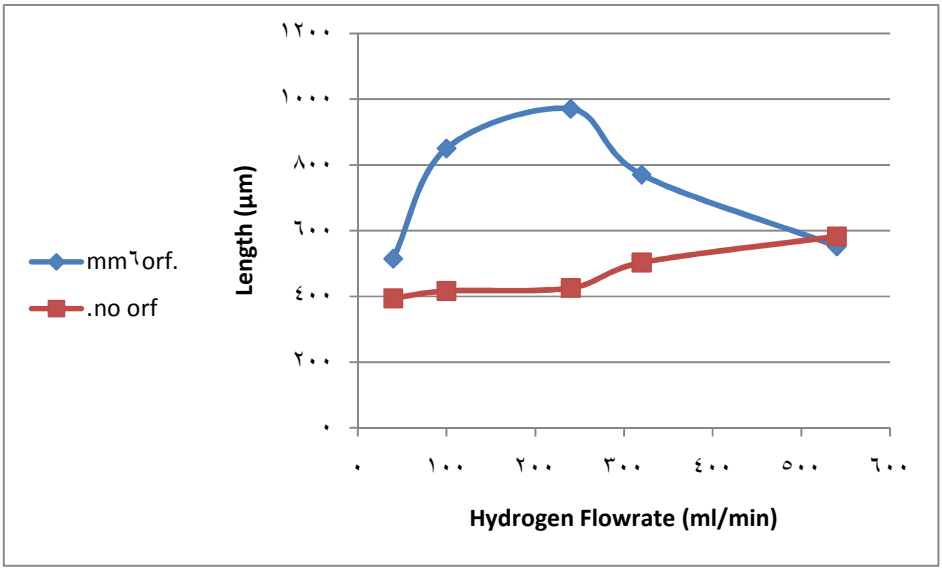

(c)

Figure 4.8: Length of CNTs produced by O-CVD without orifice and with 6 mm orifice versus hydrogen flowrate at acetylene flowrate of (a) 15 ml/min, (b) 70 ml/min and (c) 155 ml/min.

It is clear from figure 4.8 that introducing the 6mm orifice has increased the length of aligned CNTs significantly. This might be due to the flow of gases in narrow channels which give the chance for more continuous growth, beside the catalytic behaviour of the orifice which increases the number of carbon atoms able to form CNTs.

4.1.3 Effect of Reaction Time

The reaction time is the time taken by the acetylene/hydrogen/ferrocene gas mixture to flow through the tube furnace and it affects the formation the amount, purity and structure of produced CNTs. In this part, the hydrogen flowrate, acetylene flowrate, and reaction temperature were fixed at 240 ml/min, 155 ml/min and 800°C, respectively. An orifice with 6mm diameter was introduced. The reaction time was varied from 15 minute to 120 minute.

Table 4.7: The weight of deposited carbon produced by O-CVD at different reaction time with 6mm orifice at hydrogen flowrate, acetylene flowrate, and reaction temperature of 240 ml/min, 155 ml/min and 800°C, respectively.

Reaction Time (min)	Weight of Deposited Carbon (g)
15	0.113
30	0.950
60	1.197
120	2.819

It is clear from table 4.7 that when the reaction time was 15 minute only small amount of carbon nanotubes formed because the diffusion rate of Fe particles and C atoms were very low [105]. When the reaction time was increased, more acetylene dissociated and more carbon atoms started to grow as CNT up to 30 min. After 30 min, carbon impurities and soot started to appear. Muataz et al. noticed that after a certain time there was no increment in the amount of carbon deposition because all the catalyst had been consumed [105]. However, in our case we noticed that increasing the reaction time keep increasing the carbon deposition because we introduced the orifice which helps in decomposing the acetylene into carbon atoms, but since there is no enough catalyst that CNTs can grow on, the carbon deposited as impurities and soot as shown in figure 4.9, where we can noticed that increasing the reaction time decreasing the purity.

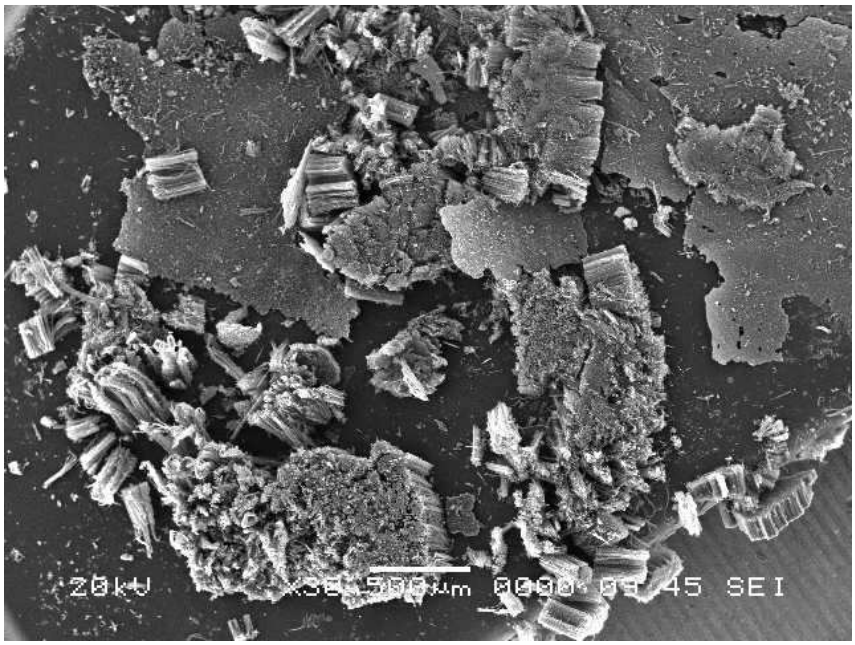

(a)

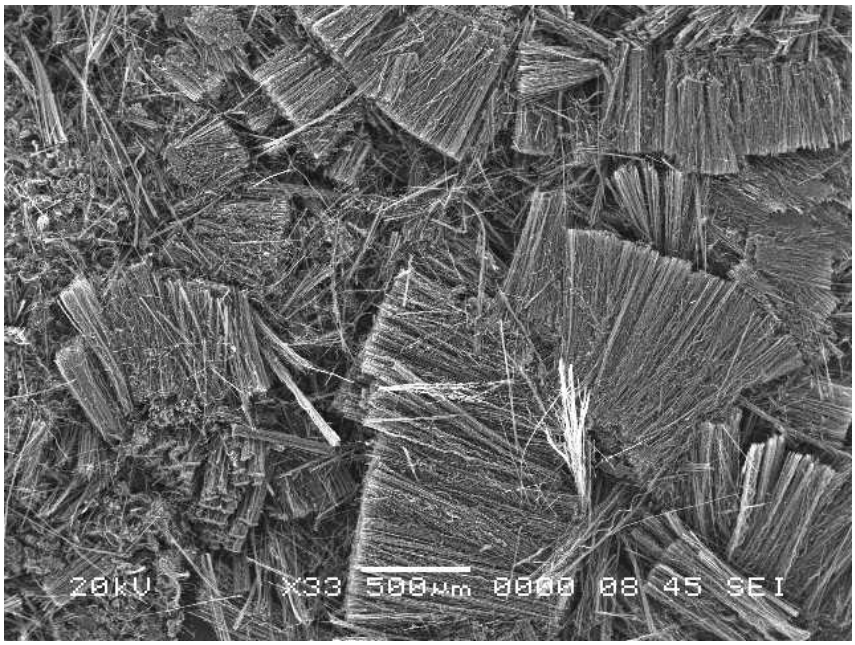

(b)

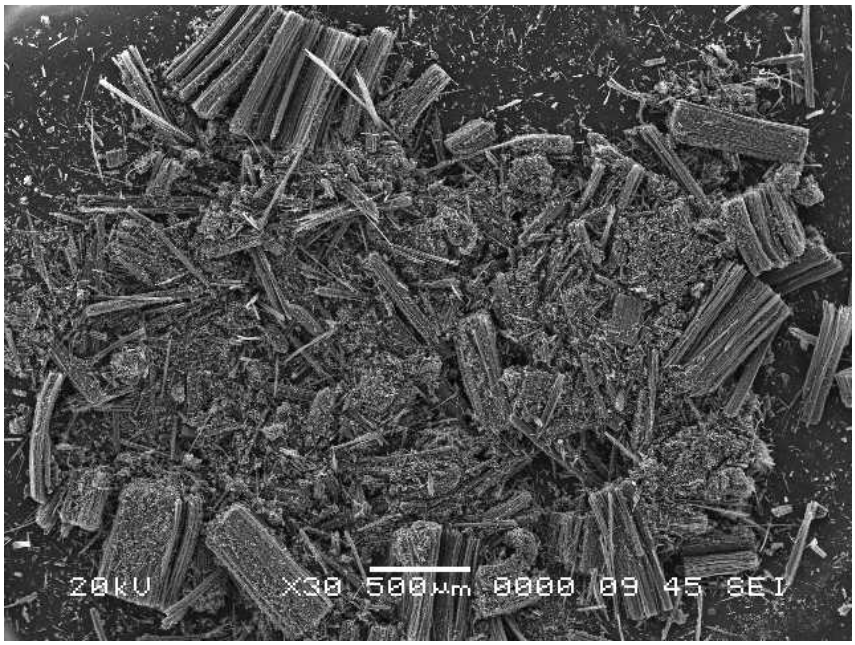

(c)

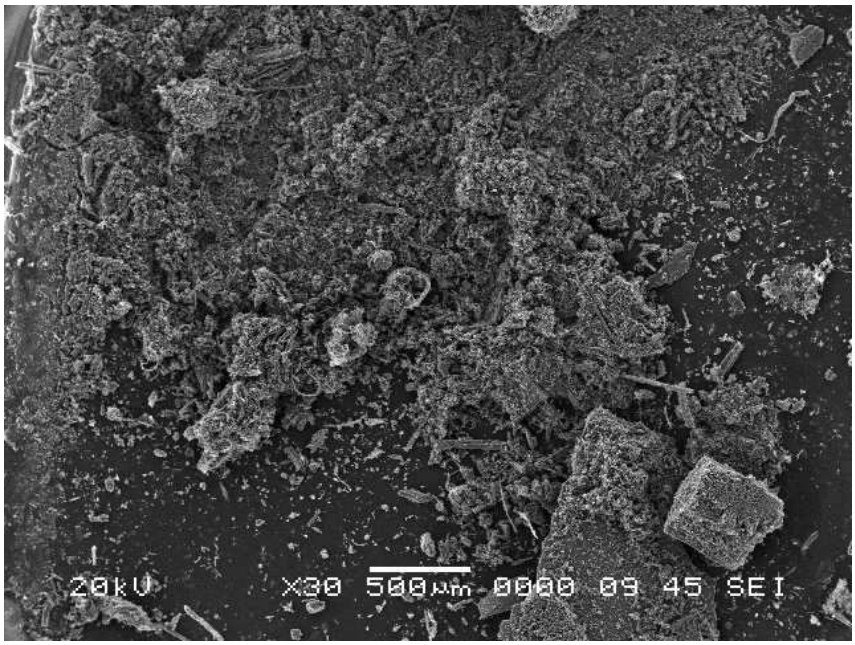

(d)

Figure 4.9: SEM images of carbon nanotubes at reaction time of (a) 15 min (b) 30 min (c) 60 min and (d) 120 min.

4.1.4 Effect of Reaction Temperature

In this study, the temperature was varied in the range (600 – 1000^{o}C) while the other parameters were as follows; hydrogen flowrate: 240 ml/min, acetylene flowrate: 155 ml/min, reaction time: 30 min and an orifice with 6mm diameter was introduced.

Figure 4.10 show the SEM images of carbon nanomaterial produced at different temperatures.

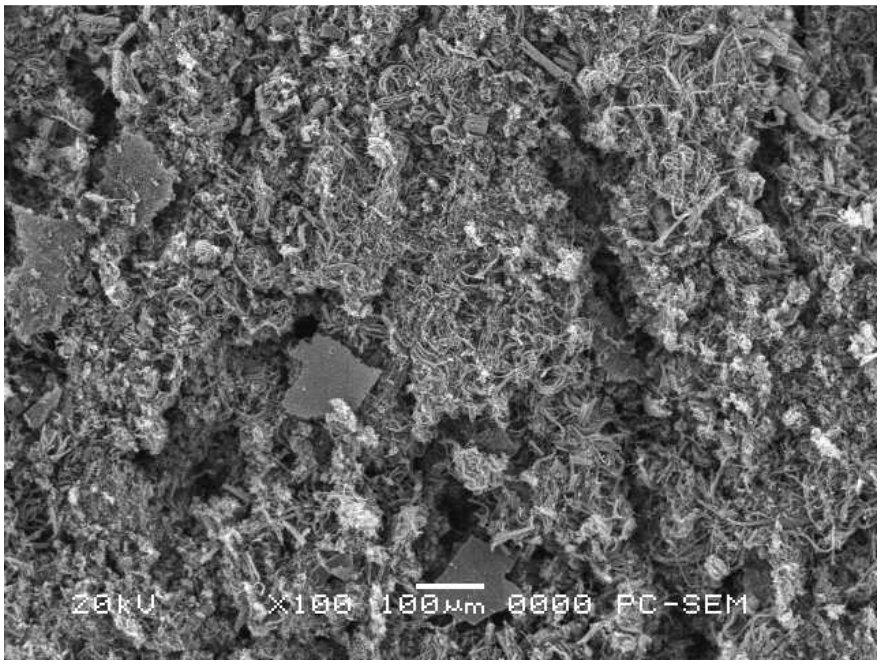

(a)

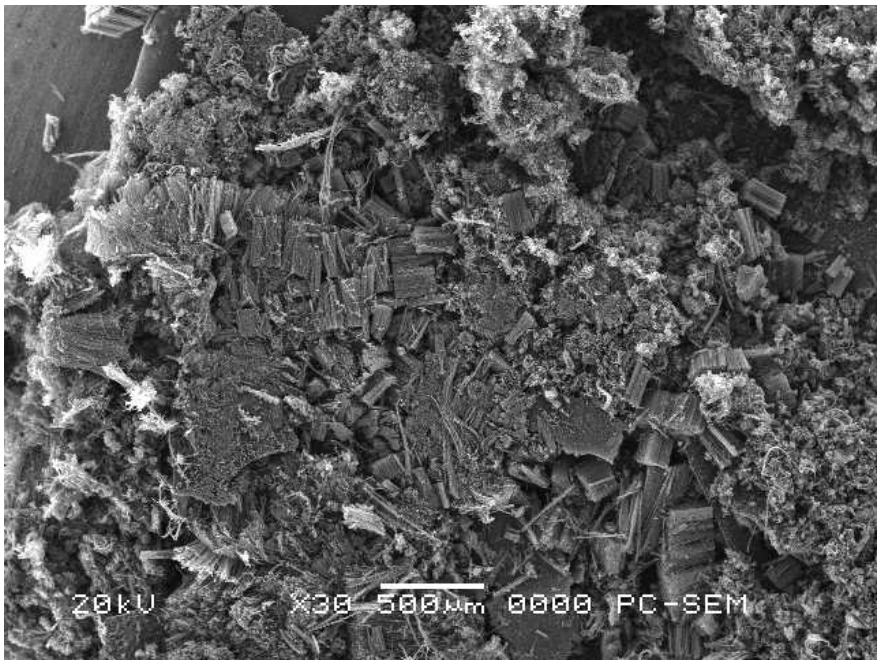

(b)

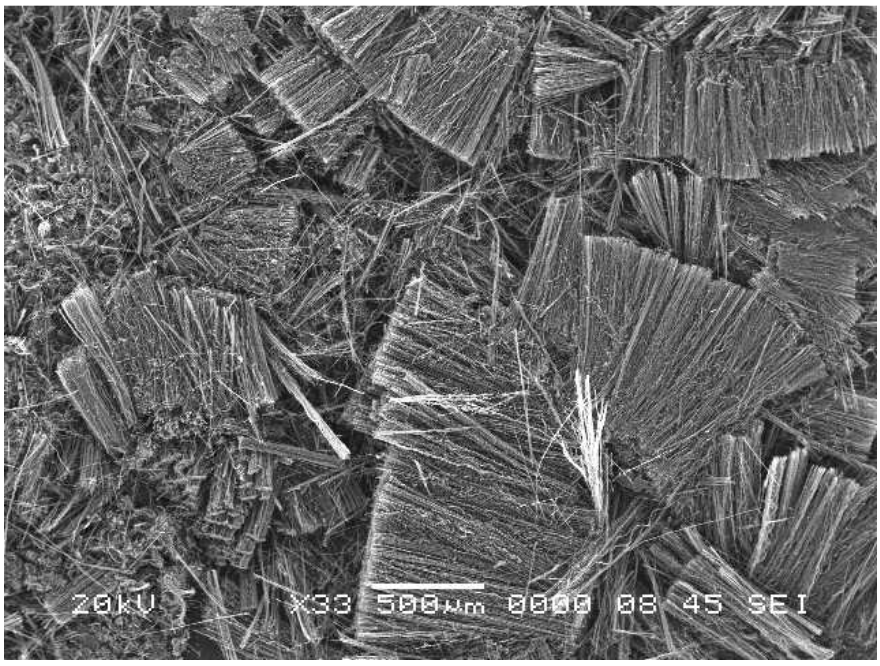

(c)

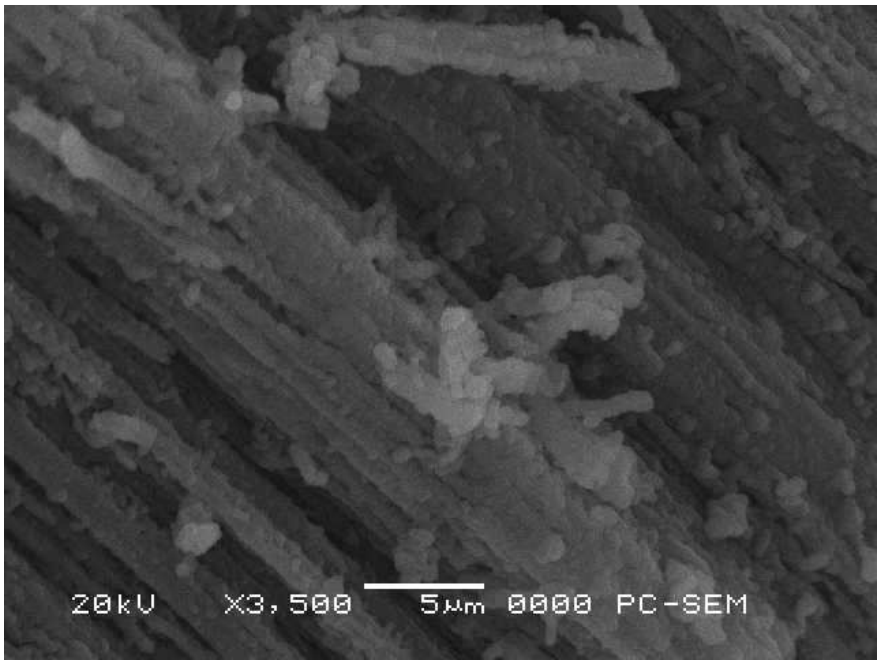

(d)

(e)

Figure 4.10: SEM images of carbon nanotubes at reaction temperature (a) 600 °C (b) 700 °C (c) 800 °C (d) 900 °C and (e) 1000 °C.

Using SEM images, it is difficult to distinguish between the CNTs and CNFs except from the size because both of them have the same surface view. However the two have different internal structure which cannot be observed using SEM technique. The difference in size had been used here to distinguish between the two materials because normally the size of CNTs are less than 100 nm while the size of CNFs are more than 100 nm. SEM images (figure 4.10(a,b and c)) show that CNTs are formed between 600 °C and 800 °C with increase in purity and yield as the temperature increases. CNF bundles were observed at 900 °C (figure 4.10(d)), suggesting that increasing the reaction temperature above 800 °C produced CNFs. When the temperature was 1000 °C, vapor grown carbon fiber would be produce as shown in figure 4.10(e).

4.1.4.1 The Role of Reaction Temperature [105]

The temperature influence on the structure of the carbon materials has been emphasized. It is generally accepted that carbon materials are formed by carbon atom dissolving, diffusing, and precipitating through the catalyst droplets in CVD process [106-108]. The dissolving, diffusing and precipitating rates of the carbon atoms are affected by both the carbon atoms concentration and the temperature. The carbon precipitation region on the Fe catalyst droplets can be distinguished into two areas, surface area and internal area. At low temperature, the carbon concentration from the decomposition of benzene over iron catalyst is certainly low. At temperature lower

than 900 °C, the dissolving and diffusing rates are limited by the low concentration of carbon atoms so that carbon atoms can only precipitate on the surface area of the catalyst droplets to form completely hollow CNTs. The diameter of CNTs gets bigger with the increase in temperature. This can probably be attributed to small catalyst droplets agglomerate at high temperature to form bigger catalyst particle which will form big CNTs. High reaction temperature will promote the decomposition of acetylene to increase the concentration of carbon atoms, which will increase the growth rate of CNTs to form bigger CNTs. With the increase of the temperature, the dissolving and diffusing rates of carbon atoms will increase, and carbon atoms can get to the internal area of the catalyst droplet to form CNFs. At high temperature, the carbon concentration is high enough for the precipitating at both side areas of the catalyst droplet to form vapor grown carbon fiber. As shown in our result, the temperature has induced the reconstruction of the metal faces of the catalyst. The change in the product from CNTs to CNFs at 900 °C was as mentioned due to the change in the catalyst faces. It shows that, at this reaction temperature the Fe catalyst reconstructs the atoms in the star shape while for CNTs the shape of the catalyst is spherical. The sizes of the CNFs catalyst are much bigger than that for CNTs as shown in figure 4.11.

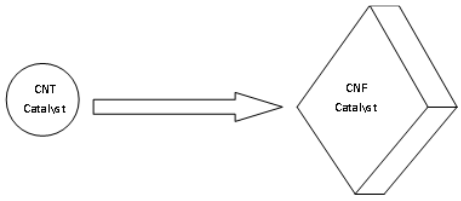

Figure 4.11: Schematic representation of the change in the size and the shape of the catalyst from CNT to CNF.

4.1.5 Finding the Optimum Conditions for Producing CNTs

By optimum conditions we mean those conditions at which the CNTs are producrd at high quality and quantity. Here we want to produce large amount of carbon nanotubes with high aspect ratio and high purity. By screening the previous results it is found that the optimum conditions are:

- Hydrogen flowrate: 240 ml/min
- Acetylene flowrate: 155 ml/min
- Orifice diameter: 6 mm
- Temperature: 800^{o}C
- Reaction time: 30 min.

The amount of produced CNT is 1.9 gram/hr with purity of 97.62% as shown in figure 4.12. Figures 4.13 and 4.14 are SEM and TEM images that show the length and diameter of optimum CNT. The length of the CNTs at optimum conditions

reaches 970 µm while the diameter is around 15 nm. These values results in aspect ratio of around 65000.

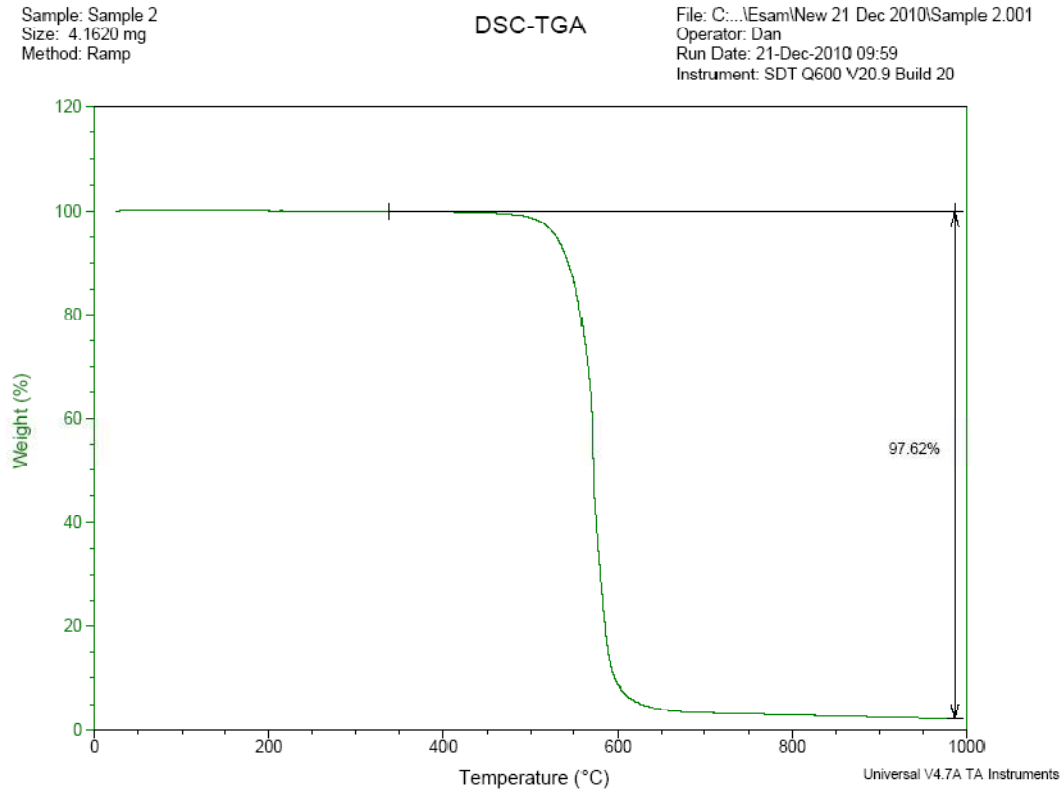

Figure 4.12: TGA curve for CNT produced at optimum conditions.

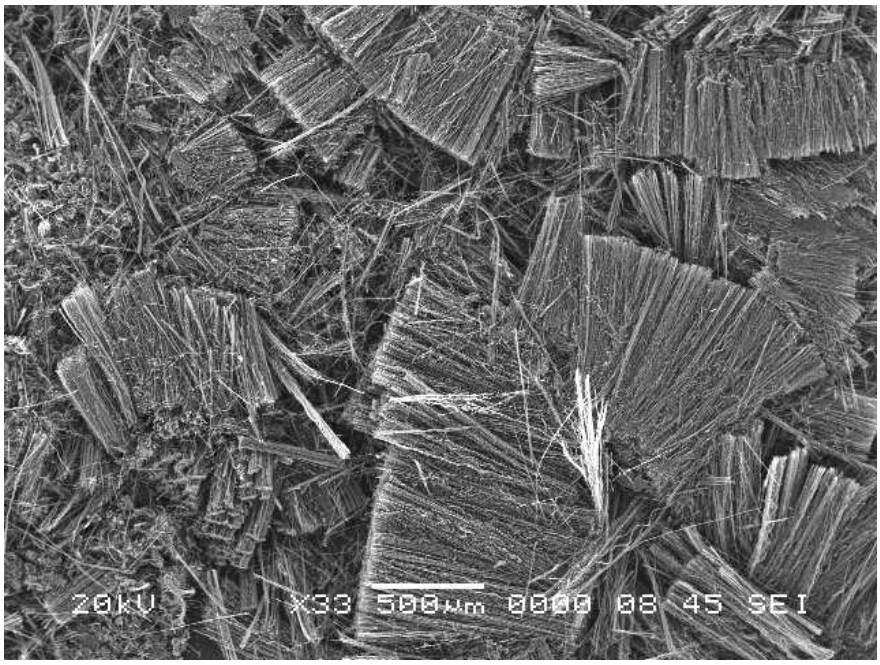

Figure 4.13: SEM image for CNT produced at optimum conditions.

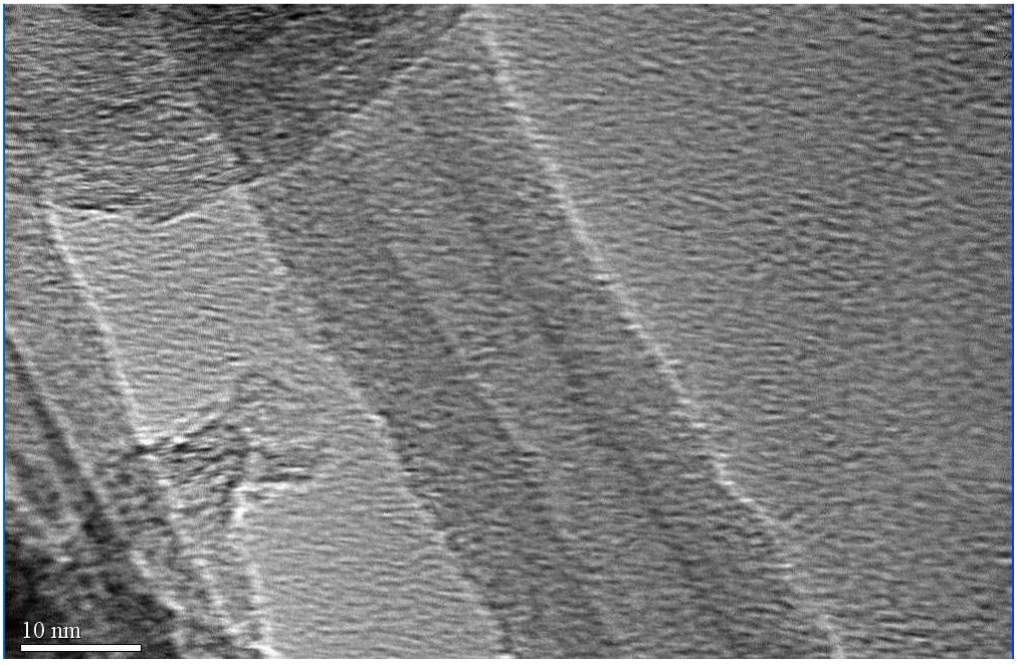

Figure 4.14: TEM image for CNT produced at optimum conditions.

4.1.6 Cost of the Production of Aligned CNTs at the Optimum Conditions

A preliminary cost calculation for the produced high quality CNT in the nanotechnlogy laboratories at KFUPM is given here. The cost calculation is based on producing CNT at the optimum conditions which are: orifice 6 mm, acetylene flowrate of 155 ml/min, hydrogen flowrate of 240 ml/min, reaction time is 30 min, reaction temperature is 800^{o}C, amount of ferrocene catalyst is 100 mg/run and argon gas is used to flush and cool down the system before and after each run.

Basis:

- 300 days/ year
- 8 hours/day
- 3 runs/day
- Each run produces 1 gram of high quality CNT.
- Which means total product is 9000 grams per year.

The following table shows the detailed cost of all items that are included in the production process.

Table 4.8: Cost of producing 1 gram of high quality CNT by O-CVD reactor.

Item	Description	Cost	Cost / gram of CNT
Reactor	2 furnaces + Ceramic tube + flow meters board (fixed cost)	30000 SR	3.33
Labor	10000 × 12 month	120000 SR/yr	13.33
Maintenance & Spare parts	Ceramic tube, Ceramic boats, miscellaneous	10000 SR/yr	1.11
Electricity	2.65 kW × 2 furnaces × 0.26 SR/kW.hr × 2 hrs	2.76 SR/run	2.76
Ferrocene Catalyst	0.1 gram × 1 SR/gram	0.1 SR/run	0.10
Argon Gas	24 cylinder/yr × 450 SR/cylinder	10800 SR/yr	1.20
H_2 Gas	550 SR/cylinder × cylinder/453067 L × 0.24 L/min × 30 min	0.009 SR/run	0.01
C_2H_2 Gas	140 SR/cylinder × cylinder/4700 L × 0.155 L/min × 30 min	0.139 SR/run	0.14
Total			**21.98**

So the total estimated cost is **21.98 SR/gram** which is **5.86 US$**.

4.2 FT-IR Spectroscopy for Functionalization of Carbon Nanotubes

In order to identify the existence of functional groups on the MWCNTs surface, Fourier transform infrared spectroscopy (FTIR) was conducted for all the nanotubes in the range of 400 to 4000 cm^{-1}. FTIR spectroscopy has been widely employed in the determination of structure of molecules [109]. Its application in the study of surface chemistry has provided one of the direct means of observing the interaction and perturbations that occur at the surface during adsorption and in determining the structure of the absorbed species. Fig. 4.15 shows the spectra of unmodified MWCNT.

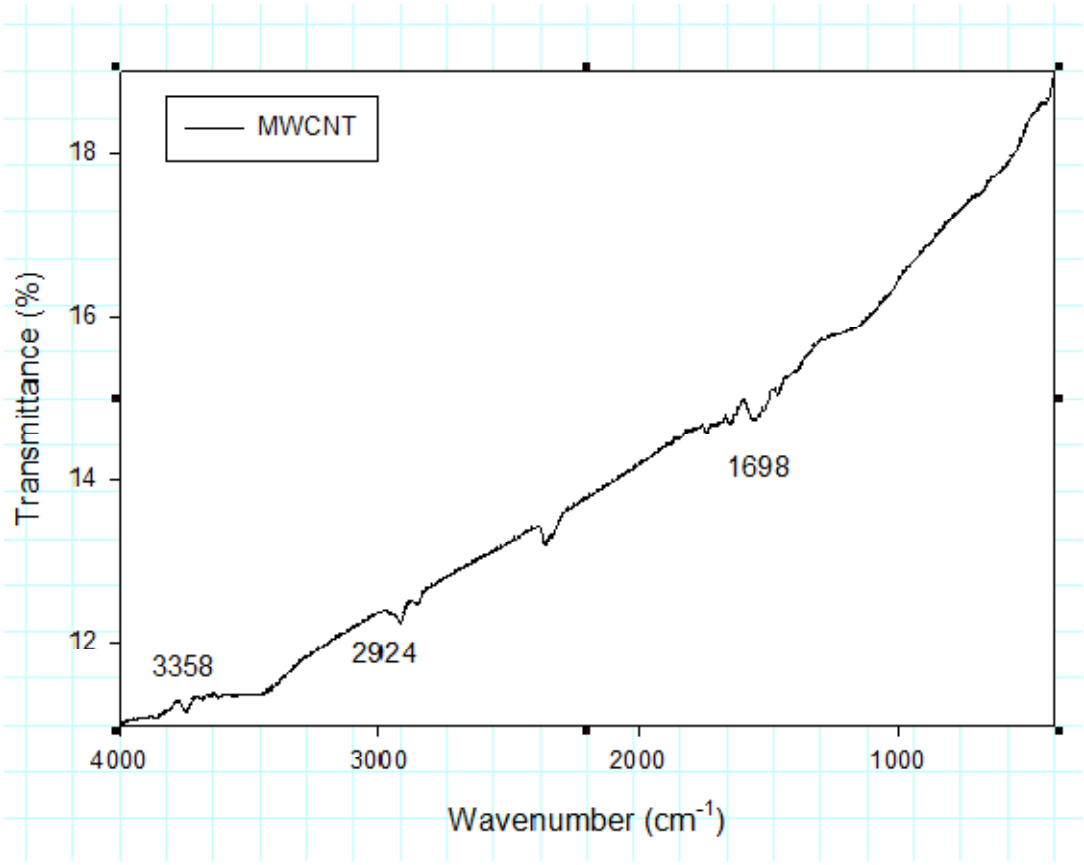

Figure 4.15: FTIR spectrum of unmodified multiwall carbon nanotubes (MWCNT)

The IR spectrum for the unmodified MWCNT shows absorption band at 3358 cm^{-1} attributed to hydrogen bonded O-H stretching, 2920 cm^{-1} which is attributed to symmetric and asymmetric CH2 stretching and 1698 cm^{-1} (assigned to carboxylic C=O stretching for acids groups. The presence of these functional groups on the surface of pure MWCNTs indicates their introduction during removal of metal catalysts in nanotubes purification processes. On acid modification of the nanotubes

with concentrated nitric acid, a new spectrum was obtained as shown in the Figure 4.16 below

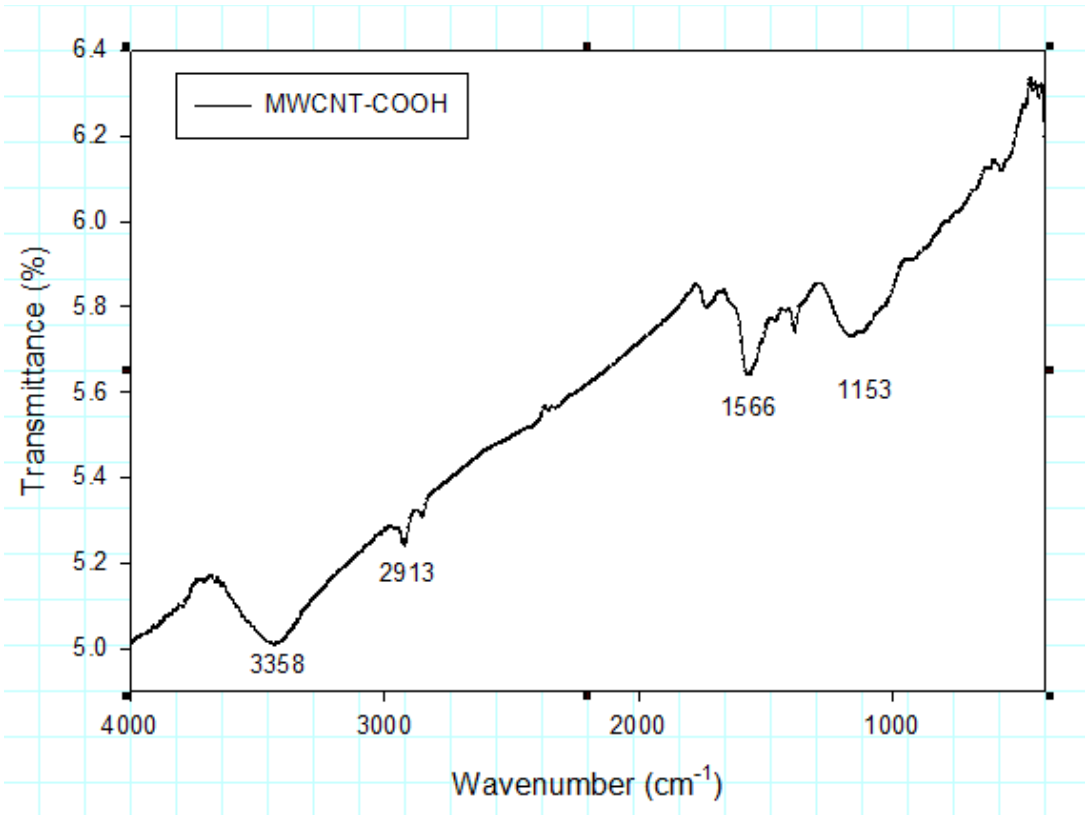

Figure 4.16: FTIR spectrum of acid modified multiwall carbon nanotubes (MWCNT-COOH)

In this new IR spectrum of CNT-COOH, an adsorption band at 3358 cm^{-1} (hydrogen bonded O-H stretch) is ascribed to the characteristic spectrum of carboxylic acid. As can be seen from figure Fig 4.16 above, this particular peak is

usually broad and can obscure other peaks within the entire region of 3400 to 2400 cm^{-1}. Moreover, carboxylic peak C=O stretching peak is observed at 1693 cm^{-1}. The existence of these peaks signified the success of surface modification of the CNTs with carboxylic acid group. Similarly, substitution of MWCNT-COOH with phenolic group (Figure 4.17) gives indicative peaks at 1452 cm^{-1} (corresponding to C-C=C asymmetric stretching for Aromatic rings) and a strong peak at 1228 cm^{-1} due C-O stretching of phenolic ester.

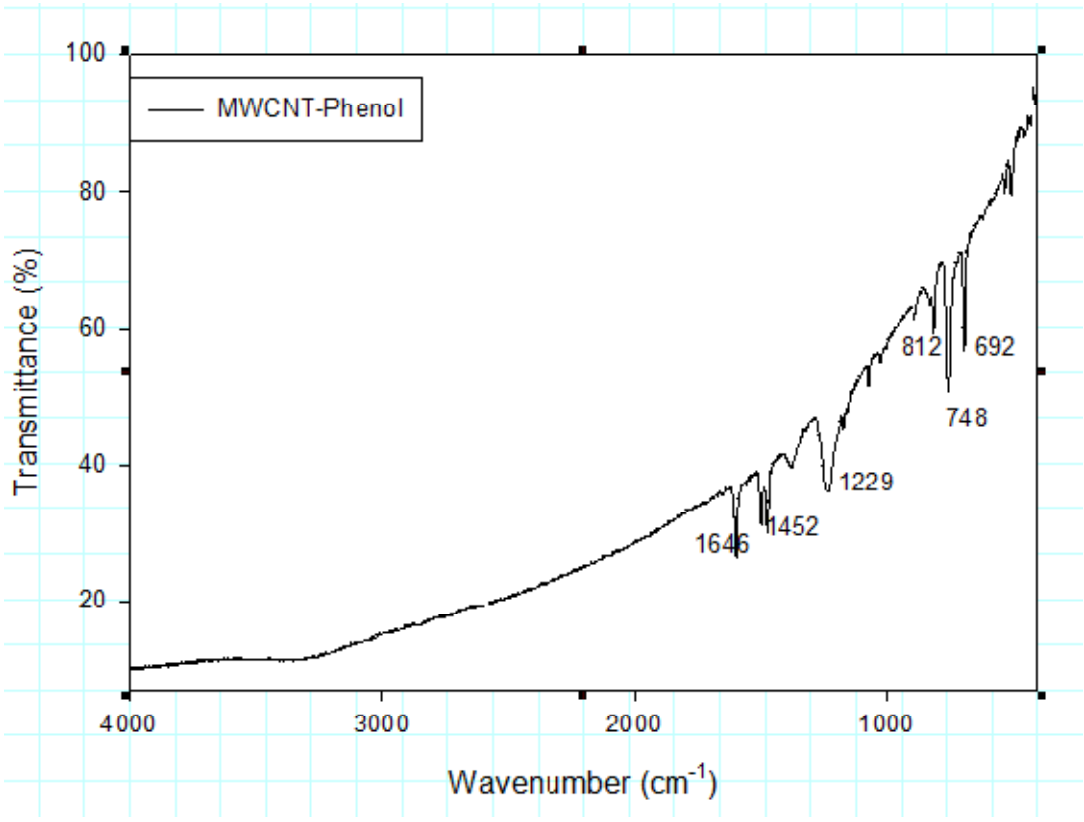

Figure 4.17: FTIR spectrum of phenol modified multiwall carbon nanotubes (MWCNT-Phenol)

Moreover, strong peaks at 812 cm^{-1}, 748 cm^{-1} and 692 cm^{-1} indicating the existence of phenoxide groups generated from the reaction between carboxylic COOH and phenyl alcohol was also indentified.

Figure 4.18 shows the IR spectrum modification of MWCNT-COOH with 1-Octadecanol.

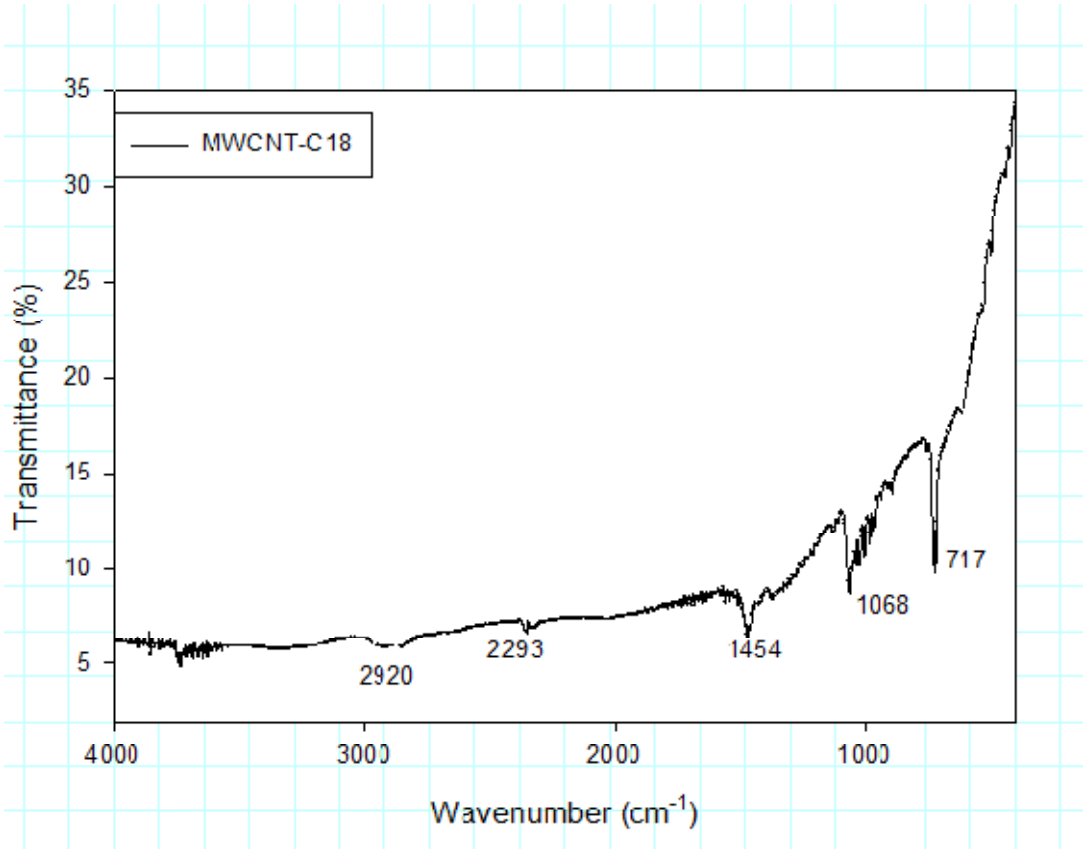

Figure 4.18: FTIR spectrum of C18 modified multiwall carbon nanotubes (MWCNT-C18)

An indicative peaks at 2920 cm^{-1} correspond to CH2 stretching of long alkyl molecule of 1-Octadecanol emanates upon modification of MWCNT-COOH to MWCNT-C18. In addition, modification with Octadecanol gives a medium C-H stretch and C-H bend of alkanes at 2293 cm^{-1} and 1454 cm^{-1} respectively. An indicative of long chain alkyl ester at 1068 cm^{-1} generated from esterification reaction of OH group of Octadecanol and COOH group of acid modified carbon nanotubes was also identified. Finally, a peak showing C-H sharp bend at 717 cm^{-1} also indicate the success of MWNCT-COOH modification with Octadecanol. Thus we have MWCNT-C18 modified carbon nanotubes.

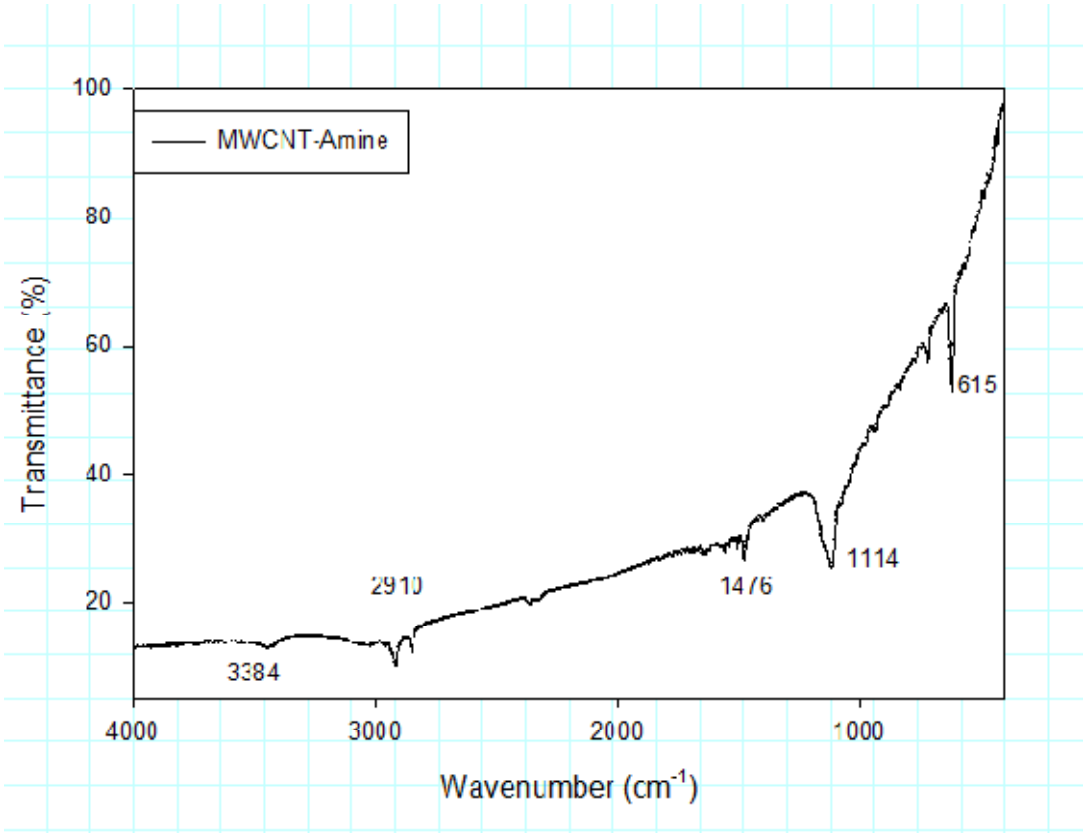

Figure 4.19: FTIR spectrum of amine modified multiwall carbon nanotubes (MWCNT-amine)

Nanotubes modification with Dodecylamine (Figure 4.19) gives a peak at 3384 cm^{-1} (N-H stretch for amides), 1476 cm^{-1} strong N-O asymmetric stretching for nitro compounds and 1114 cm^{-1} medium C-N stretch indicative peak for aliphatic amines. Lastly MWCNT-COOH modification with Dodecylamine gives N-H wag peak at 615 cm^{-1} for primary or secondary amine.

4.3 Properties of Polystyrene/CNT Nanocomposites

Polymer nanocomposites based on carbon nanotubes (CNT) are attracting attention due to their remarkable mechanical, thermal, and electrical properties. Polystyrene (PS) is a versatile polymer with the features of low price, good optical transparency, excellent electric insulation and mechanical properties. The dispersion of carbon nanotubes into PS matrix for the fabrication of PS/CNT composite has naturally stimulated significant interest among researchers [75].

In this study, PS/CNT nanocomposites were prepared by thermal bulk polymerization without any initiator. Different weight percentages of CNT, CNT-COOH, CNT-C18 and CNT-Phenol were used in order to investigate the mechanical, rheological and thermal properties of the synthesized nanocomposites.

4.3.1 Effect of Acid Treated Carbon Nanotubes on Mechanical, Rheological and Thermal Properties of PS/CNT-COOH Nanocomposites

In this part, PS/CNT and PS/CNT-COOH nanocomposites were prepared by thermal bulk polymerization without any initiator. Different weight percentages (0.1, 0.5, 1, 2 and 5 wt.%) of CNT and CNT-COOH were used in order to investigate the mechanical, rheological and thermal properties of the synthesized nanocomposites.

4.3.1.1 Mechanical Properties of PS/CNT-COOH Nanocomposites

The mechanical properties of PS in comparison to PS/CNT and PS/CNT-COOH are reported in Table 4.9. Young moduli were determined with tensile test curves obtained at ambient temperature. Pure PS has an Young's modulus of 922 MPa. With 0.1 wt.% and 0.5 wt.% of pure CNT we observed a little increase in Young's modulus to values of 937 and 1004 MPa, respectively. However, a higher increase in Young's modulus was observed upon loading with acid treated CNT. The 0.1 wt.% and 0.5 wt.% of CNT-COOH increased the Young's modulus to 1077 and 1126 MPa, respectively. With 5 wt.% of pure MWCNTs we observed a remarkable Young's modulus increase of 49.7% (1380 MPa). On the other hand, 5 wt.% of MWCNT-COOH composites show a high Young's modulus increase of 67% (1534 MPa). The acid modification of CNT seems to enhance the dispersion of the nanotubes within the PS matrix, as shown in figure 4.20 (a and b), which permit a larger matrix/filler contact area [110]. Also, stress transfer might increase because of a better interface between the matrix and the filler [110]. Similar reports are available indicating reinforcement of polymers by CNT and modified CNT [5, 97, 98].

It is noticed that Young's moduli for PS/1.0%CNT and PS/2.0%CNT composites has decreased to 884 and 878 MPa, respectively, which are below the Young's modulus of pure PS. This is due to the fact that the increasing the amount of CNT during the polymerization process results in a decrease in the molecular weight of polymer [78] and due to the formation of large agglomerates of CNTs, as shown in figure 4.20 (c

and d), which penetrates the polymer matrix and reduce the matrix/filler interaction. The following increment in Young modulus for PS/5.0%MWCNT suggests that there is a threshold value between 2 and 5 wt.% where the effect of reduction in molecular weight on reducing Young modulus has been overcome and exceeded due to the high Young modulus of CNTs filler. These results suggest that 0.5 wt.% is the best loading in terms of stress-strain properties.

Maximum stress and elongation at break values of the composites are also given in Table 4.9. It is clear that addition of MWCNT and MWCNT-COOH decreased the elongation at break values which means that the composites became stiffer in nature.

Table 4.9: Summary of mechanical properties of pure PS, PS/CNT and PS/CNT-COOH nanocomposites at different CNT loadings.

Composite	Young's modulus (MPa)	Maximum Stress (MPa)	Elongation at break (%)
PS	922.2 ± 53.9	18.62 ± 0.6	2.88 ± 0.3
PS/0.1%CNT	936.6 ± 22.5	19.66 ± 0.4	2.42 ± 0.2
PS/0.5%CNT	1004.4 ± 10.2	22.40 ± 0.4	2.54 ± 0.2
PS/1.0%CNT	884.0 ± 31.7	16.77 ± 0.9	2.38 ± 0.3
PS/2.0%CNT	877.7 ± 26.8	18.39 ± 0.9	2.26 ± 0.2
PS/5.0%CNT	1380.46 ± 66.8	17.77 ± 0.8	1.29 ± 0.2
PS/0.1%CNT-COOH	1077.0 ± 28.5	18.94 ± 0.5	2.49 ± 0.2
PS/0.5%CNT-COOH	1126.1 ± 28.5	20.27 ± 0.7	1.94 ± 0.2
PS/1.0%CNT-COOH	1057.0 ± 12.8	17.80 ± 1.0	1.77 ± 0.2
PS/2.0%CNT-COOH	1024.8 ± 43.6	15.62 ± 0.5	1.68 ± 0.2
PS/5.0%CNT-COOH	1534.03 ± 73.6	26.64 ± 0.9	1.86 ± 0.2

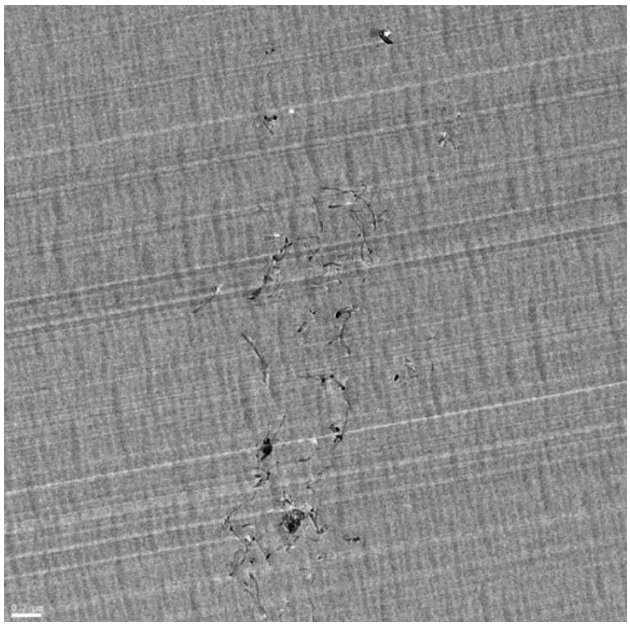

(a)

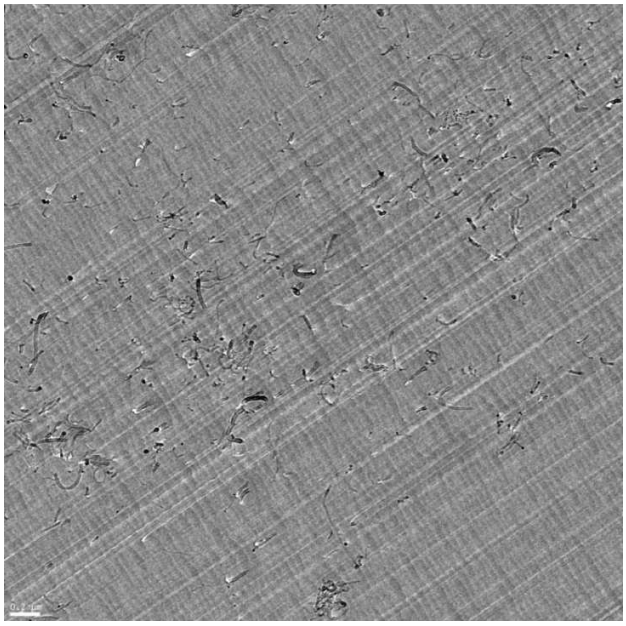

(b)

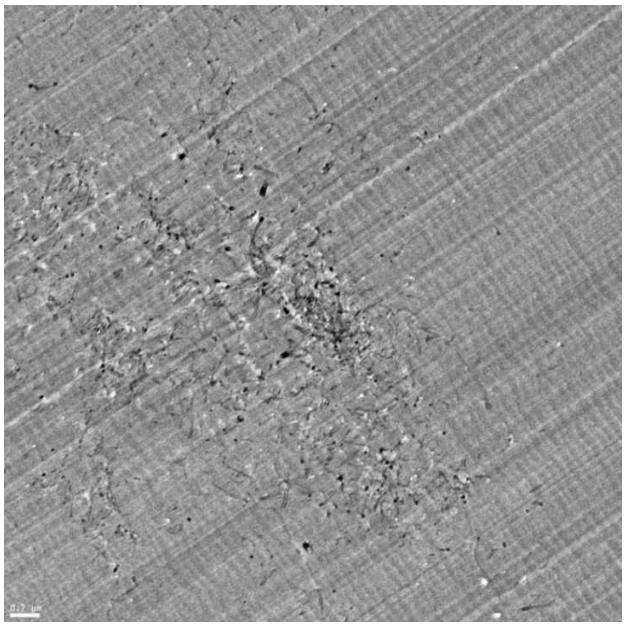

(c)

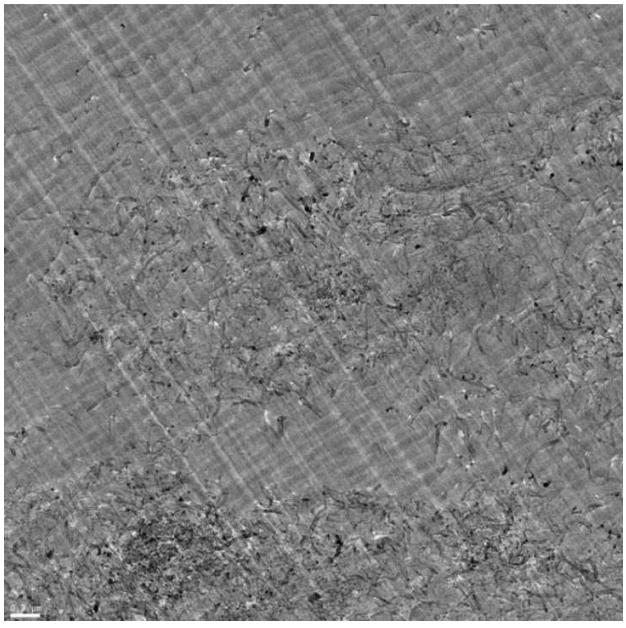

(d)

Figure 4.20: TEM images of a) 0.1wt.% CNT-COOH-PS, b) 0.5wt.% CNT-COOH-PS, c) 1wt.% CNT-COOH-PS and d) 2wt.% CNT-COOH-PS nanocomposite. (Scale is 200 nm).

4.3.1.2 Differential Scanning Calorimetry Study and Thermogravimetric Analysis

Differential scanning calorimetry allows distinguishing the influence of adding CNT to PS matrix based on the values of glass transition temperature. Table 4.10 and Figure 4.21 show the results and values of T_g obtained for PS composites with different MWCNT and MWCNT-COOH loadings. Pure PS exhibits a glass transition at 106.3^{o}C, in agreement with values reported in the literature [111]. Nanocomposites with 1 wt.% of MWCNT exhibit a change in the glass transition temperature which is 105.03^{o}C with a reduction in T_g of about 1.2^{o}C while composites with 1 wt.% of MWCNT-COOH have a T_g value of 104.6^{o}C which is below that of pure polystyrene by 1.7^{o}C. It is well known that the polystyrene glass transition temperature T_g is almost constant for molecular weight (M_n) over 10^5 g mol^{-1} [111-113]. Below this value, the glass transition temperature starts to decrease, following an empirical relation such as

$$T_g = T_g^{\infty} - \frac{C}{M_n} \qquad (4.1)$$

where C is a constant (1.2×10^5 for PS) and T_g^{∞} refers to the T_g for very large M_n. As a consequence of Eq. (1), we attribute the decrease in glass transition temperature observed to the reduction in polystyrene molecular weight formed via the polymerization in the presence of CNT.

Table 4.10: Glass transition temperature (T_g), T onset and maximum degradation temperature of PS/CNT and PS/CNT-COOH nanocomposites.

Composite	T_g (^oC)	T onset (^oC)	T max (^oC)
PS	106.26	335	400
PS/0.1%CNT	106.19	363	410
PS/1%CNT	105.03	366	412
PS/0.1%CNT-COOH	104.64	364	415
PS/1%CNT-COOH	104.62	367	420

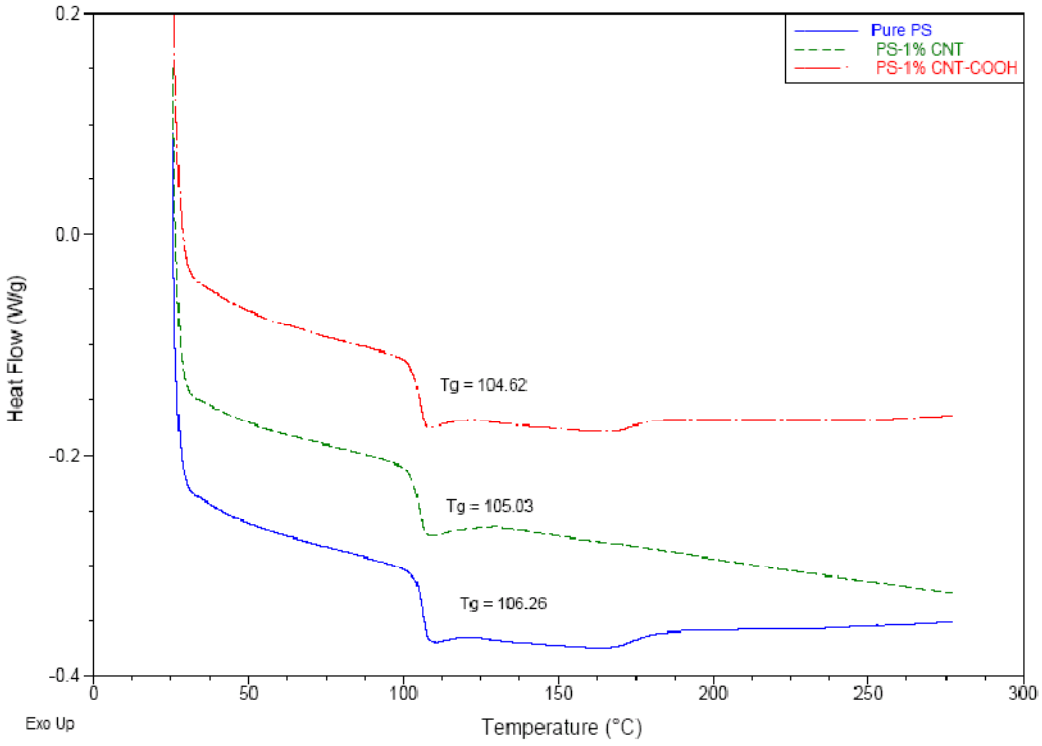

Figure 4.21: Glass Transition observed by DSC for pure PS, 1wt.% CNT-PS nanocomposite and 1wt.% CNT-COOH-PS nanocomposite.

Figure 4.22 shows the TGA and DTG curves of the virgin PS and composites of 0.1 and 1 wt% loading of both untreated and treated CNT. All the samples show a single degradation step which is the decomposition of the polymer backbone. From the TGA curves, it is seen that the acid treated composites show a slight degradation in the temperature range of 200-300^{0}C which may be due to the release of carbonyl groups associated with the treated CNT. However, this small degradation step is not reflected in the DTG curves. The DTG curves show a single peak corresponding to the maximum degradation temperature for the composites. From both TGA and DTG curves the onset of degradation and maximum degradation temperature were calculated (Table 4.10). It can be seen that the incorporation of CNT into PS has enhanced the onset of degradation to almost 30-40^{0}C for all the composites. Also the maximum degradation temperature of the composites showed an increase of 10-20^{0}C. The incorporation of CNT into PS enhanced the thermal properties significantly.

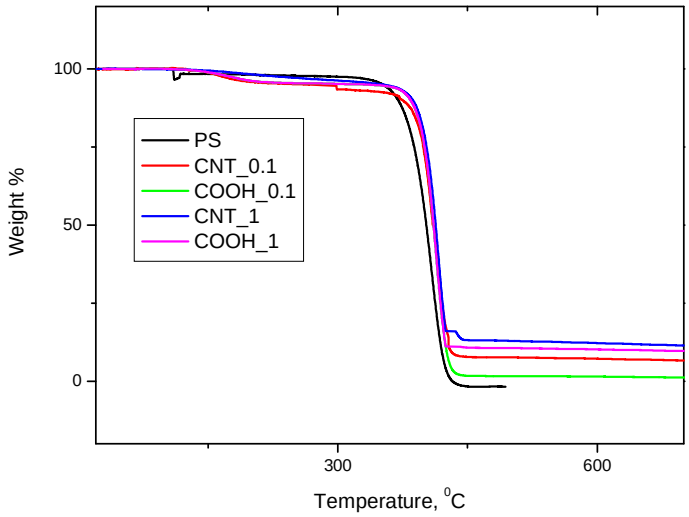

(a)

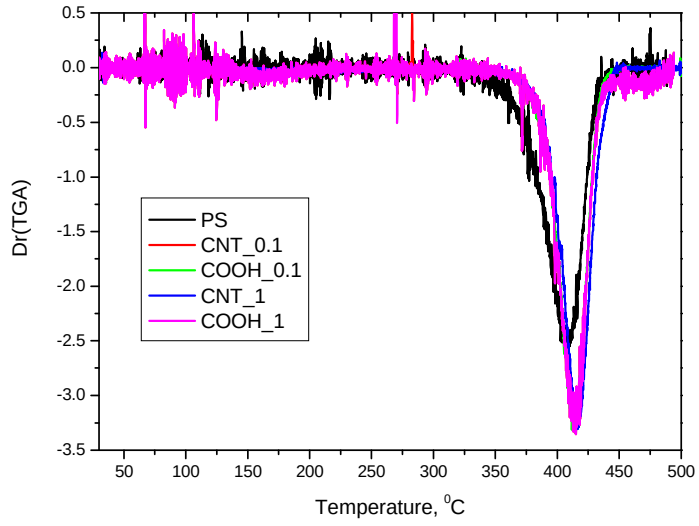

(b)

Figure 4.22: (a) TGA and (b) DTG curves of 0.1 and 1 wt% of the composites with CNT and CNT-COOH

4.3.1.3 Rheological Behavior of PS/CNT-COOH Nanocomposites

Rheology is the study of the flow behavior of a material under conditions in which they flow rather than showing elastic or plastic deformation [76]. The rheological properties of CNT/polymer nanocomposites depend on factors such as the characteristics of the filler loading, aspect ratio and dispersion, polymer molecular weight, and the interaction between the polymer and filler [76, 114-118]

The PS/CNT nanocomposites were investigated for their dynamic rheological properties. Figures 4.23-4.26 are the experimental results for the various rheological parameters obtained via dynamic melt rheology from the PS/MWCNT nanocomposites. Figure 4.23 and 4.24 are experimental results for the storage modulus, *G'*, and the loss modulus, *G''*, for the PS matrix and the composites containing 0.1, 0.5 and 1.0 wt.% loading of untreated CNT and acid treated CNT with respect to frequency. Both *G'* and *G''* increase with CNT concentration in the case of untreated CNT, while for CNT-COOH the moduli start to increase above those of pure PS since 1 wt% loading only. This results suggest that below 1 wt.% the acid treated CNT act as a plasticizer. The effect of nanotubes is more pronounced at lower frequencies and the relative effect diminishes with increase in frequency due to shear thinning. This result is in agreement with theoretical and experimental observations for fiber-reinforced composites [119-121].

Figure 4.25 shows the relationship between complex viscosity and frequency. It is obvious that in all cases, the viscous properties of the composites decreases with

increasing frequency. It is a general phenomenon that addition of fillers into polymer matrices increase the viscoelastic behavior of the polymeric materials as observed in figure 4.25 (a) for the composites with untreated CNT. However, this was not the case with 0.1 and 0.5 wt.% loadings of CNT-COOH nanocomposites. Figure 4.25 (b) shows that the complex viscosity of the composite at 0.1 and 0.5 wt.% loadings of acid treated CNT falls below that of the neat PS matrix. It can be said that at such loadings, the particle-particle interaction was not established within the matrix, for this reason, the nanotubes act as plasticizer at somewhat lower concentrations because of the miniscule nature of carbon nanotubes. However, increasing the CNT loading to 1.0 wt.% raises the composite viscosity above the threshold limit thus resulting into increase in viscous behavior of the composites above that of the neat PS matrix.

At concentrations of 5 wt.%, G' increase dramatically by almost two order of magnitude and raches a plateau in case of pure CNT at low frequencies indicating that the percolated MWCNTs may be forming a pseudo-solid-like network with strong interactions between polymer and particles [100].

Evidence of the formation of a pseudo-solid-like network of percolated MWCNTs can also be seen in Figure 4.26, where the variation of G' and G'' with frequency is compared for the pure PS sample and for the nanocomposite with the pure MWCNT concentration of 5 wt.%. While the pure PS melt shows a typical transition from elastic to viscous behavior ($G'' > G'$) at a critical frequency of 1.5 rad/s, the nanocomposite shows a predominantly elastic response ($G' > G''$, plateau in

G') over the entire frequency range. Meanwhile, 5 wt.%CNT-COOH nanocomposite does not have the same trend although the *G'* and *G''* are higher than those of 5 wt.% CNT nanocomposite.

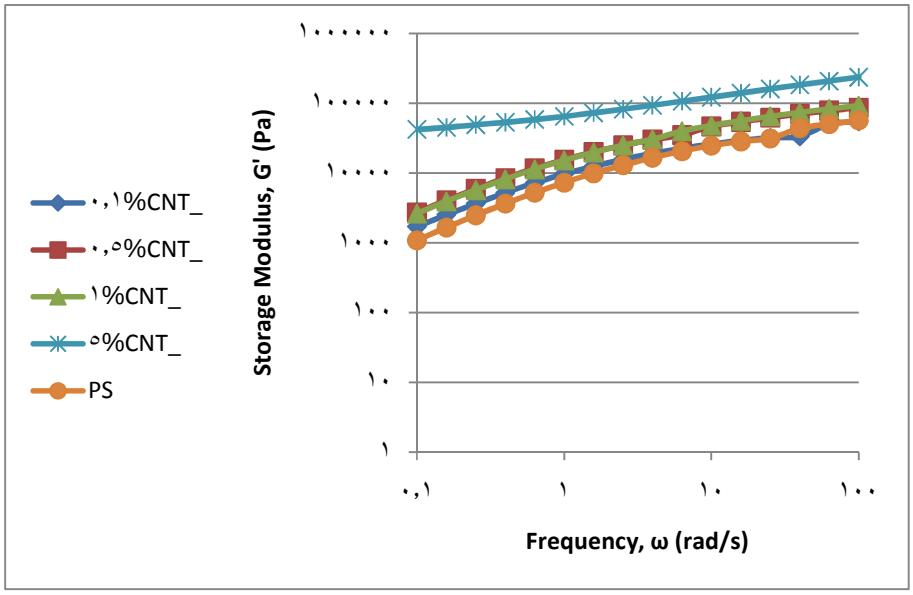

(a)

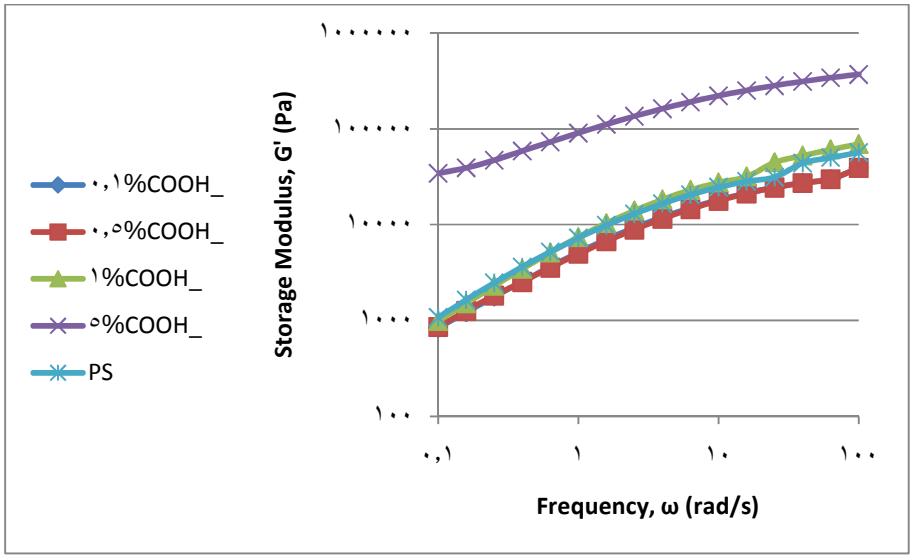

(b)

Figure 4.23: Storage Modulus (G') of the PS/CNT nanocomposites as a function of frequency at a temperature of 190^{o}C for different (a) pure CNT and (b) CNT-COOH weight percentages.

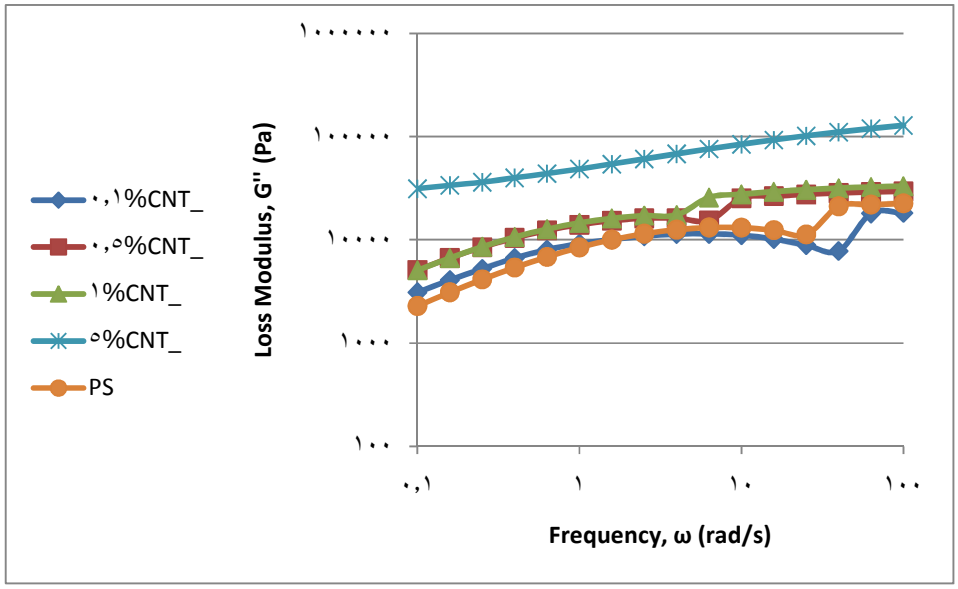

(a)

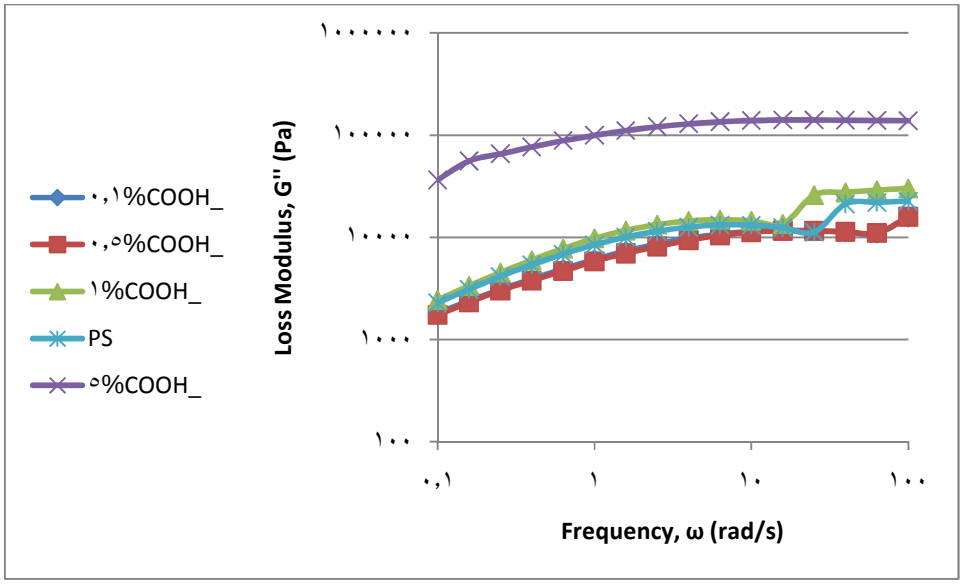

(b)

Figure 4.24: Loss Modulus (G") of the PS/CNT nanocomposites as a function of frequency at a temperature of 190^{o}C for different (a) pure CNT and (b) CNT-COOH weight percentages.

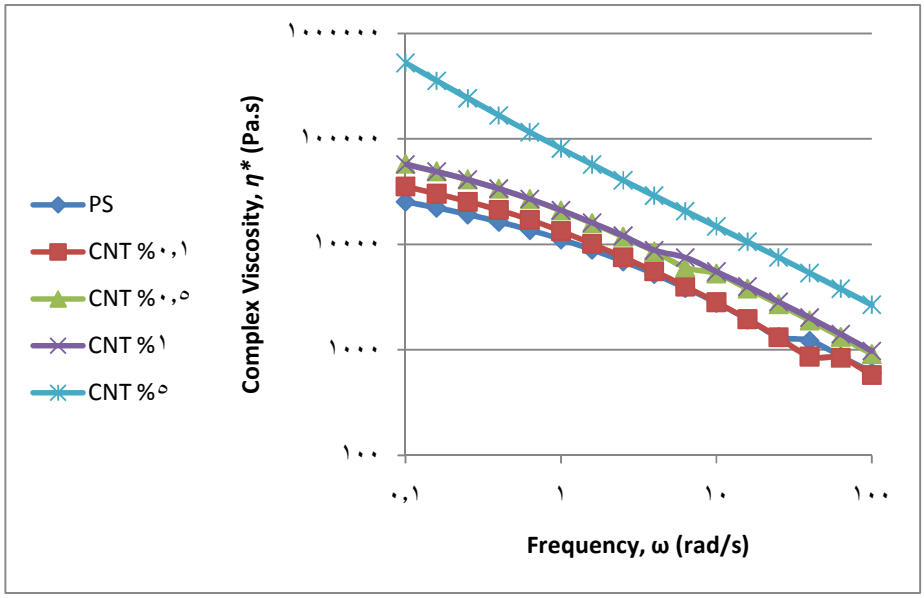

(a)

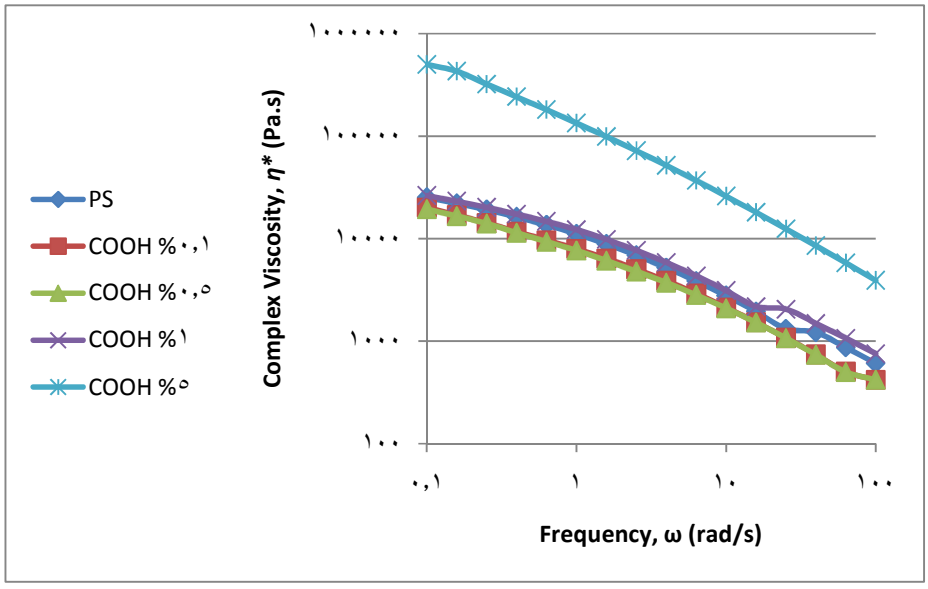

(b)

Figure 4.25: Complex Viscosity (η^*) of the PS/CNT nanocomposites as a function of frequency at a temperature of 190^{o}C for different (a) pure CNT and (b) CNT-COOH weight percentages.

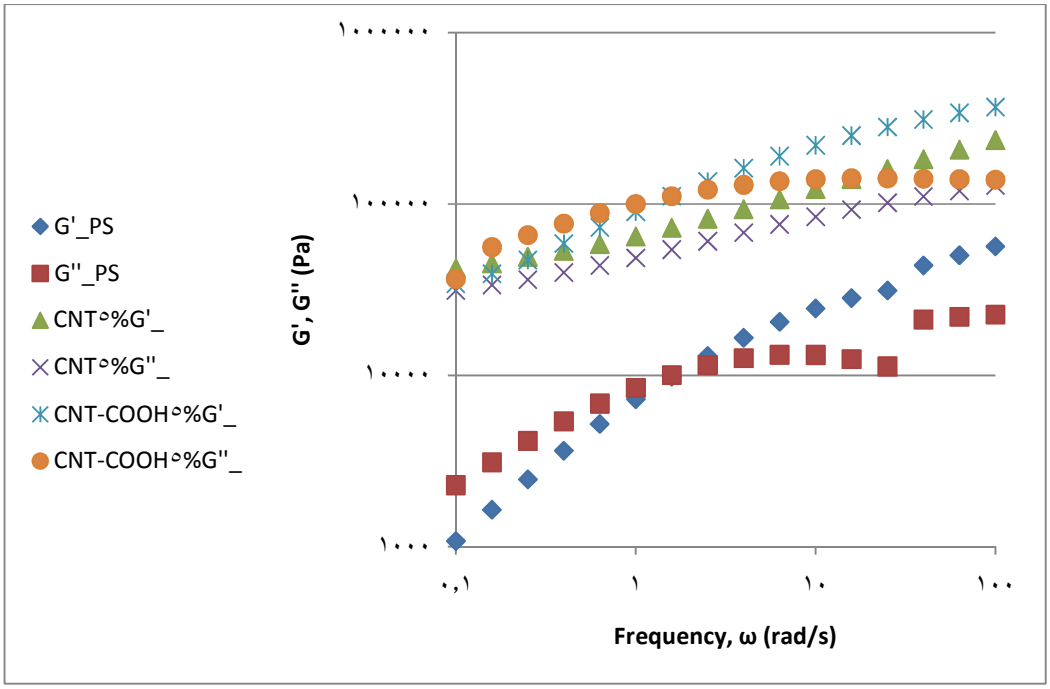

Figure 4.26: Crossover point of the storage and loss modulus curves for the pure PS, 5%CNT-PS and 5%CNT-COOH-PS nanocomposites.

4.3.2 Effect of Phenol Functionalized Carbon Nanotubes on Mechanical, Rheological and Thermal Properties of PS/CNT-Phenol Nanocomposites

In this part, the use of phenol as a functionalizing agent for CNT is reported. Phenol is aromatic in nature and is easy to form ether linkages with functional groups having –COOH or –OH moieties. PS/CNT and PS/CNT-Phenol nanocomposites were prepared by thermal bulk polymerization without any initiator, and with different weight percentages (0.1, 0.5 and 1wt.%) of CNT and CNT-Phenol. The effect of phenol functionalization of CNTs on the mechanical, thermal and rheological properties of polystyrene composites is being dealt with.

4.3.2.1 Mechanical Properties of PS/CNT-Phenol Nanocomposites

The mechanical properties of pure PS in comparison to PS/CNT-Phenol nanocomposites are reported in Table 4.11. Pure PS has a Young's modulus of 922 MPa. With 0.1 wt.% and 0.5 wt.% of unmodified CNT an increase in Young's modulus to 937 and 1004 MPa, respectively, followed by a decrease to 884 MPa for 1 wt.% are observed. The Young's moduli for PS/CNT-Phenol nanocomposites are less than the value of neat polystyrene. There are two suggested reasons for this reduction in Young's modulus; the first one is the fact that the presence of CNT during the polymerization process results in a decrease in the molecular weight of polymer [78] because CNT plays an important role as radical consumer during the polymerization

reaction and it seems that phenolic functionalization enhances this role further. The second one is the formation of large agglomerates of CNTs, as shown in figure 4.27, which penetrates the polymer matrix and reduces the filler-matrix interaction.

Maximum stress and elongation at break of the composites are also given in table 4.11. Maximum stress of 0.5 wt.% PS/CNT nanocomposite increases from 18.6 MPa of polystyrene to 22.4 MPa and the elongation at break decreased by 12% which means that the composites became more stiff. However, the maximum stress values of nanocomposites containing CNT-Phenol decreased significantly by 28%, 22% and 7% for 0.1, 0.5 and 1 wt.% of CNT-Phenol, respectively. These results suggest that 0.5 wt.% of unmodified CNT is the best loading in terms of stress-strain properties.

Table 4.11: Summary of mechanical properties of pure PS, PS/CNT and PS/CNT-Phenol nanocomposites at different CNT loadings.

Composite	Young's modulus (MPa)	Maximum Stress (MPa)	Elongation at break (%)
PS	922.2 ± 53.9	18.62 ± 0.6	2.88 ± 0.3
PS/0.1%CNT	936.6 ± 22.5	19.66 ± 0.4	2.42 ± 0.2
PS/0.5%CNT	1004.4 ± 10.2	22.40 ± 0.4	2.54 ± 0.2
PS/1.0%CNT	884.0 ± 31.7	16.77 ± 0.9	2.38 ± 0.3
PS/0.1%CNT-Phenol	781.9 ± 38.9	13.36 ± 1.7	2.87 ± 0.2
PS/0.5%CNT-Phenol	785.6 ± 75.4	14.48 ± 1.4	2.48 ± 0.2
PS/1.0%CNT-Phenol	855.5 ± 61.5	17.38 ± 1.3	2.23 ± 0.2

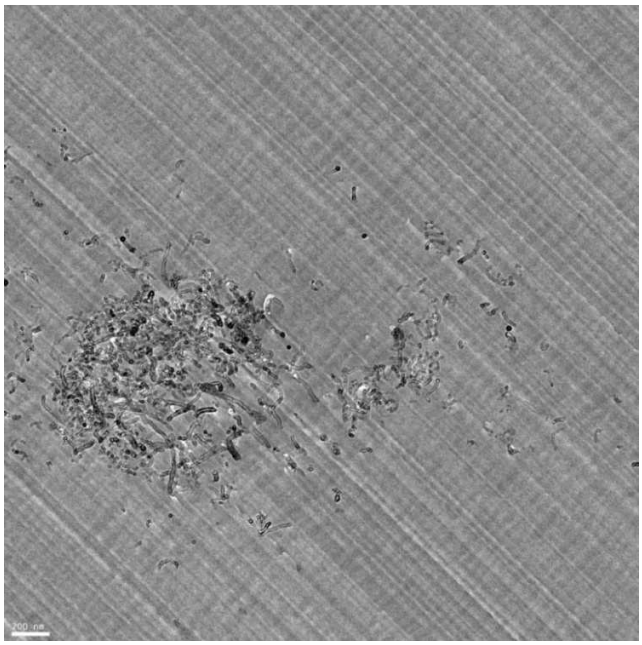

(a)

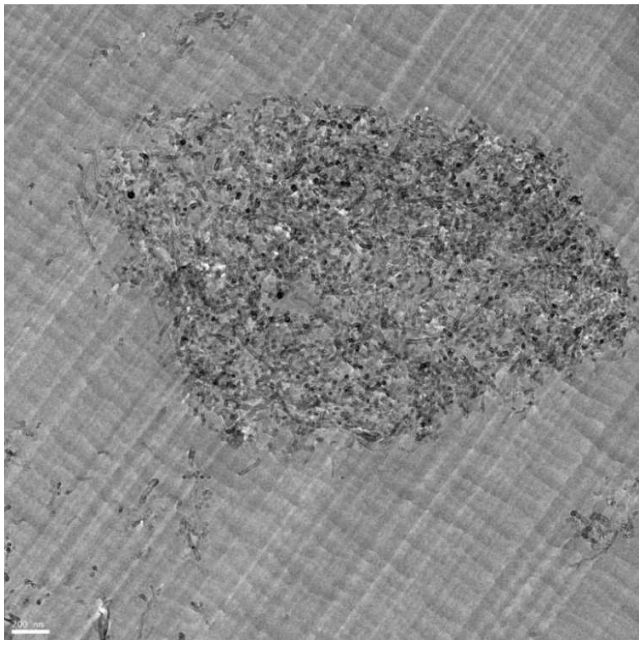

(b)

Figure 4.27: TEM images of a) PS/0.1wt.% CNT-Phenol and b) PS/1.0wt.% CNT-Phenol nanocomposite. (Scale is 200 nm).

4.3.2.2 Differential Scanning Calorimetry Study and Thermogravimetric Analysis

Differential scanning calorimetry allows distinguishing the influence of adding CNT to PS matrix based on the values of glass transition temperature. Table 4.12 and Figure 4.28 show the results and T_g obtained for PS composites with different MWCNT and MWCNT-Phenol loadings. PS exhibits a glass transition at 106.3^{o}C, which is in agreement with the reported literature values [111]. Nanocomposites with 1 wt.% of MWCNT exhibit a change in the glass transition temperature which is 105.0^{o}C with a reduction in T_g of about 1.3^{o}C while composites with 1 wt.% of MWCNT-Phenol have a T_g value of 105.3^{o}C which is below that of pure polystyrene by 1.0^{o}C.

As a consequence of Eq. (4.1), we attribute the decrease in glass transition temperature observed to the reduction in polystyrene molecular weight formed via the polymerization in the presence of CNT.

Table 4.12: Glass transition temperature (T_g), T onset and maximum degradation temperature of PS/CNT and PS/CNT-Phenol nanocomposites.

Composite	T_g (^oC)	T onset (^oC)	T max (^oC)
PS	106.26	335	400
PS/0.1%CNT	106.19	363	410
PS/1%CNT	105.03	366	412
PS/0.1%CNT-Phenol	106.26	369	412
PS/1%CNT-Phenol	105.30	370	418

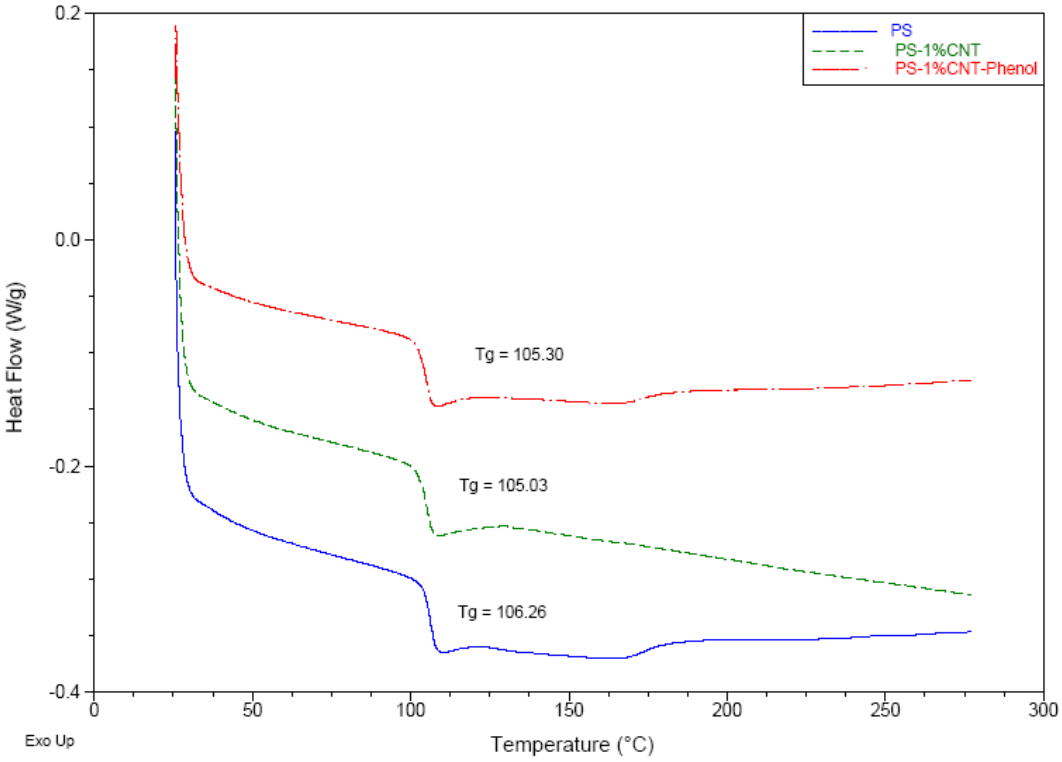

Figure 4.28: Glass Transition observed by DSC for pure PS, PS/1wt.% CNT nanocomposite and PS/1wt.% CNT-Phenol nanocomposite.

Figure 4.29 shows the TGA and DTG curves of the PS and composites of 0.1 and 1 wt% loading of both unmodified and functionalized CNT. All the samples show a single degradation step which is the decomposition of the polymer backbone. From the TGA curves, it is seen that the phenolic treated composites show a slight degradation in the temperature range of 200-300^{0}C which may be due to the release of carbonyl groups associated with the treated CNT. However, this small degradation step is not reflected in the DTG curves. The DTG curves show a single peak corresponding to the maximum degradation temperature for the composites. From both TGA and DTG curves the onset of degradation and maximum degradation temperature were calculated (Table 4.12). It can be seen that the incorporation of CNT into PS has enhanced the onset of degradation to almost 30-40^{0}C for all the composites. Also the maximum degradation temperature of the composites showed an increase of 10-20^{0}C. As a conclusion, the incorporation of CNT into PS improved the thermal properties.

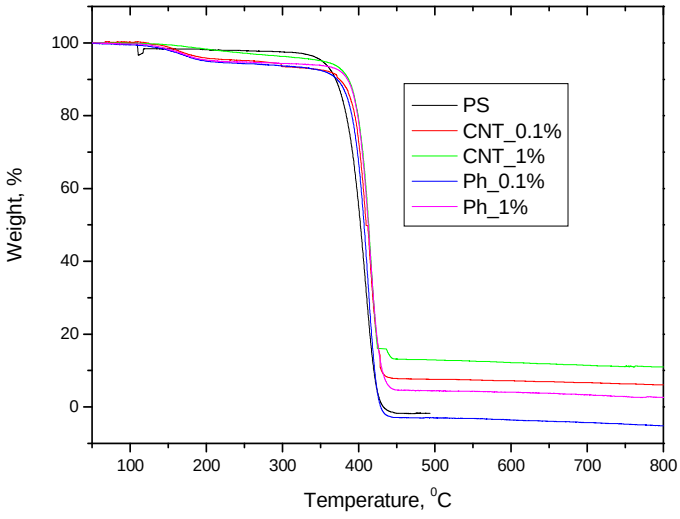

(a)

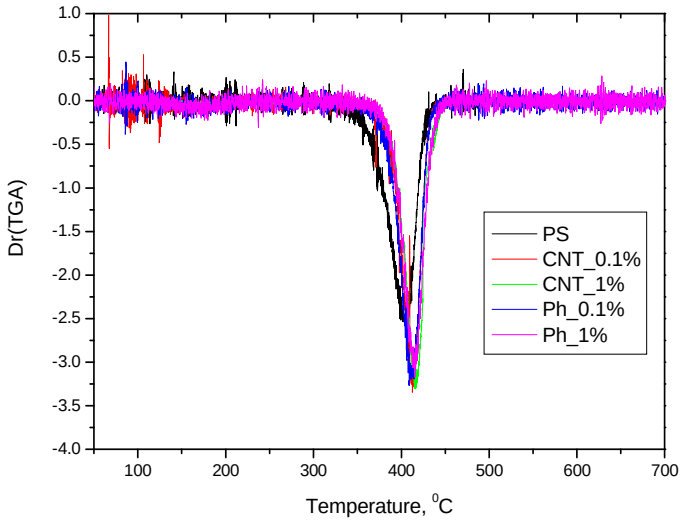

(b)

Figure 4.29: (a) TGA and (b) DTG curves of 0.1 and 1 wt% of the composites with CNT and CNT-Phenol

4.3.2.3 Rheological Behavior of PS/CNT-Phenol Nanocomposites

The PS/CNT-Phenol nanocomposites were further investigated for their dynamic rheological properties. Figures 4.30-4.32 are experimental results for the various rheological parameters obtained via dynamic melt rheology from the PS/MWCNT nanocomposites. Figure 4.30 and 4.31 are experimental results for the storage modulus, *G'*, and the loss modulus, *G''*, for the PS matrix and the composites containing 0.1, 0.5 and 1.0 wt.% loading of pure CNT and CNT-Phenol as functions of frequency. Both *G'* and *G''* increase with CNT concentration in case of pure CNT, while for CNT-Phenol only for 1 wt.% the moduli start to increase above those of pure PS. This results suggest that below 1 wt.% the CNT-Phenol act as a plasticizer. The effect of nanotubes is more pronounced at lower frequencies and the relative effect diminishes with increasing frequency due to shear thinning. This result is in agreement with theoretical and experimental observations for fiber-reinforced composites [119-121].

Figure 4.32 shows the relationship between complex viscosity and frequency. It is obvious that in all cases, the viscous properties of the composites decreases with increasing frequency. It is a general phenomenon that addition of fillers into polymer matrices increased the viscoelastic behavior of the polymeric materials as observed in figure 4.32(a) for the composites with pure CNT. However, this was not the case with 0.1 and 0.5 wt.% loadings of CNT-Phenol nanocomposites. Figure 4.32(b) shows that the complex viscosity of the composite at 0.1 and 0.5 wt.% loadings of CNT-Phenol

falls below that of the neat PS matrix. It can be said that at such loadings, the particle-particle interaction was not established within the matrix, for this reason, the nanotubes act as plasticizer at somewhat lower concentrations because of the miniscule nature of carbon nanotubes. However, increasing the CNT-Phenol loading to 1.0 wt.% raises the composite viscosity above the threshold limit thus resulting into increase in vicious behavior of the composites above that of the neat PS matrix.

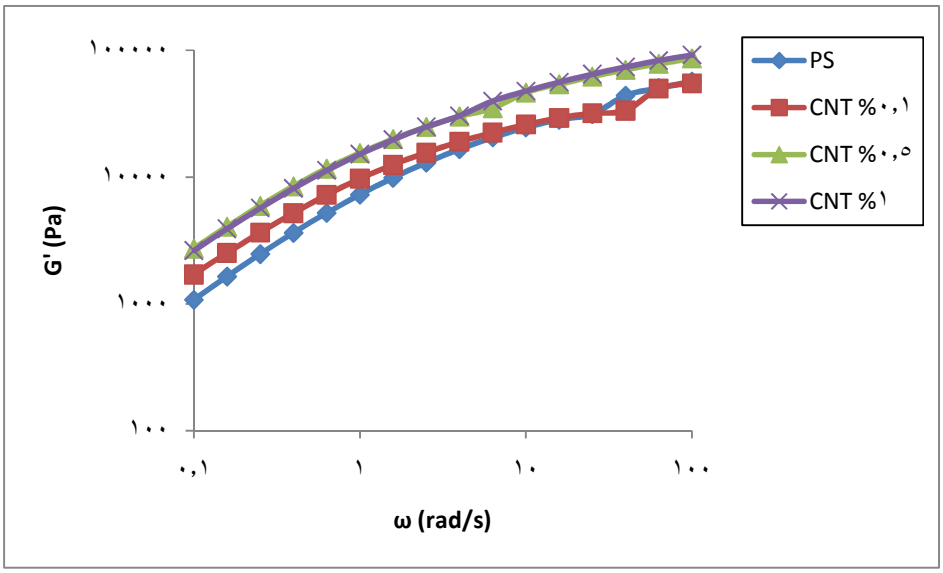

(a)

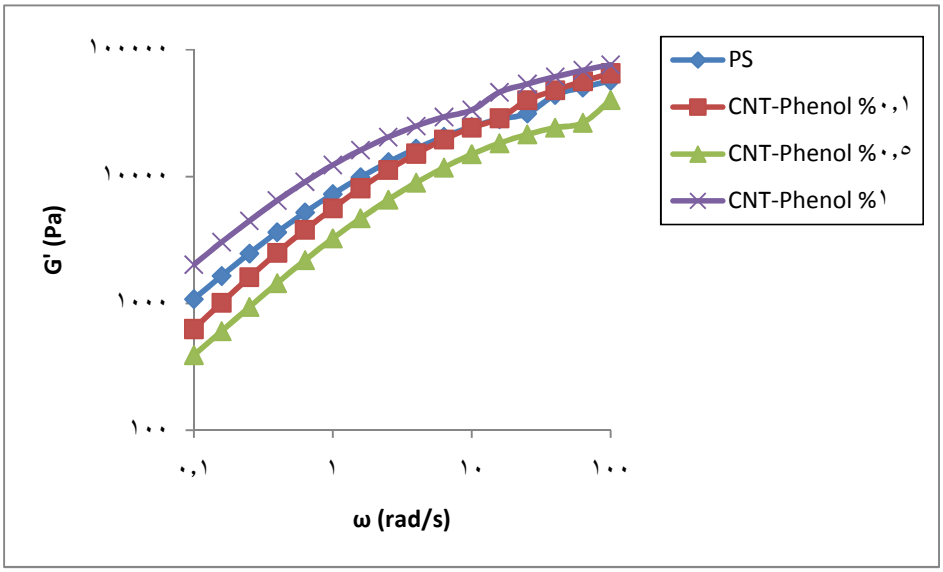

(b)

Figure 4.30: Storage Modulus (G') of the PS/CNT nanocomposites as a function of frequency at a temperature of 190^{o}C for different (a) pure CNT and (b) CNT-Phenol weight percentages.

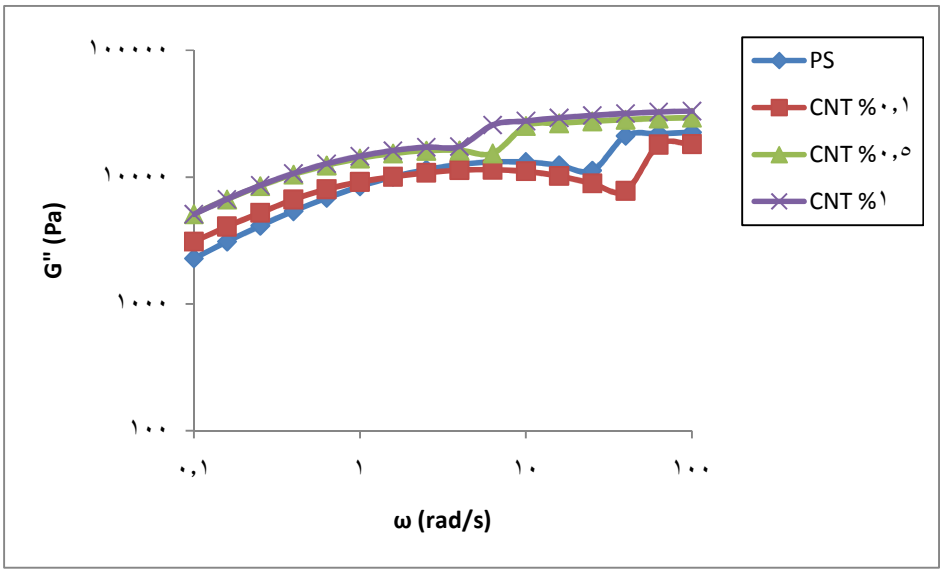

(a)

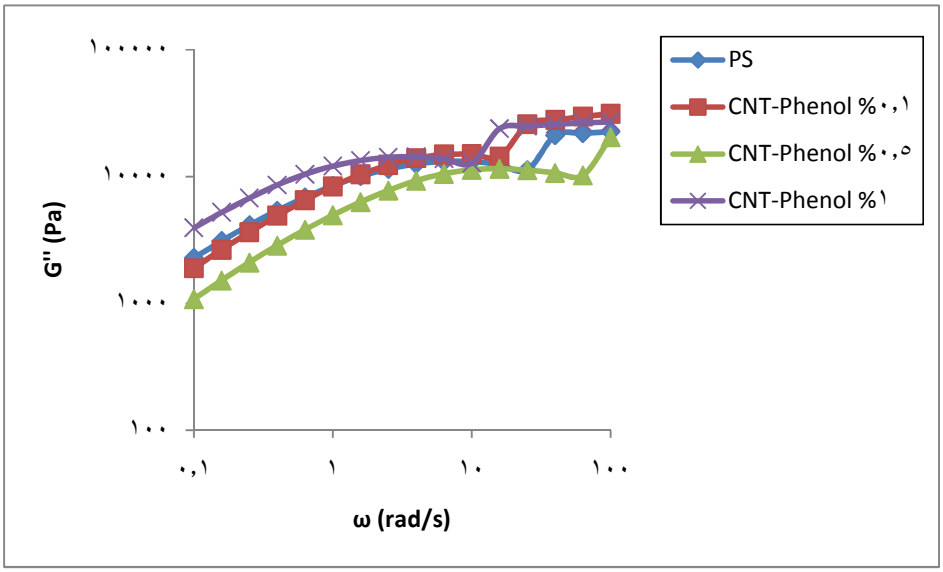

(b)

Figure 4.31: Loss Modulus (G") of the PS/CNT nanocomposites as a function of frequency at a temperature of 190°C for different (a) pure CNT and (b) CNT- Phenol weight percentages.

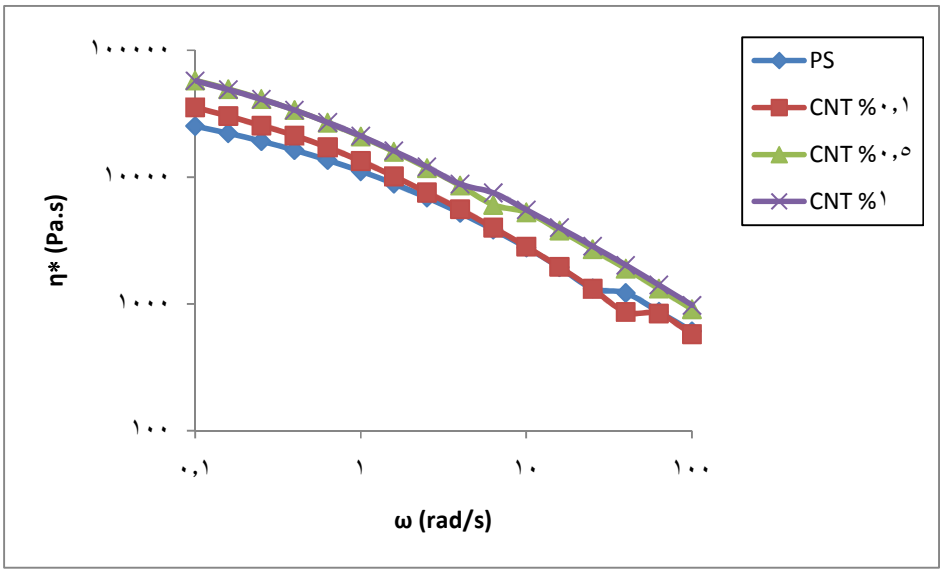

(a)

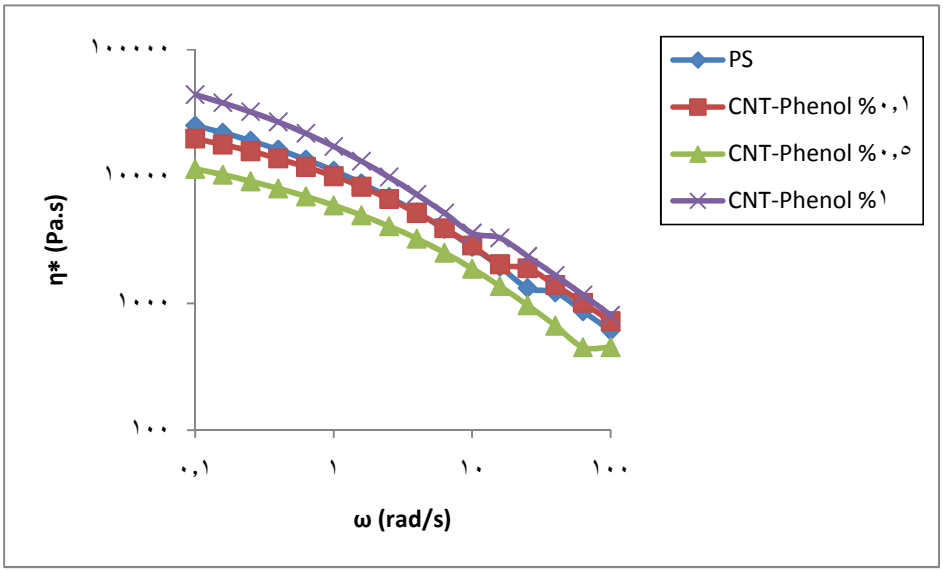

(b)

Figure 4.32: Complex Viscosity (η^*) of the PS/CNT nanocomposites as a function of frequency at a temperature of 190^{o}C for different (a) pure CNT and (b) CNT- Phenol weight percentages.

4.3.3 Effect of 1-Octadecanol Functionalized Carbon Nanotubes on Mechanical, Rheological and Thermal Properties of PS/CNT-Phenol Nanocomposites

In this part, the use of ($C_{18}H_{38}O$), as a functionalizing agent for CNT is reported. PS/CNT and PS/CNT-C18 nanocomposites were prepared by thermal bulk polymerization without any initiator. The effect of CNT-C18 on the mechanical, thermal and rheological properties of polystyrene composites is being dealt with.

4.3.3.1 Mechanical Properties of PS/CNT-C18 Nanocomposites

The mechanical properties of PS in comparison to PS/CNT-C18 nanocomposites are reported in Table 4.13. Pure PS has an Young's modulus of 922 MPa. With 0.1 wt.% and 0.5 wt.% of pure CNT we observed a little increase in Young's modulus to values of 937 and 1004 MPa, respectively. However, a remarkable increase in Young's modulus was observed upon loading with functionalized CNT-C18. The 0.1 wt.% and 0.5 wt.% of CNT-COOH increased the Young's modulus to 987 and 1102 MPa, respectively. The acid modification of CNT seems to enhance the dispersion of the nanotubes within the PS matrix, as shown in figure 4.33, which permit a larger matrix/filler contact area [110]. Also, stress transfer might increase because of a better interface between the matrix and the filler [110]. Similar reports are available indicating reinforcement of polymers by CNT and modified CNT [5, 97, 98].

It is noticed that Young's moduli for PS/1.0%CNT and PS/1.0%CNT-C18 composites has decreased to 884 and 860 MPa, respectively, which are below the Young's modulus of pure PS. This is due to the fact that the presence of CNT during the polymerization process results in a decrease in the molecular weight of polymer [78]. Also, some agglomerates started to appear (Figure 4.33-c), which penetrates the polymer matrix and reduces the filler-matrix interaction. These results suggest that 0.5 wt.% is the best loading to increase the Young's modulus.

Maximum stress and elongation at break values of the composites are also given in Table 4.13. It is clear that addition of CNT and CNT-C18 decreased the elongation at break values which means that the composites became stiffer in nature.

Table 4.13: Summary of mechanical properties of pure PS, PS/CNT and PS/CNT-C18 nanocomposites at different CNT loadings.

Composite	Young's modulus (MPa)	Maximum Stress (MPa)	Elongation at break (%)
PS	922.2 ± 53.9	18.62 ± 0.6	2.88 ± 0.3
PS/0.1%CNT	936.6 ± 22.5	19.66 ± 0.4	2.42 ± 0.2
PS/0.5%CNT	1004.4 ± 10.2	22.40 ± 0.4	2.54 ± 0.2
PS/1.0%CNT	884.0 ± 31.7	16.77 ± 0.9	2.38 ± 0.3
PS/0.1%CNT-C18	986.5 ± 23.6	18.96 ± 1.7	2.56 ± 0.2
PS/0.5%CNT-C18	1101.9 ± 71.7	20.17 ± 0.9	2.14 ± 0.2
PS/1.0%CNT-C18	860.1 ± 49.6	17.13 ± 1.4	2.29 ± 0.2

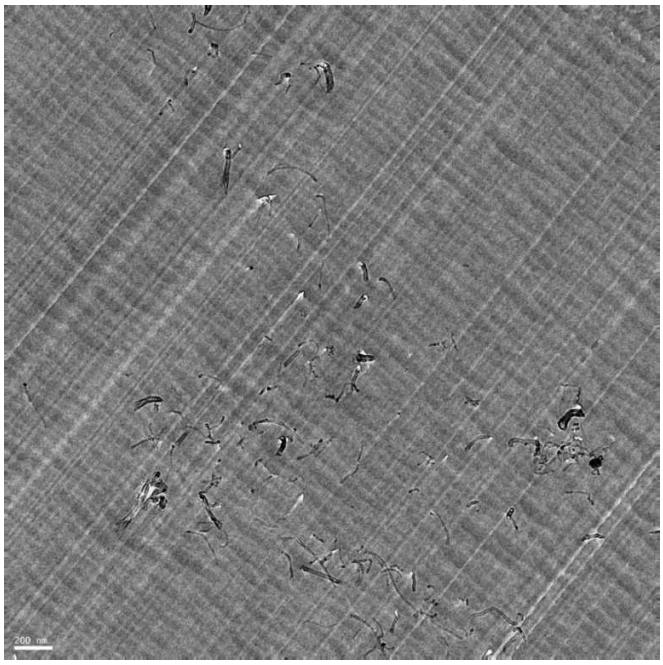

(a)

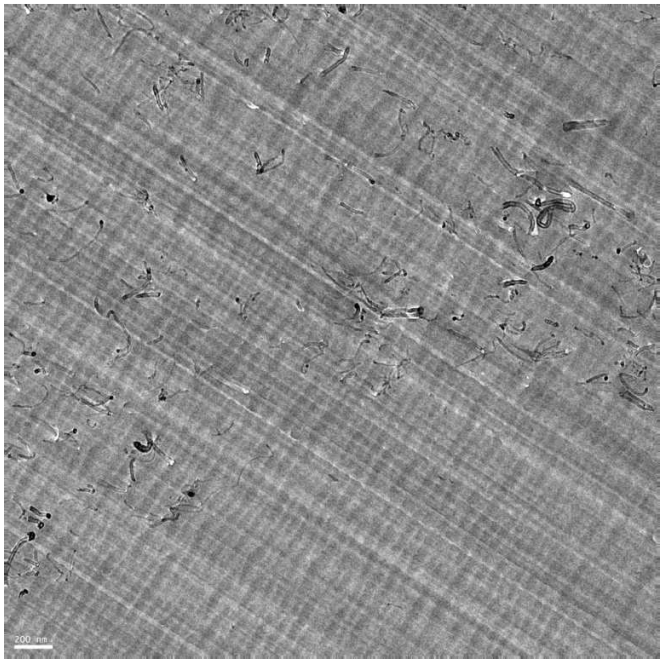

(b)

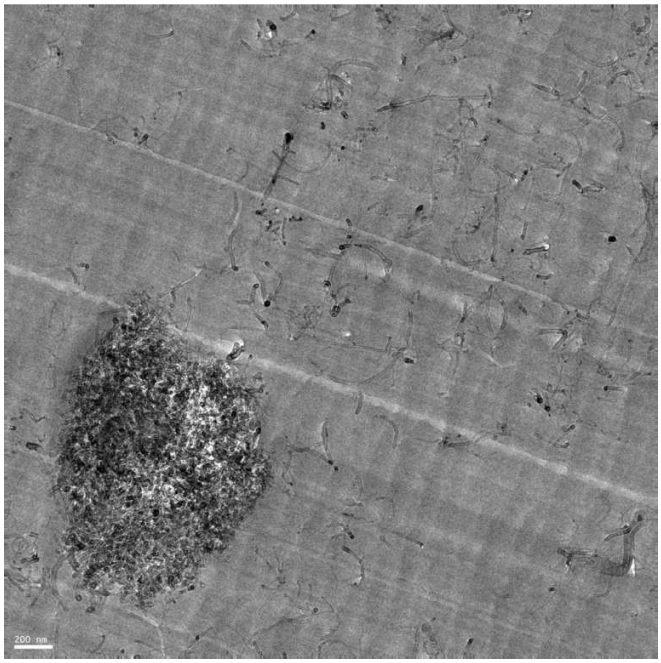

(c)

Figure 4.33: TEM images of a) PS/0.1wt.% CNT-C18, b) PS/0.5wt.% CNT-C18 and c) PS/1.0wt.% CNT-C18 nanocomposite. (Scale is 200 nm).

4.3.3.2 Differential Scanning Calorimetry Study and Thermogravimetric Analysis

Differential scanning calorimetry allows distinguishing the influence of adding CNT to PS matrix based on the values of glass transition temperature. Table 4.14 and Figure 4.34 show the results and values of T_g obtained for PS composites with 0.1wt.% and 1wt.% CNT and CNT-C18 loadings. Pure PS exhibits a glass transition at 106.3^{o}C, in agreement with values reported in the literature [111]. Nanocomposites with 1 wt.% of CNT exhibit a change in the glass transition temperature which is 105.03^{o}C with a reduction in T_g of about 1.2^{o}C while composites with 1 wt.% of CNT-C18 have a T_g value of 92.1^{o}C which is significantly below that of pure polystyrene by 14^{o}C.

As a consequence of Eq. (4.1), we attribute the decrease in glass transition temperature observed to the reduction in polystyrene molecular weight formed via the polymerization in the presence of CNT and CNT-C18 because CNT plays an important role as radical consumer during the polymerization reaction and it seems that 1-octadecanol functionalization enhances this role further. This is in agreement with the reduction in Young's modulus observed previously.

Table 4.14: Glass transition temperature (T_g), T onset and maximum degradation temperature of PS/CNT and PS/CNT-C18 nanocomposites.

Composite	T_g (^oC)	T onset (^oC)	T max (^oC)
PS	106.26	335	400
PS/0.1%CNT	106.19	363	410
PS/1.0%CNT	105.03	366	415
PS/0.1%CNT-C18	104.37	363	410
PS/1.0%CNT-C18	92.15	365	412

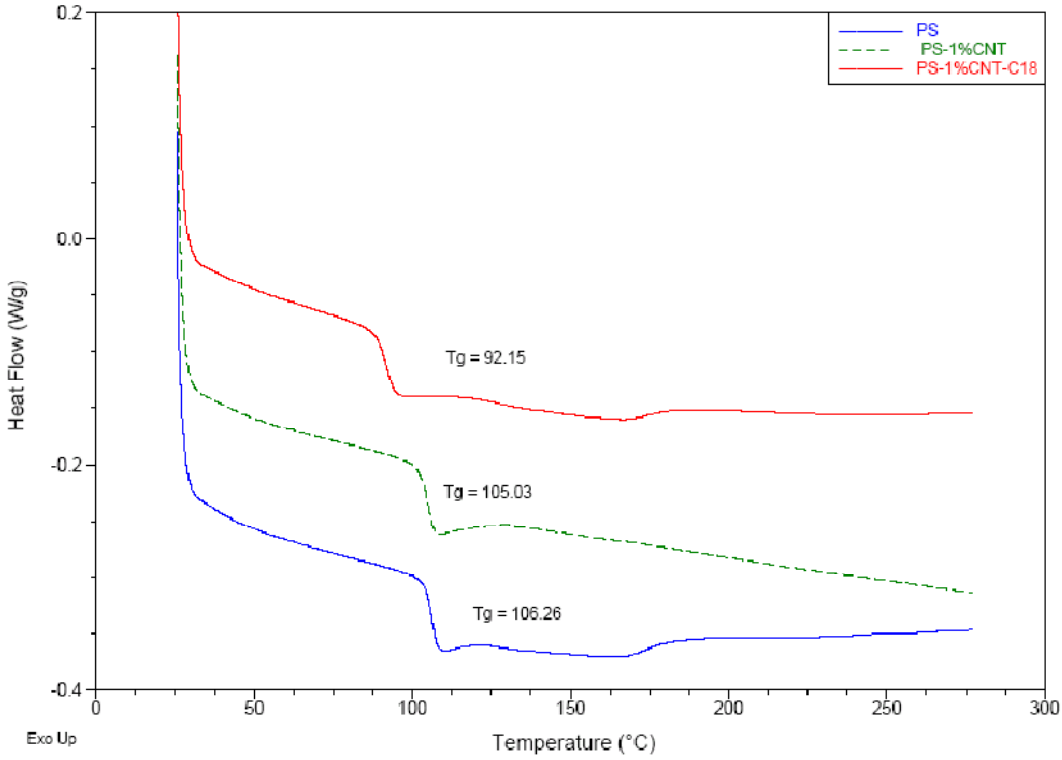

Figure 4.34: Glass Transition observed by DSC for pure PS, PS/1wt.% CNT nanocomposite and PS/1wt.% CNT-C18 nanocomposite.

Figure 4.35 shows the TGA and DTG curves of the virgin PS and composites of 0.1 and 1 wt% loading of both CNT CNT-C18. All the samples show a single degradation step which is the decomposition of the polymer backbone. From the TGA curves, it is seen that the PS/CNT-C18 nanocomposites show a slight degradation in the temperature range of 200-300^{0}C which may be due to the release of C18 groups associated with the treated CNT. However, this small degradation step is not reflected in the DTG curves. The DTG curves show a single peak corresponding to the maximum degradation temperature for the composites. From both TGA and DTG curves the onset of degradation and maximum degradation temperature were calculated (Table 4.14). It can be seen that the incorporation of CNT into PS has enhanced the onset of degradation to almost 28-31^{0}C for all the composites. Also the maximum degradation temperature of the composites showed an increase of 10-15^{0}C. In short, the incorporation of CNT into PS enhanced the thermal properties significantly.

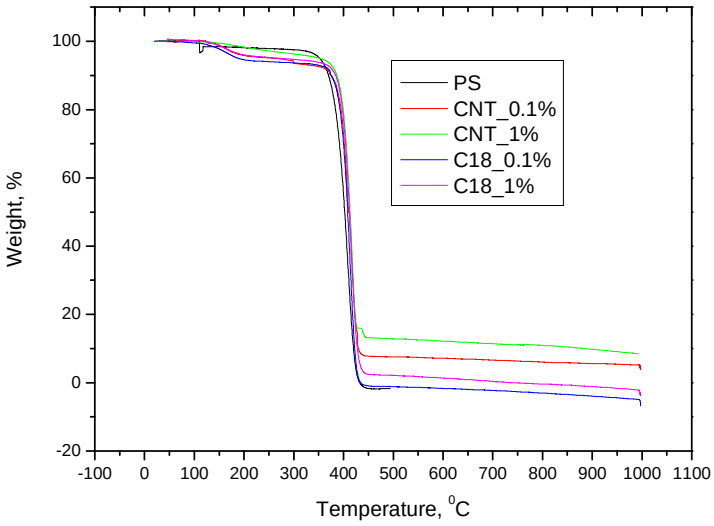

(a)

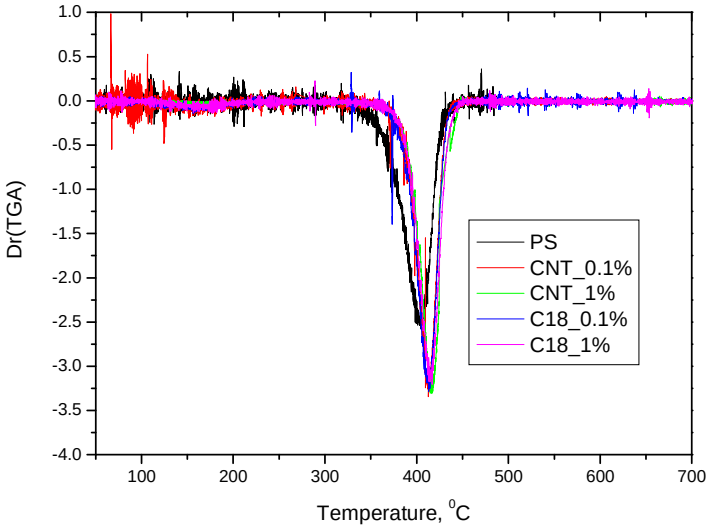

(b)

Figure 4.35: (a) TGA and (b) DTG curves of 0.1 and 1 wt% of the composites with CNT and CNT-C18

4.3.3.3 Rheological Behavior of PS/CNT-C18 Nanocomposites

The PS/CNT-C18 nanocomposites were further investigated for their dynamic rheological properties. Figures 4.36-4.38 are experimental results for the various rheological parameters obtained via dynamic melt rheology from the PS/CNT nanocomposites. Figures 4.36 and 4.37 are experimental results for the storage modulus, *G'*, and the loss modulus, *G''*, for the PS matrix and the composites containing 0.1, and 1.0 wt.% loadings of pure CNT and CNT-C18 as functions of frequency. Data collected at a temperature of 190^{o}C. Both *G'* and *G''* increase with increasing the CNT concentration in case of pure CNT, while for CNT-C18 the moduli are below those of pure PS, especially for loading of 0.1wt.%. These results suggest that the CNT-C18 act as a plasticizer. The effect of nanotubes is more pronounced at lower frequencies and the relative effect diminishes with increasing frequency due to shear thinning. This result is in agreement with theoretical and experimental observations for fiber-reinforced composites [119-121].

Figure 4.38 shows the relationship between complex viscosity and frequency. It is obvious that in all cases, the viscous properties of the composites decreases with increasing frequency. It is a general phenomenon that addition of fillers into polymer matrices increased the viscoelastic behavior of the polymeric materials as observed in figure 4.38-a for the composites with pure CNT. However, this was not the case with 0.1 and 1.0 wt.% loadings of CNT-C18 nanocomposites. Figure 4.38-b shows that the complex viscosity of PS/1.0wt.%CNT-C18 nanocomposite does not differ

significantly from that of neat PS. However, the complex viscosity of the composite at 0.1wt.% loading of CNT-C18 falls below that of the neat PS matrix. It can be said that at such loading, the particle-particle interaction was not established within the matrix, for this reason, the nanotubes act as plasticizer at somewhat lower concentrations because of the miniscule nature of carbon nanotubes.

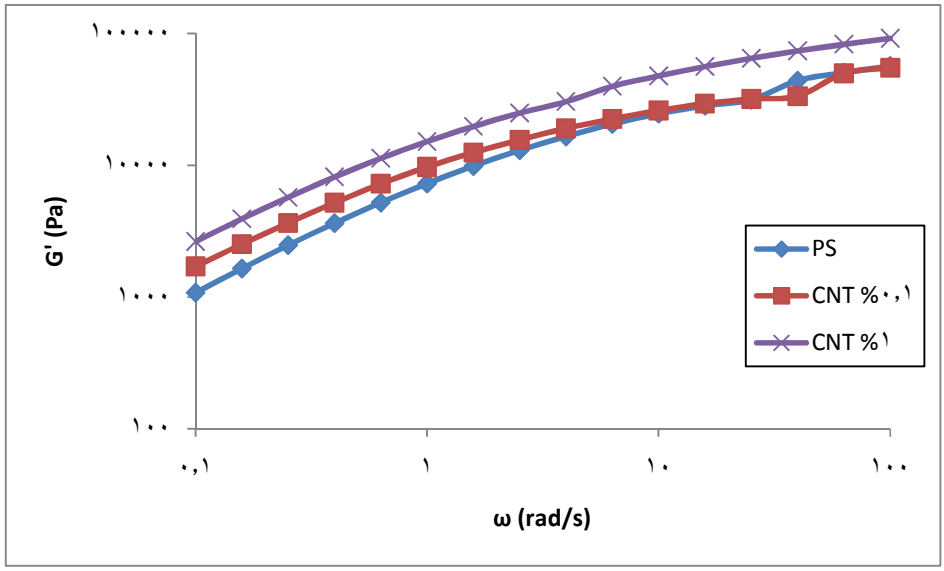

(a)

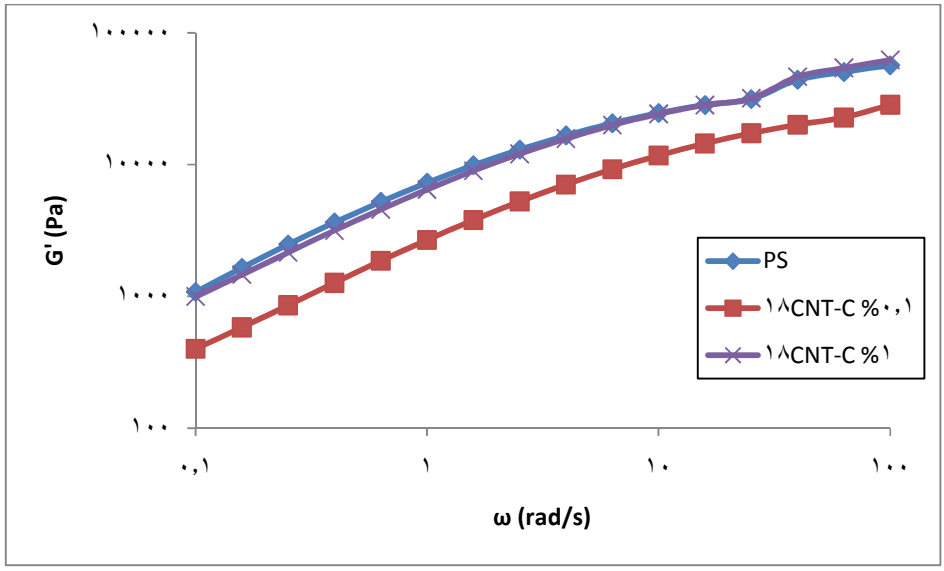

(b)

Figure 4.36: Storage Modulus (G') of the PS/CNT nanocomposites as a function of frequency at a temperature of 190^{o}C for different (a) pure CNT and (b) CNT-C18 weight percentages.

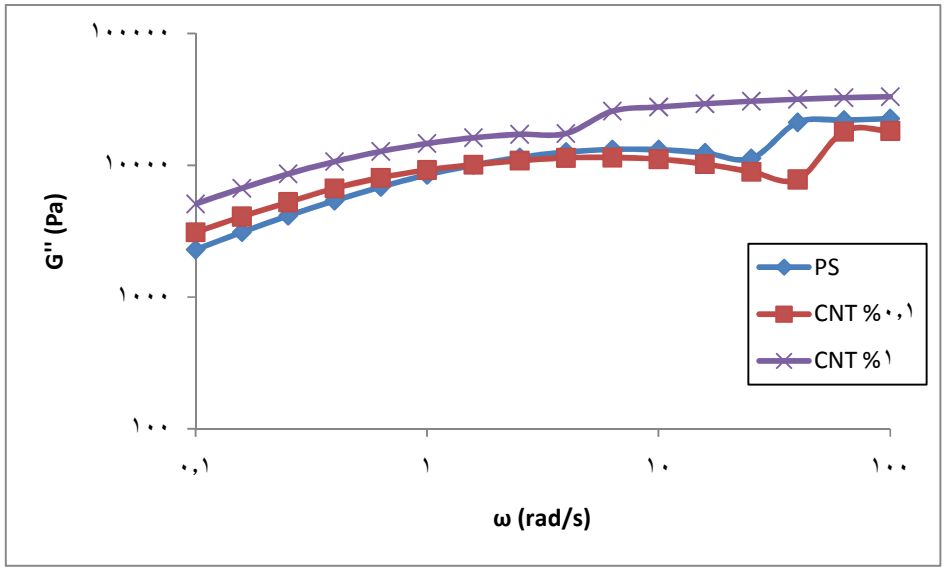

(a)

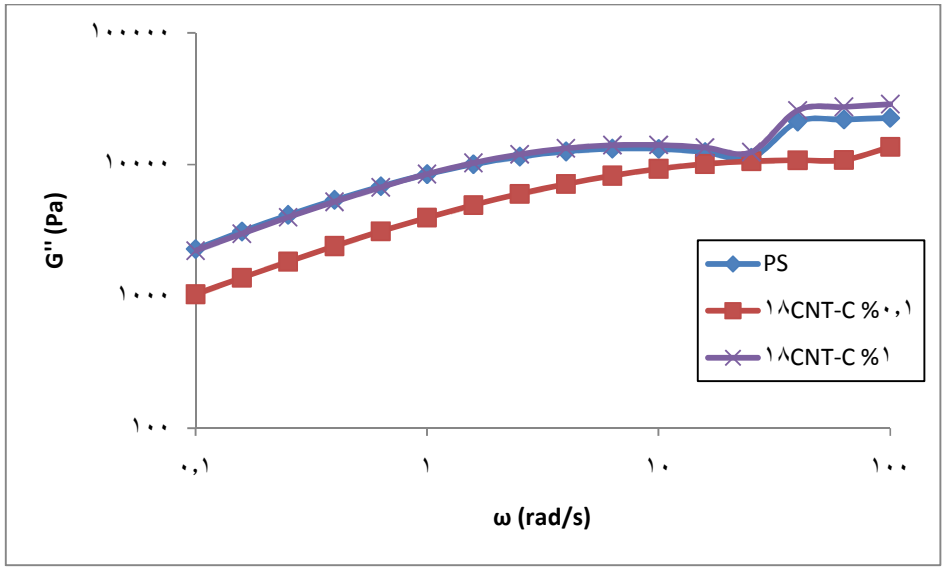

(b)

Figure 4.37: Loss Modulus (G") of the PS/CNT nanocomposites as a function of frequency at a temperature of 190^{o}C for different (a) pure CNT and (b) CNT- C18 weight percentages.

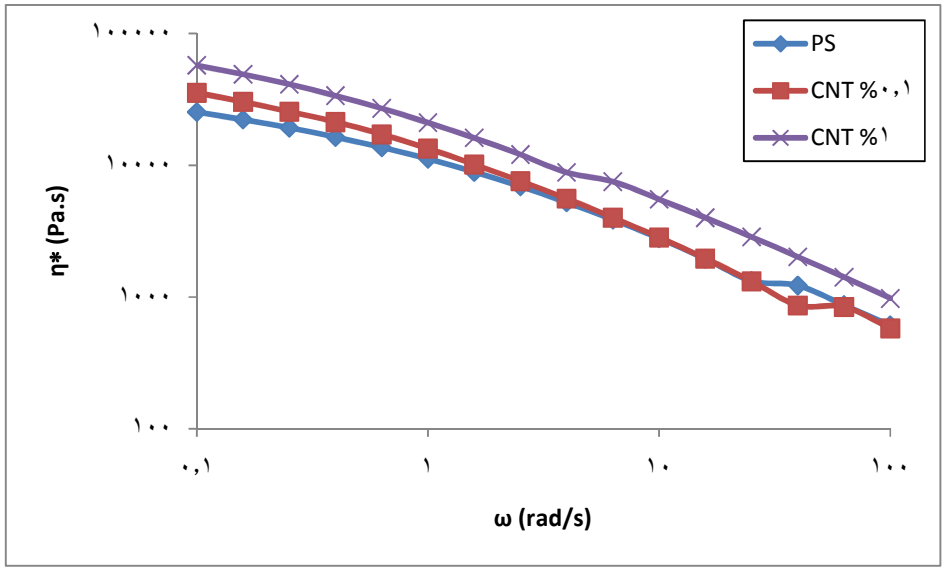

(a)

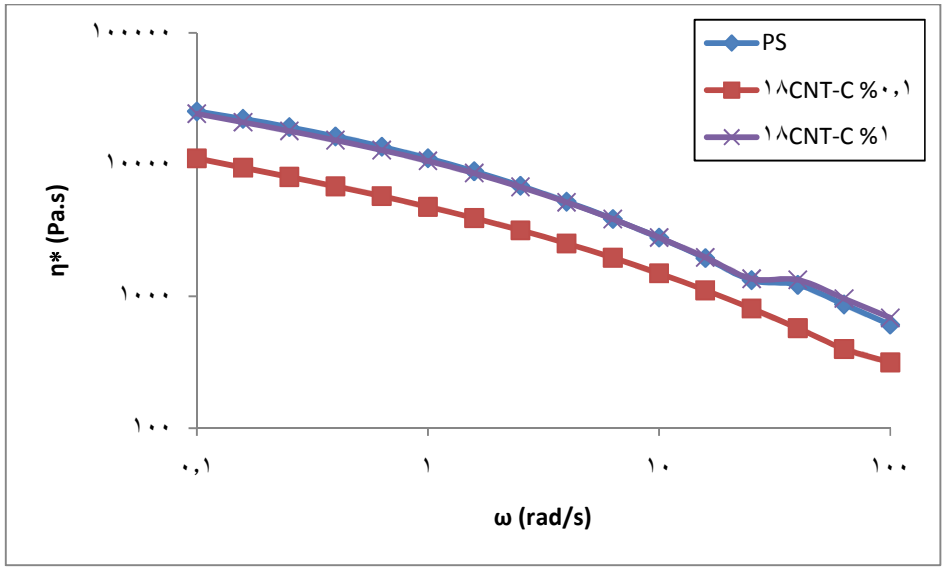

(b)

Figure 4.38: Complex Viscosity (η^*) of the PS/CNT nanocomposites as a function of frequency at a temperature of 190^{o}C for different (a) pure CNT and (b) CNT- C18 weight percentages.

4.4 Effect of Carbon Nanotubes as Inhibitor of Styrene Polymerization

In handling and storage of styrene monomer, the styrene temperature must be controlled at around 10^{o}C to prevent styrene polymerization. Also, a polymerization inhibitor must be added. In hot climates and during the transportation of styrene, the initial inhibitor level should be increased to avoid autocatalytic polymerization which becomes self-sustaining above 20^{o}C [122].

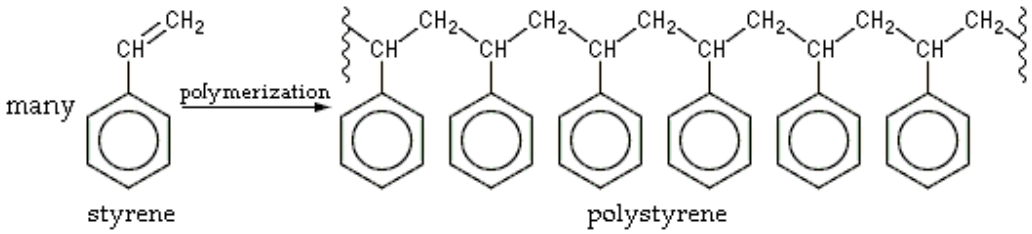

Figure 4.39: Polymerization of styrene monomer to polystyrene.

In literature there are some studies on the inhibition of radical polymerisation in the presence of carbonaceous nanomaterials (carbon nanotubes or fullerenes) [123-129]. These substances exhibit different inhibition activity under varied conditions of the polymerization reaction; kind of monomer, solvent or initiator. They can be the effective inhibitors or retarders, e.g., in the polymerisation of methyl methacrylate [123, 124, 128] and acrylonitrile [129] both fullerenes C60 and single wall carbon nanotubes (SWCNT) exhibit the action of slowing down the process, hence they are retarders, whereas fullerene C60 is a typical inhibitor in the polymerisation of styrene [125] and vinyl acetate [126].

Three different weight percentages of MWCNTs (0.1, 1 and 5 wt %) were mixed with fixed amount of styrene monomer (10 ml) in the round bottom flask. The polymerization temperature was fixed at 115 ^{o}C while polymerization time was varied from 1-6 hr. The conversion of styrene monomer with and without CNTs was calculated using the following equation:

$$\%conversion = \left(\frac{\text{weight of recovered polystyrene}}{\text{initial weight of styrene monomer}}\right) \times 100\%$$

Figure 4.40 shows the conversions of styrene monomer to polystyrene at different polymerization time. By increasing the polymerization time the degree of polymerization increases. Figure 4.40 is clearly showing that the addition of MWCNTs reduces the polymerization rate. For example after one hour polymerization the conversion of the pure styrene (without MWCNTs) to polystyrene reaches 20%, while by adding small amount of CNTs such as 0.1 wt% the conversion was reduced by 50% and became only 10%. Further increase in the amount of CNTs leads to reduce the conversion of styrene significantly. At 5 wt% of CNTs in styrene and after one hour of polymerization time, the styrene remains as monomer and there was not any polymerization which indicates that the CNTs inhibit the reaction and stop any polymerization process. After 6 hours of polymerization time the conversions of styrene without addition of CNTs reaches up to ~ 90 %, while by adding CNTs at 0.1, 1 and 5 wt% the conversions were 80.1, 58.9 and 51.4 %, respectively, and all are less than the conversion of pure styrene without MWCNT. This is due to the fact that MWCNT have electron affinities similar to those of fullerenes, and therefore be predicted to behave as radical traps in chain reactions such as polymerization.

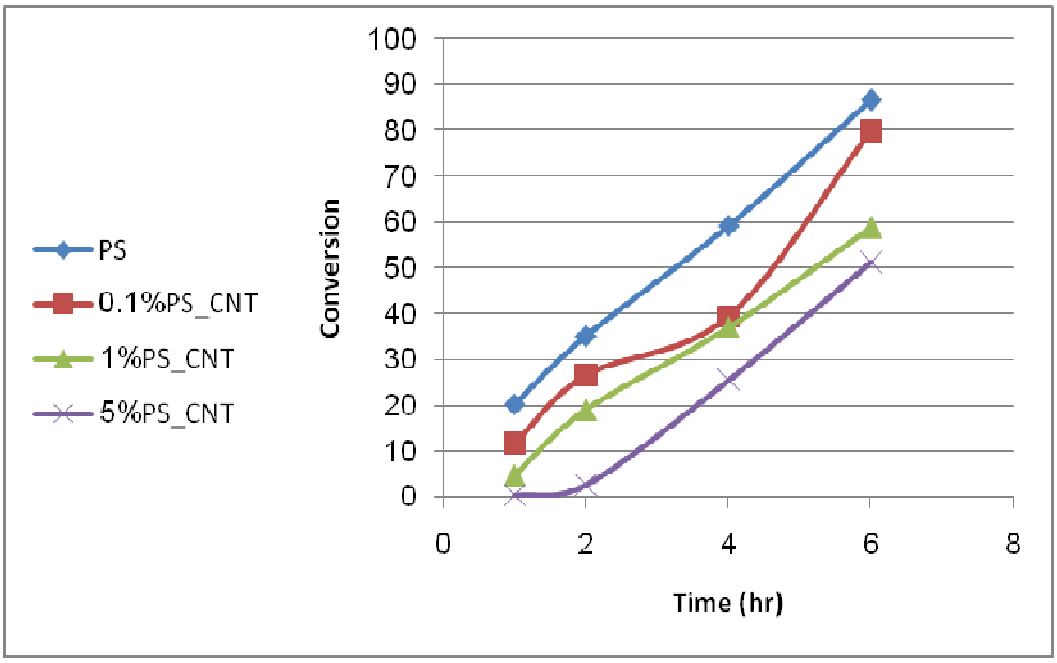

Figure 4.40: Conversion of styrene monomer to polystyrene using 0.1, 1 and 5 wt% of MWCNT at 115^{o}C.

Great reduction in the conversion of styrene monomer to polystyrene was achieved when the MWCNTs were functionalized with different functional groups such Amine and carboxylic groups as shown in figure 4.41. No significant polymerization was occurring after one hour of polymerization time when MWCNT-Amine or MWCNT-COOH were added with only 1 wt%, which indicates that the functional group on the surface of MWCNTs plays a major role on the sharp reduction of the conversion. After 6 hours the conversion does not go beyond 34% for amine functional group and 65% for carboxylic functional group which proves the good efficiency of modified MWCNTs with functional group in inhibiting the polymerization of styrene.

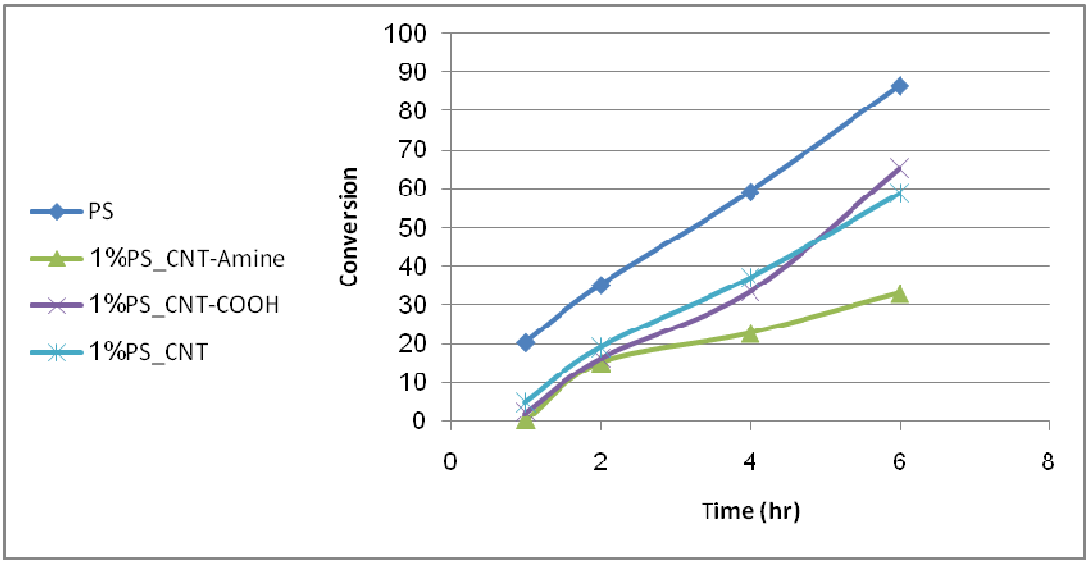

Figure 4.41: Conversion of styrene monomer to polystyrene using 1 wt% of MWCNT, MWCNT-COOH and MWCNT-Amine at 115^{o}C.

In conclusion, the non modified MWCNTs and modified MWCNTs-Amine and MWCNT-COOH shows a clear reduction in the conversion of styrene monomer to polystyrene at high temperature (115 ^{O}C) and different polymerization time from 1-6 hours, which prove that they are good candidates as polymerization inhibitors by adding them to the styrene monomer solution.

4.5 Comparison between Low and High Aspect Ratio CNTs

In this section we compare the Young's modulus of PS/CNT nanocomposites prepared by in-situ polymerization with high aspect ratio (HAR) CNT which was produced by O-CVD reactor and has an aspect ratio of 65000 with the Young's modulus of the nanocomposites which were prepared with commercial CNT with an aspect ratio of 3000.

Table 4.15: Young's modulus of PS/CNT nanocomposite prepared by in-situ polymerization at different CNT loadings.

CNT Loading (wt.%)	Young's Modulus (MPa)	
	Commercial CNT	HAR CNT
0	922.2	922.2
0.1	936.6	1091.1
0.5	1004.4	706.5
1.0	804.0	554.1

It is seen from table 4.15 that 0.1 wt.% of commercial CNT increases the Young's modulus by only 1.5% while HAR CNT increases it by 18.3%. This is due to the significant effect of increasing the aspect ratio of CNT. Even the 0.5% of commercial CNT increases the Young's modulus by 8.9% which is still less than the half of the increment by HAR CNT.

Increasing the loading of HAR CNT to 0.5 wt.% and 1 wt.% causes a sharp decrease in Young's modulus because it decreases the degree of polymerization and acting as polymerization inhibitor is more dominating than acting as a filler as explained in sections 4.3 and 4.4.

CHAPTER FIVE

CONCLUSIONS AND RECOMMENDATIONS

5.1 Conclusions

- Orifice chemical vapor deposition (O-CVD) reactor was designed and fabricated locally to produce well aligned multiwall carbon nanotube with high aspect ratio.
- The reaction parameters were varied to study their effect and to find the optimum conditions. These parameters are; reaction temperature (600-1000^{o}C), hydrogen flowrate (40-540 ml/min), acetylene flowrate (15-155 ml/min), and orifice diameter (3, 6, 12 mm).
- The optimum conditions were found to be; hydrogen flowrate: 240 ml/min, acetylene flowrate: 155 ml/min, orifice diameter: 6 mm, temperature: 800^{o}C, reaction time: 30 min. The amount of produced CNT is 1.9 gram/hr with purity of 97.62% with a low cost of 5.8 $US.

- Multiwall carbon nanotubes (MWCNT) were functionalized by acid treatment, phenol group and 1-octadecanol group and characterized using Fourier Transform Infrared Spectroscopy (FTIR).
- Polystyrene (PS)/CNT nanocomposites were prepared by thermal bulk polymerization without any initiator at different loadings of CNT.
- The tensile tests showed that maximum improvement by 68% in Young's modulus was obtained at 5wt.% loading of CNT-COOH.
- The DSC study showed a decrease in glass transition temperature (T_g) values of PS in the nanocomposites.
- The rheological study was conducted at 190^{o}C and shows that the addition of untreated CNTs increases the viscoelastic behavior of the PS matrix, while the functioalized CNTs act as plasticizer at loadings of 0.1% and 0.5%.
- Thermogravimetric analysis shows that the incorporation of CNT into PS enhanced the thermal properties of the matrix polymer.
- The non modified MWCNTs and modified MWCNTs-Amine and MWCNT-COOH shows a clear reduction in the conversion of styrene monomer to polystyrene at high temperature (115 ^{O}C) and different polymerization time from 1-6 hours, which prove that they are good candidates as polymerization inhibitors by adding them to the styrene monomer solution.

- Using 0.1 wt.% of high aspect ratio (HAR) CNT produced by the O-CVD reactor in PS/CNT nanocomposites increases the Young's modulus of the composite by 18.3%, and this is 12 times higher than the increment obtained by using the commercial CNT.

5.2 Recommendations

The following recommendations might be made for future related studies:

- Study the fluid dynamics and the reaction kinetics of the O-CVD reactor and develop mathematical model for.
- Use different hydrocarbons as carbon source and different catalysis in the process of producing CNT by O-CVD
- Use HAR CNT in preparing nanocmposites of different polymers and with different preparation techniques.
- Study the effect of CNT as polymerization inhibitor for different monomers other than styrene and at different temperatures.

APPENDIX

Appendix A

Results for 3mm and 12mm orifices

Table A.1: The weight, purity and lenght of CNTs produced by O-CVD at different acetylene and hydrogen flowrates with 3mm orifice at reaction temperature and reaction time of 800^{o}C and 30 min respectively.

Orifice Diameter (mm)	Acetylene Flowrate (ml/min)	Hydrogen Flowrate (ml/min)	weight of Deposited Carbon (g)	Purity %	Length of CNTs (µm)
3	15	40	0.1023	94.95	194.4
3	15	100	0.1437	31.535	133.3
3	15	240	0.2015	10.37	476.9
3	15	320	0.1617	7.895	171.7
3	15	540	0.1836	75.45	350
3	70	40	0.754	83.77	---
3	70	100	0.4398	100	---
3	70	240	0.6312	99.44	---
3	70	320	0.577	---	---
3	70	540	0.8896	52.545	---
3	155	40	0.733	6.825	---
3	155	100	0.3384	73.11	284.2
3	155	240	0.9721	93.905	---
3	155	320	1.0003	96.65	---
3	155	540	0.7881	92.345	---

Table A.2: The weight, purity and lenght of CNTs produced by O-CVD at different acetylene and hydrogen flowrates with 3mm orifice at reaction temperature and reaction time of 800^{o}C and 30 min respectively.

Orifice Diameter (mm)	Acetylene Flowrate (ml/min)	Hydrogen Flowrate (ml/min)	weight of Deposited Carbon (g)	Purity %	Length of CNTs (µm)
12	15	40	0.3544	40.345	500
12	15	100	0.1628	20.665	230.8
12	15	240	0.2303	19.725	85
12	15	320	0.1764	12.555	76.9
12	15	540	0.1555	67.235	100
12	70	40	0.286	95.975	323.1
12	70	100	0.0905	72.095	509.8
12	70	240	0.0558	17.675	292.3
12	70	320	0.3295	1.63	442.3
12	70	540	0.3168	2.38	555.6
12	155	40	0.3824	87.04	---
12	155	100	0.3003	90.645	---
12	155	240	0.2935	97.61	---
12	155	320	0.4069	93.42	722.2
12	155	540	0.2706	42.855	250

REFERENCES

[1] Paradise M, Goswami T. Carbon nanotubes – Production and industrial applications, Materials & Design 2007;28:1477-89.

[2] O'Connell MJ. Carbon nanotubes properties and applications, New York: Taylor & Francis; 2006

[3] See CH, Harris AT. A review of carbon nanotube synthesis via fluidized-bed chemical vapor deposition, Ind. Eng. Chem. Res 2009;46:997-1012.

[4] Harris P. Carbon nanotube science, Cambridge: Cambridge University Press; 2009: 43-72.

[5] Coleman JN, Khan U, BlauWJ, Gun'ko YK. Small but strong: A review of the mechanical properties of carbon nanotube–polymer composites, Carbon 2006;44:1624-52.

[6] Qian D, Dickey EC, Andrews R, Rantell T. Load transfer and deformation mechanisms in carbon nanotube–polystyrene composites. Appl Phys Lett 2000;76(20):2868-70.

[7] Iijima, S., (1991). Helical Microtubules of Graphitic Carbon. Nature 354: 56-58.

[8] Ebbesen, T. W. and P.M. Ajayan (1992). Large-Scale Synthesis of Carbon Nanotubes. Nature, 358 (6383): 220-222.

[9] Bethune, D. S., C. H. Kiang, M. S. de Vries, G. Gorman, R. Savoy, J. Vazquez and R. Beyers, (1993). Nature: 363, 605.

[10] Thess, A., R. P. Lee, H.J. Nikolaev, P. Dai, J. Petit, C. H. Robert, Y. H. Xu, S. G. Lee, A. G. Kim, D. T. Rinzler, G. E. Colbert, D. Scuseria, J. E. Tomanek and R.E. Smalley (1996).Crystalline ropes of metallic carbon nanotubes. Science 273 (52): 483-487.

[11] Yacamán-José, M., M. Miki-Yoshida, L. Rendón and J. G. Santiesteban (1993).Catalytic growth of carbon microtubules with fullerene structure. Applied Physics Letters 62(6) 657-659.

[12] Dresselhaus, M. G. Dresselhaus and S. Riichiro (1998). Physical Properties of Carbon Nanotubes. London: Imperial College Press.

[13] Satishkumar, B., P. Thomas, A. Govindaraj and C. Rao (2000). Y-junction carbon nanotubes. Applied Physics Letters 77(16): 2530-2532.

[14] Schujman, B. S., R. Vajtai., B. Biswas, L. J Schowalter and P. Ajayan (2002). Electrical behavior of isolated multiwall carbon nanotubes characterized by scanning surface potential microscopy. Applied physics letters 81(3): 541 – 543.

[15] Collins, P. and P. Avouris (2000). Nanotubes for electronics. Scientific American 62-69.

[16] Dong, Q., J. W Gregory., K. L Wing. Y. Min-Feng, and S. R Rodney (2002). Mechanics of carbon nanotubes. Applied Mechanics Review 55(6): 495-532.

[17] Schadler, L. S., S. C. Giannaris and P. M. Ajayan (1998). Load transfer in carbon nanotube epoxy composites. Applied Physics Letters 73(26): 3842-3844.

[18] Wagner, H., O. Lourie, Y. Feldman and R. Tenne (1998). Stress-induces fragmentation of multiwall carbon nanotubes in a polymer matrix. Applied Physics Letters 72(2): 188-190.

[19] Sahoo N G, Rana S, Cho J W, Li L, Chan S H. Polymer nanocomposites based on functionalized carbon nanotubes. Progress in Polymer Science 2010;35:837–867.

[20] Ching-Hwa, K., G. William, B. Robert and S. Donald (1995). Carbon nanotubes with single-layer walls. Carbon 33(7): 903-914

[21] Journet, C. and P. Bernier (1998). Production of carbon nanotubes. Applied Physics A-Materials Science & Processing 67 (1): 1-9.

[22] Jung, S. H., M. R Kim, S. H Jeong, S. U Kim, O. J. Lee, K. H, Lee, J. H Suh, and C. K. Park (2003). High-yield synthesis of multi-walled carbon nanotubes by

arc discharge in liquid nitrogen. Applied Physics A-Materials Science & Processing 76(2): 285-286.

[23] Andreas T., L. Roland, N. Pavel, D. Hongjie, P. Pierre, R. Jerome, X. Chunhui, H. L. Young, G. K. Seong, G. R. Andrew, T. C.Daniel, S. Gustavo, T. David, E. F. John, and E. S. Richard (1996). Crystalline Ropes of Metallic Carbon Nanotubes. Science, 273: 483-487.

[24] Hugh, O. P. (1999). Handbook of chemical vapor deposition (cvd) principles, Technology, and Applications. Second Edition William Andrew publishing, llc Norwich, New York, USA

[25] Tomita, A., K. Yoshida, Y. Nishiyama and Y. Tamai (1971). Formation of pyrolytic carbon from benzene over nickel and some properties of the carbon formed. Cabon 10: 601-611.

[26] Hulteen, J. C., H. X. Chen, C. K. Chambliss and C. R Martin (1997). Template synthesis of carbon nanotubule and nanofiber arrays. Nanostrctured Materials 9: 133-136.

[27] Jipeng, C., Z. Xiaobin, L. Fu, T. Jiangping, L. Huanming, S. Yanlin., and C. Fei (2004). Long bundles of aligned carbon nanofibers obtained by vertical floating catalyst method. Materials Chemistry and Physics 87: 241–245.

[28] Sinnot, S. B., R. Andrews, D. Qian, A. M. Rao, Z. Mao, E. C., Dickey, and F. Derbyshire (1999). Model of carbon nanotube growth through chemical vapor Deposition. Chemical Physics Letters 315: 25-30.

[29] Yudasaka, M., K. Rie, M. Takeo, O. Yoshimasa, Y. Susumu, and O. Etsuro (1995). Specific conditions for Ni catalyzed carbon nanotube growth by chemical vapor deposition. Applied Physics Letters, 67: 17-22.

[30] Xin Qing Wang, Liang Li, Ning Jie Chu, Ya Pi Liu, Hong Xiao Jin, Hong Liang Ge (2009). Lamellar Fe/Al_2O_3 catalyst for high-yield production of multi-walled carbon nanotubes bundles. *Materials Research Bulletin, Volume 44, Issue 2, Pages 422-425*.

[31] Maohui, G., and S. Klaus (1994). Bundles of carbon nanotubes generated by vapor-phase growth. Applied Physics T. 64-69.

[32] Yih-Ming L., Y. Sung, T. Chen, H. Wang and M. Ger (2007) Low temperature growth of carbon nanotubes by thermal chemical vapor deposition using non-isothermal deposited Ni–P–Pd as co-catalyst. Materials Chemistry and Physics Volume 106, Issues 2-3, 399-405

[33] Illayathambi K., R. Andrews, D. Qian, M. Mengu (2009). Growth kinetics of MWCNTs synthesized by a continuous-feed CVD method. Carbon 47 384 – 395

[34] Li, Y. Y., S. D. Bae, A. Sakoda and M. Suzuki (2001). Formation of vapor grown carbon fibers with sulfuric catalyst precursors and nitrogen as carrier gas. Carbon 39:91–100.

[35] Pavel, N., J. B. Michael, R. B. Kelley, R. Frank, T. C. Daniel, K. A., Smith and E. S. Richard (1999). Gas-phase catalytic growth of single-walled carbon nanotubes from carbon monoxide. Chemical Physics Letters 313: 91–97.

[36] Cheol, J. L., C. Seung, K. Hyoun-Woo, P. Chong-Yun and Y. Cheol-Woong (2002). Large-scale production of aligned carbon nanotubes by the vapor phase growth method. Chemical Physics Letters 359:109–114.

[37] Liu, B.C., S.C. Lyu, T.J. Lee, S.K. Choi, S.J. Eum, C.W. Yang, C.Y. Park and C.J. Lee (2003). Synthesis of single- and double-walled carbon nanotubes by catalytic decomposition of methane. Chemical Physics Letters 373: 475–479.

[38] Tatsuki, H., T. Kawakubo, J. Kimura, R. Taniguchi, A. Okamoto, T. Okazaki, T. Sugai, Y. Ozeki, M. Yoshikawa and H. Shinohara (2003). Selective synthesis of double-wall carbon nanotubes by CCVD of acetylene using zeolite supports. Chemical Physics Letters 382:679–685.

[39] Jieshan, Q., A. Yuliang, Z. Zhao, Y. Li, Y. Zhou (2004). Catalytic synthesis of single-walled carbon nanotubes from coal gas by chemical vapor deposition method. Fuel Processing Technology 85: 913– 920.

[40] Yoichi, M., Y. Miyauchi, S. Chiashi, S. Maruyama (2003). Characterization of single-walled carbon nanotubes catalytically synthesized from alcohol. Chemical Physics Letters 374: 53–58.

[41] Kobayashia, Y., H. Nakashimaa, D. Takagib and Y. Hommaa (2004). CVD growth of single-walled carbon nanotubes using size-controlled nanoparticle catalyst. Thin Solid Films 464–465:286– 289.

[42] Flahaut, E., C. Laurent, A. Peigney (2005). Catalytic CVD synthesis of double and triple-walled carbon nanotubes by the control of the catalyst preparation. Carbon 43: 375–383.

[43] Kim, Y.A., T. Hayashi, M. Endo, Y. Kaburagi, T. Tsukada, J. Shan, K. Osato and S. Tsuruoka (2005). Synthesis and structural characterization of thin multi-walled carbon nanotubes with a partially facetted cross-section by a floating reactant method. Carbon 43: 2243–2250.

[44] Pinault, M., M. Mayne-L'Hermite , C. Reynaud , V. Pichot , P. Launois and D. Ballutaud (2005). Growth of multiwalled carbon nanotubes during the initial stages of aerosol-assisted CCVD. Carbon 43 (2005) 2968–2976.

[45] Jing K., T. S. Hyongsok, M. C. Alan, F. Q. Calvin and D. Hongjie (1998). Synthesis of individual singlewalled carbon nanotubes on patterned siliconwafers. Nature 395.

[46] Zoltán B., G. Halasi, B. Korbély and K. Hernadi (2008). CVD-synthesis of multiwall carbon nanotubes over potassium-doped supported catalysts. Applied Catalysis A: General Volume 344, Issues 1-2 , 191-197

[47] Bei, C. and W. Ping (2005). Aligned carbon nanotubes by catalytic decomposition of C_2H_2 over Ni–Cr alloy. Carbon 43: 3172–317.

[48] Firoozeh Danafara, Fakhru'l-Razi, Mohd Amran Mohd Sallehа, Dayang Radiah Awang Biak (2009). Fluidized bed catalytic chemical vapor deposition synthesis of carbon nanotubes—A review. Chemical Engineering Journal 155, 37–48

[49] A.A. Muataz, A. Fakhru'l-Razi, C. Guan, E. Mahdi, A. Rinaldi, Effect of reaction temperature on the production of carbon nanotubes, NANO: Brief Rep. Rev. 1 (2006) 251–257.

[50] K. Kim, W.S. Jung, S.Y. Bae, J. Park, J. Choi, J. Choo, Investigation on the temperature-dependent growth rate of carbon nanotubes using chemical vapor deposition of ferrocene and acetylene, Chem. Phys. Lett. 401 (2005) 459–464.

[51] S.Y. Son, Y. Lee, S.Won, D.H. Lee, High-quality multiwalled carbon nanotubes from catalytic decomposition of carboneous materials in gas–solid fluidized beds, Ind. Eng. Chem. Res. 47 (2008) 2166–2175.

[52] Buchholz, D. B.; Doherty, S. P.; Chang, R. P. H. Mechanism for the growth of multiwalled carbon-nanotubes from carbon black. *Carbon* 2003, *41* (8), 1625.

[53] Lavrentiev, V.; Abe, H.; Yamamoto, S.; Naramoto, H.; Narumi, K. Formation of carbon nanotubes under conditions of Co+C60 film. *Physica B* 2002, *323* (1-4), 303.

[54] Resasco, D. E.; Alvarez, W. E.; Pompeo, F.; Balzano, L.; Herrera, J. E.; Kitiyanan, B.; Borgna, A. A scalable process for production of singlewalled carbon nanotubes (SWNTs) by catalytic disproportionation of CO on a solid catalyst. *J. Nanopart. Res.* 2002, *4* (1-2), 131.

[55] Li, Y. L.; Kinloch, I. A.; Shaffer, M. S. P.; Geng, J.; Johnson, B.; Windle, A. H. Synthesis of single-walled carbon nanotubes by a fluidizedbed method. *Chem. Phys. Lett.* 2004, *384* (1-3), 98.

[56] Wang, Y.; Wei, F.; Luo, G.; Yu, H.; Gu, G. The large-scale production of carbon nanotubes in a nano-agglomerate fluidized-bed reactor. *Chem. Phys. Lett.* 2002, *364* (5-6), 568.

[57] Perez-Cabero, M.; Rodriguez-Ramos, I.; Guerrero-Ruiz, A. Characterization of carbon nanotubes and carbon nanofibers prepared by catalytic decomposition of acetylene in a fluidized bed reactor. *J. Catal.* 2003, *215* (2), 305.

[58] Cheng, H. M.; Li, F.; Su, G.; Pan, H. Y.; He, L. L.; Sun, X.; Dresselhaus, M. S. Large-scale and low-cost synthesis of single-walled carbon nanotubes by the catalytic pyrolysis of hydrocarbons. *Appl. Phys. Lett.* 1998, *72* (25), 3282.

[59] Kumar, M.; Ando, Y. Controlling the diameter distribution of carbon nanotubes grown from camphor on a zeolite support. *Carbon* 2005, *43* (3), 533.

[60] Maruyama, S.; Kojima, R.; Miyauchi, Y.; Chiashi, S.; Kohno, M. Low temperature synthesis of high-purity single-walled carbon nanotubes from alcohol. *Chem. Phys. Lett.* 2002, *360* (3-4), 229.

[61] Murakami, Y.; Miyauchi, Y.; Chiashi, S.; Maruyama, S. Characterization of single-walled carbon nanotubes catalytically synthesized from alcohol. *Chem. Phys. Lett.* 2003, *374* (1-2), 53.

[62] Inoue, S.; Nakajima, T.; Kikuchi, Y. Synthesis of single-wall carbon nanotubes from alcohol using Fe/Co, Mo/Co, Rh/Pd catalysts. *Chem. Phys. Lett.* 2005, *406* (1-3), 184.

[63] Li, Q.; Yan, H.; Zhang, J.; Liu, Z. Effect of hydrocarbons precursors on the formation of carbon nanotubes in chemical vapor deposition. *Carbon* 2004, *42* (4), 829.

[64] Hernadi, K.; Fonseca, A.; Nagy, J. B.; Siska, A.; Kiricsi, I. Production of nanotubes by the catalytic decomposition of different carboncontaining compounds. *Appl. Catal., A* 2000, *199* (2), 245.

[65] Qian, W.; Yu, H.; Wei, F.; Zhang, Q.; Wang, Z. Synthesis of carbon nanotubes from liquefied petroleum gas containing sulfur. *Carbon* 2002, *40* (15), 2968.

[66] Lee, Y. T.; Park, J. Temperature dependent growth of vertically aligned carbon nanotubes in the range 800-1100 °C. *J. Phys. Chem. B* 2002, *106* (31), 7614.

[67] Liu, B. C.; Lyu, S. C.; Jung, S. I.; Kang, H. K.; Yang, C. W.; Park, J. W.; Park, C. Y.; Lee, C. J. Single-walled carbon nanotubes produced by catalytic chemical vapor deposition of acetylene over Fe-Mo/MgO catalyst. *Chem. Phys. Lett.* 2004, *383* (1-2), 104.

[68] Wong E W, Sheehan P E, Lieber C M. Nanobeam mechanics: elasticity, strength and toughness of nanorods and nanotubes. Science 1997;277:1971-1975.

[69] Yu M, Lourie O, Dyer M J, Moloni K, Kelly T F, Ruoff R S. Strength and breaking mechanism of multiwalled carbon nanotubes under tensile load. Science 2000;287:637-640.

[70] Coleman J N, Blau W J, Dalton A B, Munoz E, Collins S, Kim B G, Razal J, Selvidge M, Vieiro G, Baughman R H. Improving the Mechanical Properties of Single-Walled Carbon Nanotube Sheets by Intercalation of Polymeric Adhesives. Appl. Phys. Lett. 2003;82:1682-1684.

[71] Byrne M T, McNamee W P, Gun'ko Y K. Chemical functionalization of carbon nanotubes for the mechanical reinforcement of polystyrene composites. Nanotechnology 2008;19:415707 (8pp)

[72] Kota A K, Cipriano B H, Duesterberg M K, Gershon A L, Powell D, Raghavan S R, Bruck H A. Electrical and Rheological Percolation in Polystyrene/MWCNT composites. Macromolecules 2007;40:7400-7406

[73] Biercuk M J, Llaguno M C, Radosavljevic M, Hyun J K, Johnson A T. Carbon nano-tube composites for thermal management. Appl. Phys. Lett. 2002;80:2767–2769.

[74] Shi D, Lian J, He P, Wang L M, Xiao F, Yang L, Schulz M J, Mast D B. Plasma coating of carbon nanofibers for enhanced dispersion and interfacial bonding in polymer composites. Appl. Phys. Lett. 2003;83:5301–5303.

[75] Chen X, Tao F, Wang J, Yang H, Zou J, Chen X, Feng X. Concise route to styryl-modified multi-walled carbon nanotubes for polystyrene matrix and enhanced mechanical properties and thermal stability of composite. Materials Science and Engineering A 2009;499:469-475.

[76] Ma PC, Siddiqui N A, Marom G, Kim JK. Dispersion and functionalization of carbon nanotubes for polymer-based nanocomposites: A review. Composites: Part A 2010;41:1345–1367.

[77] Safadi B., Andrews R., Grulke E. A.: Multiwalled carbon nanotube polymer composites: Synthesis and characterization of thin films. J. Appl. Polym. Sci., 84, 2660–2669 (2002).

[78] Kim S. T., Choi H. J., Hong S. M.: Bulk polymerized polystyrene in the presence of multiwalled carbon nanotubes. Colloid Polym Sci, 285, 593-598 (2007).

[79] Zhang, Z., J. Zhang, P. Chen, B. Zhang, J. He and G. H. Hu, 2006, Enhanced interactions between multi-walled carbon nanotubes and polystyrene induced by melt mixing, Carbon 44, 692-698.

[80] Ajayan, P., O. Stephan, C. Colliex and D. Trauth (1994). Aligned carbon nanotube arrays formed by cutting a polymer resin-nanotube composite. Science 265: 1212-1214.

[81] Peigney, A., C. H. Laurent, E. Flahaut and A. Rousset (2000). Carbon nanotubes in novel ceramic matrix nanocomposites. Ceramics International 26: 677-683.

[82] Dresselhaus, M., G. Dresselhaus and P. Avouris (2001). Carbon Nanotubes: Synthesis, Structure, Properties, and Applications, Germany: Springer-Verlag Berlin HeidleberG.

[83] Allaouia, A., S. Baia, H. M. Chengb, J. B. Baia (2002). Mechanical and electrical properties of a MWNT/epoxy composite. Composites Science and Technology 62:1993–1998.

[84] Sandler, J. K., W. Kirk, J. E. Kinloch, I. A. Shafferl, M. S. P. Windle (2003). Ultra-low electrical percolation threshold in carbon-nanotube-epoxy composites. Polymer 44 5893–5899.

[85] Gong, X., J. Liu, S. Baskaran, R. D. Voise and J. S. Young (2000). Surfactant assisted processing of carbon nanotube/polymer composites. Chemistry of Materials12: 1049-1052.

[86] Bonard, J. M., J. P. Salvetat, T. Stockli, W. A. de Heer, and A. Chatelain (1998). Field Emission from Single-Wall Carbon Nanotube Films. Applied Physics Letters 73: 918-920.

[87] Zhu, W., C. Bower and O. Zhou, G. Kochanski and S. Jin (1999). Large current density from carbon nanotube field emitters. Applied Physics Letters 75 (6): 873-875.

[88] Dean, K.A and B. R. Chalamala (1999). Field emission microscopy of carbon nanotube caps. Journal of Applied Physics 85: 3832-3836.

[89] Jia, Z., Z. Wang, C. Xu, J. Liang, B. Wei, D. Wu and S. Zhu (1999). Study on poly (methly methacrylate)/carbon nanotube composites. Materials Science and Engineering A, 271: 395-400.

[90] Carole, A. C., R. Diana, L. David and H. Mayerb (2002). Distribution and alignment of carbon nanotubes and nanofibrils in a polymer matrix. Composites Science and Technology 62:1105–1112.

[91] Shaffer, M. S. P. and A. H. Windle (1999). Fabrication and characterization of carbon nanotube/poly (vinyl alcohol) composites. Advanced Materials 11: 937-941.

[92] Jin, L., C. Bower and O. Zhou (1998). Alignment of carbon nanotubes in a polymer matrix by mechanical stretching. Applied Physics Letters 73(9): 1197-1199.

[93] Haggenmueller, R., H. H. Gommans, A. G. Rinzler, J. E. Fischer and K. I. Winey (2000). Aligned single-wall carbon nanotubes in composites by melt processing methods. Chemical Physics Letters 330: 219-225.

[94] Hsu-Chiang, K., C. Ma, W. Chang, S. Yuen, H. Wu, T. Lee (2005). Synthesis, thermal, mechanical and Rheological properties of multiwall carbon nanotube/waterborne polyurethane nanocomposite. Composites Science and Technology 65: 1703–1710.

[95] Tony, M., P. Po¨tschke, P. Halley, M. Murphy, D. Martin, S. Bell, G. Brennan, D. Bein, P. Lemoine and J. Quinn (2005). Polyethylene multiwalled carbon nanotube composites. Polymer 46: 8222–8232.

[96] Thostenson E. T., Chou T. W.: Aligned multi-walled carbon nanotube-reinforced composites: processing and mechanical characterization. J. Phys. D: Appl. Phys., 35, L77-L80 (2002).

[97] Andrews R., Jacques D., Minot M., Rantell T.: Fabrication of carbon multiwall nanotube/polymer composites by shear mixing. Macromol. Mater. Eng., 287, 395-403 (2002).

[98] Mitchell C. A., Bahr J. L., Arepalli S., Tour J. M., Krishnamoorti R.: Dispersion of functionalized carbon nanotubes in polystyrene. Macromolecules, 35, 8825-8830 (2002).

[99] Choi H. J., Zhang K., Lim J. Y.: Multi-walled carbon nanotube/polystyrene composites prepared by in-situ bulk sonochemical polymerization. Journal of Nanoscience and Nanotechnology, 7, 3400-3403 (2007).

[100] Kota A. K., Cipriano B. H., Duesterberg M. K., Gershon A. L., Powell D., Raghavan S. R., Bruck H. A.: Electrical and Rheological Percolation in Polystyrene/MWCNT composites. Macromolecules, 40, 7400-7406 (2007).

[101] Abuilaiwi F. A., Laoui T., Al-Harthi M., Atieh M. A.: Modification and functionalization of multiwalled carbon nanotube (MWCNT) via Fischer esterification. The Arabian Journal for Science and Engineering, 35, 37-48 (2010).

[102] A.M. Shanmugharaj, J.H. Bae, Kwang Yong Lee, Woo Hyun Noh, Se Hyoung Lee and Sung Hun Ryu. Physical and chemical characteristics of multiwalled carbon nanotubes functionalized with aminosilane and its influence on the properties of natural rubber composites. Composites Science and Technology. Vol 67, Issue 9, (2007) 1813-1822

[103] M. Hughes, G. Z. Chen, M. Shaffer, D. J. Fray, and A. H. Windle, Electrochemical Capacitance of a Nanoporous Composite of Carbon Nanotubes and Polypyrrole, *Chem. Mater.*, 14(2002), pp. 1610–1613.

[104] Yue-Ying, F., C. Hui-Ming, W. Yong-Liang, S. Ge and S. Zu-Hong (2000). Tailoring the diameters of vapor-grown carbon nanofibers. Carbon 38: 921–927

[105] Atieh, M. A. Synthesis, characterization and application of carbon nanotubes and carbon nanofiber. PhD dissertation, Univeristi Putra Malaysia, 2005.

[106] Oberun, A., M. Endo and T. Koyama (1976). Filamentous growth of carbon through benzene decomposition. Journal of Crystal Growth 32: 335-349.

[107] Munehiro, I., O. Toshihiko, M. Kenji and E. Morinobu (1992). Formation of vapor-grown carbon fibers in CO-CO_2—H_2 mixtures, influence of carrier gas composition. Carbon 35: 59-463.

[108] Munehiro, I., O. Toshihiko and M. Kenji (1993). Preparation of vapor-grown carbon fibers by floating catalyst method in linz-donawitz-converter gas: influence of catalyst size. Carbon 33(5): 699-703

[109] Socrates G., Infrared Characteristic Group and Frequencies, John Wiley & Sons, New York, 1980

[110] Fragneaud B, Masenelli-Varlot K, Gonzalez-Montiel A, Terrones M, Cavaillé J Y. Mechanical behavior of polystyrene grafted carbon nanotubes/polystyrene nanocomposites. Composites Science and Technology 2008;68:3265–3271.

[111] Rieger J.: The glass transition temperature of polystyrene. Journal of Thermal Analysis, 46, 965-972 (1996).

[112] Williams M. L., Landel R. F., Ferry J. D.: The temperature dependence of relaxation mechanisms in amorphous polymers and other glass-forming liquids. J Am Chem Soc, 77, 3701–3707 (1955).

[113] Goldbeck-Wood G., Bliznyuk V., Burlakov V., Assender H., Briggs A., Tsukahara Y., Anderson K., Windle A.: Surface structure of polystyrenes: comparison of lattice chain simulations and scanning probe microscopy. American Physical Society, Annual March Meeting, March 12 - 16, 2001, Washington State Convention Center Seattle.

[114] Liu C, Zhang J, He J, Hu G. Gelation in carbon nanotube/polymer composites. Polymer 2003;44:7529–7532.

[115] Du F., Scogna R. C., Zhou W., Brand S., Fischer J. E., Winey K. I.: Nanotube networks in polymer nanocomposites: rheology and electrical conductivity. Macromolecules, 37, 9048–9055 (2004).

[116] Huang Y Y, Ahir S V, Terentjev E M. Dispersion rheology of carbon nanotubes in a polymer matrix. Phys Rev B 2006;73:125422.

[117] Fan Z., Advani S. G.: Rheology of multiwall carbon nanotube suspensions.: J. Rheol., 51, 585–604 (2007).

[118] Abbasi S, Carreau P J, Derdouri A, Moan M. Rheological properties and percolation in suspensions of multiwalled carbon nanotubes in polycarbonate. Rheol Acta 2009;48:943–959.

[119] Potschke P., Fornes T. D., Paul T. R.: Rheological behavior of multiwalled carbon nanotube/polycarbonate composites.: Polymer, 43, 3247-3255 (2002).

[120] Mutel A. T., Kamal M. R.: Rheological properties of fiber-reinforce polymer melts. in ' Two Phase Polymer Systems' (ed.: Utracki L. A.) Carl Hanser, Munich, Chapter 12, 305-331 (1991).

[121] Kitano T., Kataoka T., Nagatsuka Y.: Shear flow rheological properties of vinylon-and glass-fiber reinforced polyethylene melts. Rheol Acta, 23, 20-30 (1984).

[122]www.sabic.com/me/en/productsandservices/chemicals/styrenemonomer.asp
x

[123] Seno M, Fukunaga H, Sato T. Kinetic and ESR studies on radical polymerization of methyl methacrylate in the presence of fullerene. J Polym Sci: Part A: Polym Chem 1998;36:2905–12.

[124] Kirkwood K, Stewart D, Imrie CT. Role of C60 in the free radical polymerization of methyl methacrylate. J Polym Sci: Part A: Polym Chem 1997;35:3323–5.

[125] Chen Y, Lin K-Ch. Radical polymerization of styrene in the presence of C60. J Polym Sci: Part A: Polym Chem 1999;37:2969–75.

[126] Seno M, Maeda M, Sato T. Effect of fullerene on radical polymerization of vinyl acetate. J Polym Sci: Part A: Polym Chem 2000;38:2572–8.

[127] Deng J et al. Carbon nanotube—polyaniline hybrid materials. Eur Polym J 2002;38:2497–501.

[128] Onderko K, Pabin-Szafko B, Szafko J. Poly (methyl methacrylate)/ carbon nanotubes composites. Karbo 2004;49(4): 175–81.

[129] Barbara Pabin–Szafko, Ewa Wiśniewska, Jerzy Szafko, Carbon nanotubes and fullerene in the solution polymerisation of acrylonitrile European Polymer Journal 42 (2006) 1516–1520

VITA

- Issam Thaher Ahmad Amr.
- Nationality: Jordanian - Born in Jeddah, 31/3/1979.
- Married with two daughters.
- Received B.Sc. degree in Chemical Engineering from The University of Jordan in June 2002.
- Received Master of Science degree in Chemical Engineering from King Fahd University of Petroleum & Minerals in May 2006.
- Received Doctor of Philosophy degree in Chemical Engineering from King Fahd University of Petroleum & Minerals in January 2011.
- Worked as Research Assistant at King Fahd University of Petroleum & Minerals (Feb. 2004 – Nov. 2006).
- Worked as Lecturer B at King Fahd University of Petroleum & Minerals (Nov. 2006 – Jun 2011).
- Present Address:

  P. O. Box: 8344 – Dhahran 31261 – Saudi Arabia

  Tel.: 966 501277073
- Permanent Address:

  Amman – Jordan

  Tel.: 962 795022270
- Email: esamamr@gmail.com